AN EXPERIMENTAL STUDY OF THE BOUNDARY-LAYER CHARACTERISTICS FOR TWO-PHASE (GAS-LIQUID SPRAY) FLOW OVER A CIRCULAR CYLINDER

Thosis for the Degree of Ph. D. MICHIGAN STATE UNIVERSITY
Harold E. Wright
1966



This is to certify that the

thesis entitled

AN EXPERIMENTAL STUDY OF THE BOUNDARY-LAYER CHARACTERISTICS FOR TWO-PHASE (GAS-LIQUID SPRAY) FLOW OVER A CIRCULAR CYLINDER

presented by

Harold E. Wright

has been accepted towards fulfillment of the requirements for

Ph.D. degree in Mechanics

Department of Metallurgy, Mechanics and Materials Science

Major professor

Lawrence E. Malvern

Date Unoust 5, 1966

ABSTRACT

AN EXPERIMENTAL STUDY OF THE BOUNDARY-LAYER CHARACTERISTICS FOR TWO-PHASE (GAS-LIQUID SPRAY) FLOW OVER A CIRCULAR CYLINDER

by Harold E. Wright

This research is concerned with the transverse flow of a two-phase (air-water spray) mixture over a right circular cylinder for a range of gas Reynolds numbers from 1×10^4 to 2×10^5 , with mass ratios of water to air less than 0.1. The particular area of investigation is the region of the flow field where the boundary-layer separates from the cylinder.

This research includes an experimental investigation of the flow field in the region of the cylinder and some of its boundary-layer properties. As a result of the investigation two experimental tools for two-phase boundary-layer studies were successfully developed: A technique for the measurement of the pressure profile was developed, utilizing liquid-filled pressure lines from which a small amount of water is injected into the liquid boundary layer. For the case considered, a maximum error of 5.2 per cent was found at the point of pressure minimum in comparison with a standard method in single-phase flow. The second technique developed was a method for visually observing the point of boundary-layer separation. A mixture of distilled water and wetting agent was injected into the liquid boundary layer, which promoted the formation of small gas bubbles, whose motion

disclosed the point of boundary-layer separation. The results of these observations agreed with those interpreted from the observed pressure profiles.

The pressure profiles were measured for the case of two-phase flow for a gas Reynolds number of 5.64 × 10⁴ and three different water nozzle pressures. In each case the point of pressure minimum shifted downstream approximately 6 degrees while the separation point shifted downstream 14 degrees when compared to single-phase flow at the same gas Reynolds number. The rate of growth of the liquid-boundary-layer thickness was observed to be high in the region between the point of pressure minimum and the separation point. A bubble of water was observed to be located downstream of the separation point, and vortices were observed. It was by these vortices that water was discharged from the cylinder. It is believed that the presence of the relatively thick liquid boundary layer in the region of the separation point and the presence of the water bubble provided the external flow with a contour sufficiently different from a cylinder to produce the observed reduction in the slope of the pressure profile in this region.

Two analytical models were considered: the first assumed a laminar boundary-layer system, while the second considered turbulent flow. Neither analytical model gave good agreement with experimentally-observed separation points.

AN EXPERIMENTAL STUDY OF THE BOUNDARY-LAYER CHARACTERISTICS FOR TWO-PHASE (GAS-LIQUID SPRAY) FLOW OVER A CIRCULAR CYLINDER

by

Harold E. Wright

A THESIS

Submitted to
Michigan State University
in partial fulfillment of the requirements
for the degree of

DOCTOR OF PHILOSOPHY

Department of Metallurgy, Mechanics and Materials Science

ACKNOWLEDGMENTS

I gratefully acknowledge my indebtedness to Dr. Max Scherberg of the Aerospace Research Laboratories of the United States Air Force, who suggested the problem and gave valuable guidance and counsel throughout the project.

I wish to express my sincere graditude to my major professor, Dr. L. E. Malvern for his continued encouragement, patience, suggestions and technical guidance throughout my entire Ph.D. program. I am grateful to my research professor, Dr. J. E. Lay, for his many suggestions and technical advice on problems encountered in the research. I hereby acknowledge my appreciation to the other members of my guidance committee, Dr. W. A. Bradley, Dr. J. F. Foss and Dr. R. H. Wasserman.

I am grateful to the United States Air Force for the opportunity to pursue this research. In particular, I am indebted to the Air Force Institute of Technology (AFIT) and the Aerospace Research Laboratories who provided facilities and instrumentation. I want to thank Mr. W. W. Baker, laboratory technician of AFIT for his assistance throughout the experimental phase of the research.

Finally, I wish to thank my wife and children for the sacrifice they made in order for me to pursue this research.

CONTENTS

																									PAGE
ACKNOWLE	EDGME	NTS .						•	•	•	•	•	•	•	•		•	•	•	•	•	•	•	•	ii
LIST OF	FIGUE	RES		•	•		•	•	•	•		•		•		•	•	•	•	•	•	•	•		v
LIST OF	TABLE	ES.						•	•	•	•	•	•	•	•	•	•		•	•	•	•	•	•	ix
NOMENCLA	ATURE			•	•		•		•	•	•	•	•	•	•	•	•	•	•			•	•		x
CHAPTER																									
I.	INTRO	DUCT:	ION				•	•	•	•	•	•		•	•	•	•	•	•	•	•	•	•	•	1
		Gener																				•	•		1
	1.2		The																		•	•	•		4
II.	ANAL	YSIS						•	•												•	•	•		8
	2.1	Gene				-						-										•	•	•	8
	2.2	Gas I	Bour s in		_		-										-					•		•	9
	2.3	Turb	uleı Lar																				•	•	19
III.	EXPE	RIMEN'	ΓAL	ME	тн	ODS	S Al	ND	AP	PA	RA	ıΤU	IS				•	•			•			•	25
	3.1																								25
		Gene:																							
	3.2	The																							26
	3.3	The																							27
	3.4	The 1	Wate	er-	-Sp:	ray	' S	yst	tem	1	•	•	•	•	•	•	•	•	•	•	•		•	•	28
	3.5	The 1	Wind	d-I	un:	ne]	. T	est	: S	Sec	ti	on	l												28
	3.6	The '																							
			zzlo																						28
	3.7	Butt																							29
		C	eri.	ry - c	va.	, T A 6	: a.					. L	11	1 0	156	:1.	•	•	•	•	•	•	•	•	
	3.8	Summ																							29
	3.9	The '	ſes [.]	t S	Spe	cin	ien	ar	nd	Сс	nt	ro	1	Pa	ne	21	•	•	•	•	•	•	•	•	29
IV.	EXPE	RIMEN'	TAL	PF	ROC:	EDU	JRE	•	•	•	•	•	•	•	•	•	•	•	•	•	•	•	•	•	32
	4.1	Dete																					•	•	32
	4.2	Dete:												-						_					
			d D:	-																					36
	4.3	Meas	ure	ner	nt (of	th	e I	iic	ui	.d-	·Fi	lm	1	'hi	ck	ne	ess	3						38

CONTENTS (contd.)

CHAPTER		PAGE
IV.	EXPERIMENTAL PROCEDURE (contd.)	
	4.4 The Determination of the Ratio of the Mass	
	of Water Flow to Mass of Air Flow	39
	4.5 Measurement of the Liquid-Film Velocity	41
	4.6 The Determination of the Boundary-Layer Separation Point	42
	osparacion roine	' -
٧.	NUMERICAL PROCEDURES	44
	5.1 The Scope of the Numerical Procedures	44
	5.2 Polynomial Fitted to Experimental Data	44
	5.3 The Runge-Kutta Numerical Procedure	44
	5.4 Numerical Procedures for the Laminar	
	Gas Boundary-Layer Model	50
	5.5 Numerical Procedure for the Turbulent	
	Gas Boundary-Layer Model	51
	das boundary bayer noder	91
VI.	RESULTS	52
	6.1 Preliminary Remarks	52
	6.2 Wind-Tunnel Evaluation in Single-Phase Flow	53
	6.3 Experimental Results in Two-Phase Flow	57
	6.4 Results of Analytical Investigation	68
	6.5 Summary of Results	71
	ore summary or negation	, _
VII.	SUMMARY AND CONCLUSIONS	75
APPENDIX	K	
Α	GRAVITATIONAL EFFECTS	79
В	FIGURES	81
С	TABLES	131
_		
D	BIBLIOGRAPHY	143

LIST OF FIGURES

FIGURE		PAGE
1	Boundary Layer Quantities for Gas Boundary Layer	82
2	Schematic Drawing of AFIT 10"×10" Wind Tunnel	83
3	AFIT 10"×10" Wind Tunnel	84
4	Test Section of AFIT 10"×10" Wind Tunnel	85
5	Schematic of Test Cylinder	86
6	One and One-Half Inch Diameter Test Cylinder	87
7	Schematic Drawing of Pressure Measuring System	88
8	Pressure Measuring System	89
9	Calibration Curve for Statham Pressure Transducer with 14 Volts DC Applied Voltage	90
10	Pressure Correction for Change in Elevation Between Pressure Tap on Test Cylinder and Transducer vs Angle of Cylinder Rotation, Calibration Constant equal 1.840 Millivolt Per Inch Water Pressure	91
11	Grid Wire Layout for Droplet Velocity Ud Measurement	92
12	Apparatus for Measurement of Liquid Film Thickness	93
13	Liquid Film Thickness vs Probe Voltage, Φ = 90°, $P_{\mathbf{W}}$ = 20 psig	94
14	Droplet Capture Tube Apparatus	95
15	(a) One-Half Inch Capture Tube(b) Three-Eighths Inch Capture Tube	95
16	Schematic Drawing of Schlieren Apparatus	96
17	Boundary-Layer Separation in Single-Phase Flow with Forward Stagnation Point at Top of Cylinder, Reynolds Number 5.64×10 ⁴	97

LIST OF FIGURES (contd.)

FIGURE	PAGE
18	Runge-Kutta Subroutine
19	Computer Flow Chart for Runge-Kutta Subroutine 99
20	Computer Program for Equation (2.15) 100
21	Computer Program for Equations (2.25) and (2.26) 101
22	Average Nusselt Number vs Reynolds Number for Single-Phase Flow (Wind Tunnel Evaluation) 102
23	Pressure Coefficient vs Φ, 1.5 Inch Diameter Cylinder, Single-Phase Flow 103
24	Pressure Coefficient vs Φ, 1.5 Inch Diameter Cylinder for Single-Phase Flow, Re = 5.64×10 ⁴ 104
25	Hysteresis Effects in Pressure Measuring System, Single-Phase Flow, Re = 5.64×10 ⁴ 105
26	Pressure on Cylinder vs Φ for 1.5 Inch Diameter Cylinder Single-Phase Flow, Re = 5.64×10 ⁴ 106
27	Difference Between Actual and Observed Pressure, Observed Pressure Measured by Water Injection Method
28	Pressure vs Φ for Gas Reynolds Number equal 5.64×10 ⁴ , Nozzle Water Pressure equal 20 psig 108
29	Pressure Coefficient vs Φ for Two-Phase Flow Over 1.5 Inch Diameter Cylinder, Nozzle Water Pressure equal 15 psig, Red = 522, Gas Reynolds Number equal 5.64×10 ⁴
30	Pressure Coefficient vs Ф for Two-Phase Flow Over 1.5 Inch Diameter Cylinder, Nozzle Water Pressure equal 20 psig, Red = 458, Gas Reynolds Number equal 5.64×10 ⁴
31	Pressure Coefficient vs Ф for Two-Phase Flow Over 1.5 Inch Diameter Cylinder, Nozzle Water Pressure equal 25 psig, Red = 380, Gas Reynolds Number equal 5.64×10 ⁴
32	Per Cent of Observations vs Fraction of Standard Deviation, Gas Reynolds Number equal 5.64×10 ⁴ , Nozzle Water Pressure equal 15 psig 112

LIST OF FIGURES (contd.)

FIGURE		PAGE
33	Per Cent of Observations vs Fraction of Standard Deviation, Gas Reynolds Number equal 5.64×10 ⁴ , Nozzle Water Pressure equal 20 psig	113
34	Per Cent of Observations vs Fraction of Standard Deviation, Gas Reynolds Number equal 5.64×10 ⁴ , Nozzle Water Pressure equal 25 psig	114
35	Liquid Boundary-Layer Thickness vs Φ for Gas Reynolds Number equal 5.64×10 ⁴ , Nozzle Water Pressure equal 15 psig	115
36	Liquid Boundary-Layer Thickness vs Φ for Gas Reynolds Number equal 5.64×10 ⁴ , Nozzle Water Pressure equal 20 psig	116
37	Liquid Boundary-Layer Thickness vs Φ for Gas Reynolds Number equal 5.64×10 ⁴ , Nozzle Water Pressure equal 25 psig	117
38	Liquid-Gas Interface Velocity vs Φ for Gas Reynolds Number equal 5.64×10 ⁴ , Nozzle Water Pressure equal 15 psig	118
39	Liquid-Gas Interface Velocity vs Φ for Gas Reynolds Number equal 5.64×10 ⁴ , Nozzle Water Pressure equal 20 psig	119
40	Liquid-Gas Interface Velocity vs Φ for Gas Reynolds Number equal 5.64×10 ⁴ , Nozzle Water Pressure equal 25 psig	120
41	Boundary-Layer Separation for Gas Reynolds Number equal 5.64×10 ⁴ and Water Pressure equal 20 psig at Spray Nozzle	121
42	Water Spray Distribution Milliliters Per Minute Along Axis of Test Cylinder, for 1/2 Inch Collecting Tube, Nozzle Nr. 2116, Gas Reynolds Number equal 5.64×10 ⁴ and Water Pressure at Spray Nozzle equal 20 psig	122
43	Coordinate Plot of Water Spray Distribution Over Test Segment of Cylinder in Milliliters Per Minute for One-Half Inch Capture Tube, Gas Reynolds Number equal 5.64×10 ⁴ , Water Pressure at Spray Nozzle equal 20 psig and Average Mass Ratio of Water to Air	
	equal 0.045	123

LIST OF FIGURES (contd.)

FIGURE		PAGE
44	Water Vortex Separating from Liquid Film and Indicating Direction of Vortex Rotation	124
45	Series of Vortices Extending into Liquid Boundary Layer	124
46	Boundary-Layer Separation for Gas Reynolds Number equal 3.55×10 ⁴ and Water Pressure equal 20 psig at Spray Nozzle	125
47	Boundary-Layer Separation for Gas Reynolds Number equal 1.04×10 ⁵ and Water Pressure equal 20 psig at Spray Nozzle	125
48	Velocity Pressure vs Φ for Gas Reynolds Number equal 5.64×10 ⁴ , Nozzle Water Pressure equal 15 psig	126
49	Velocity Pressure vs Φ for Gas Reynolds Number equal 5.64×10 ⁴ , Nozzle Water Pressure equal 20 psig	127
50	Velocity Pressure vs Φ for Gas Reynolds Number equal 5.64×10 ⁴ , Nozzle Water Pressure equal 25 psig	128
51	Boundary-Layer Separation on a Vertical Cylinder in Horizontal Two-Phase Flow, Gas Reynolds Number equal 5.64×10 ⁴	129
52	Boundary-Layer Separation on a Vertical Cylinder in Horizontal Two-Phase Flow with Dye Injected into Liquid Boundary Layer, Gas Reynolds Number	
	equal 5.64×10 ⁴	130

LIST OF TABLES

TABLE		PAGE
1	Heat Transfer Data	132
2	Velocity Profiles	133
3	Velocity Pressure in Inches Water, with Test Cylinder Removed, at Test Station in AFIT 10"×10" Vertical Wind Tunnel, Run No l	134
4	Velocity Pressure in Inches Water, with Test Cylinder Removed, at Test Station in AFIT 10"×10" Vertical Wind Tunnel, Run No 2	135
5	Velocity Pressure in Inches Water, with Test Cylinder Removed, at Test Station in AFIT 10"×10" Vertical Wind Tunnel, Run No 3	136
6	Velocity Pressure in Inches Water, with Test Cylinder Removed, at Test Station in AFIT 10"×10" Vertical Wind Tunnel, Run No 4	. 137
7	Velocity Pressure in Inches Water, with Test Cylinder Removed, at Test Station in AFIT 10"×10" Vertical Wind Tunnel, Run No 5	. 138
8	Droplet Velocity Data	139
9	Droplet Size Distribution and Reynolds Number Data	. 140
10	Laminar Boundary Layer Data	141
11	Turbulent Boundary Layer Data	142

NOMENCLATURE

Α area pressure coefficient $C_{\mathbf{P}}$ particle diameter (liquid or solid) d D cylinder diameter Н δ^*/θ boundary layer dimensionless shape factor for turbulent flow h average heat transfer coefficient k gas thermal conductivity l constant distance measured from the gas-liquid interface to an arbritrary point in the external flow field number of frames (photographic) m n film speed in frames per second number of observations N Nu average gas Nusselt number based on cylinder diameter Ρ pressure $P_{\mathbf{w}}$ water pressure at spray nozzle P_{s} static pressure velocity pressure q Q heat flow per unit time cylinder radius R gas Reynolds number based on cylinder diameter Re droplet Reynolds number based on droplet diameter and gas Red properties ($Re_d = d (U_\infty - U_d)/v$) $U_S\theta/\nu$, Reynolds number based on momentum thickness and gas Rea

properties

NOMENCLATURE (contd.)

- S distance
- Tw surface temperature
- T_∞ gas temperature at infinity
- U velocity inside of gas boundary layer in x direction
- Ud particle (solid or liquid) velocity at infinity
- U₀ velocity at outer edge of liquid film
- Us velocity at edge of gas boundary layer
- U_{∞} velocity of gas at infinity
- u' nonsteady velocity disturbance in x direction
- v' nonsteady velocity disturbance in y direction
- w' nonsteady velocity disturbance in z direction
- x coordinate along the interface between the liquid film and the gas boundary layer
- y coordinate normal to interface and measured from interface
- Y $\left(\frac{\delta}{R}\right)^2 \frac{Re}{2}$, dimensionless gas boundary-layer thickness
- α difference between arithmetic mean value and observed value of droplet population
- β 1 $\frac{U_0}{U_c}$, dimensionless velocity ratio
- δ gas boundary-layer thickness
- δ_{L} liquid boundary layer thickness
- $\delta^{\mbox{\scriptsize 18}}$ gas boundary-layer displacement thickness defined by Equation (2.4)
- ε intensity of turbulence
- η Y/ δ , dimensionless coordinate normal to the surface (interface)
- θ gas boundary-layer momentum thickness defined by Equation (2.5)
- λ dimensionless parameter for laminar flow
- μ dynamic viscosity of gas

NOMENCLATURE (contd.)

- ν kinematic viscosity of gas
- ρ density of gas
- ρ_{∞} density of gas at infinity
- σ standard deviation defined by Equation (4.2)
- τ₀ shear stress at liquid-gas interface
- x/R, dimensionless coordinate along the surface (interface)

CHAPTER I

INTRODUCTION

1.1 General Discussion and Purpose

One of the first examples of artificially created two-phase flow for the purpose of significantly increasing the attainable levels of surface heat-transfer rates was accomplished in the nuclear power field by addition of solid particles, such as graphite dust, to the coolant flow (1). Following this Elperin 1961 (2) reported in the Russian literature that, by the addition of a small amount of water in droplet form to the coolant air, it was possible to increase the surface heat-transfer rate by an order of magnitude in flow across a bundle of tubes.

Until Elperin published his paper on two-phase flow the major emphasis was the investigation of such flows in open and closed conduits. One of the first major contributions in the field of two-phase flow was by Martinelli et al. in 1941 (3), which was superseded by a Lockhart and Martinelli article in 1949 (4). These publications attempted to develop a procedure for the calculation of pressure loss in pipes for each of the four possible modes of flow:

- 1. Liquid and gas in turbulent flow.
- 2. Liquid in laminar flow and gas in turbulent flow.
- 3. Liquid in turbulent flow and gas in laminar flow.
- 4. Both liquid and gas in laminar flow.

Later McManus 1956 (5) made an extensive experimental investigation of the flow properties for a two-phase (air-water) flow in circular tubes. Here pipe flow in horizontal flow and vertical up-flow and down-flow configurations were considered. The investigation considered a range of from one-hundred-per cent air to one-hundred-per cent water for each pipe configuration.

The purpose of the present study is to investigate boundary layers which are developed on a circular cylinder when subjected to transverse flow of a two-phase mixture. The two-phase mixture is to be composed of air as the primary fluid stream, which is conveying a small amount of liquid (water) in droplet form.

The two-phase mixture will develop on the leading surface of the cylinder surrounding the stagnation point two hydrodynamic boundary layers and, for the case of a heated or cooled cylinder, two thermodynamic boundary layers. These boundary layers are composed first of a liquid film which wets the cylinder, and overlaying this film (boundary layer) will be a two-phase mixture boundary layer. This assumes that water droplets will flow in the gas boundary layer, so that it is in fact a two-phase boundary layer. In general, there will also be a thermal boundary layer within the liquid boundary layer and one within the gas (two-phase) boundary layer, possibly extending beyond the hydrodynamic boundary layer into the free stream. This makes a possible total of four boundary layers, two hydrodynamic and two thermal.

For the case of transverse flow over a cylinder the curved surface will provide the necessary conditions for the development of a pressure gradient in the flow direction. This gradient for the case

of low-speed flow will first be negative and later be positive. One would assume that it is possible for boundary-layer separation to occur in the region of the positive pressure gradient. This indeed takes place, and as a result of this separation the local heat-transfer rate is affected. The region of flow in the neighborhood of the separation point is the major subject of this investigation.

The present investigation was divided into three distinct parts:

First, an analytical investigation of the boundary layer was developed, as presented in Chapter II. Two flow models were considered, both utilizing numerical procedures for their solutions. Chapter V presents the numerical procedures and the computer programs for the two models. The results of the analytical investigations are given in Chapter VI. The second part of the investigation was the collection of the required experimental data for the above computer solutions. Chapter III presents a description of the apparatus, and Chapter IV presents the experimental procedure, including a description of the technique developed for the measurement of the pressure profile around the test cylinder. The third segment of the investigation was the experimental determination of the boundary-layer separation point. The system developed for this observation is presented in Chapter IV, and the results are given in Chapter VI.

Discussion of the results is given in Chapter VII. Included there are also conclusions and recommendations for further research.

1.2 Some Theories of Boundary-Layer Behavior

in Two-Phase Flow

A brief history of the development of some of the boundary-layer theories for two-phase flow will be reviewed. In order to keep the history brief only those articles pertaining to gas-liquid droplet and gas-solid particle flow will be reviewed.

Chiu 1962 (6), assuming laminar flow, made an analysis for the case of two-phase (gas-solid particle) flow over a flat plate. Two salient features of the analysis may reflect similar situations for the problems at hand.

The first was the assumption of laminar two-phase flow. Here a gas flow which initially is assumed laminar will remain laminar, providing the solid particle Reynolds number remains in the neighborhood of unity. The mechanism which would cause the flow field to become turbulent was the wake produced by the particle. For this analysis the solid particle Reynolds number was determined by the expression

$$Re_{d} = \frac{d(U_{\infty} - U_{d})}{v} \tag{1.1}$$

where d is the diameter of the particle, U_{∞} - $U_{\rm d}$ the velocity difference between the gas and the particle at infinity and ν the gas kinematic viscosity. It should be observed that a velocity difference of ten feet per second would limit the particle diameter to a few microns. This places a rather severe constraint on the system, as in most practical cases the liquid droplet diameter would be much greater than a few microns. In fact the particle momentum must be sufficiently

high in order that the particle may cross the gas streamlines and impinge upon the cylinder.

The second item of importance was the assumption that the solid particles did not contribute to the pressure of the system. Thus, the system pressure was equated to the partial pressure of the gas. For the case of small mass ratios of water to total mass flow, negligible blockage of the tunnel may be assumed.

Tribus 1952 (7) made an analysis of the trajectories of water drops around streamlined bodies. Here the investigation was concerned with the icing of surfaces. Two significant conclusions were made. First, the liquid catch rate is strongly controlled by the droplet size. The larger drops would cross the gas stream lines and impinge on the cylinder, while the smaller drops are deflected by the gas streamlines and may flow around the cylinder without making contact. The second conclusion was that only the section of the cylinder near the stagnation point was wetted by the drops. The included angle of the wetted surface is a function of droplet size. This analysis would indicate that one should explore those systems that provide large droplets and relatively low gas stream velocities, if the objective is to increase the level of heat-transfer rate.

Tifford 1964 (8) made an analysis of two-phase flow (gas-liquid spray) for the case of flow over a flat plate. Again no pressure gradient existed, and flow separation could not take place. Because of the assumptions that were made, the results only predicted that the heat-transfer rate and wall shearing stress could be maximized. Thus, for given free-stream single-phase flow conditions there exists an optimum liquid spray rate. Here it was assumed that the flat plate

was isothermal, and that the velocity and temperature at the outer edge of the liquid film remained constant.

Goldstein, Yang and Clark 1965 (9) made an analytical investigation of the liquid film formed on a cylinder in two-phase flow. This analysis was based on the assumption that the flow remains laminar. The analysis also assumed that the cylinder liquid catch rate was controlled by the particle trajectory. The trajectory analysis followed the analysis as outlined by Tribus (7). In order to solve the problem, the pressure on the cylinder was assumed to be the same as that developed by single-phase flow (given by $U_S = 2U_\infty \sin \phi$). The shear stress between the liquid film and the gas boundary layer was assumed to be the same as that produced by single-phase flow over a dry cylinder. Further, the analysis only gave results for that part of the cylinder where the potential flow was still accelerating. Thus, only a negative pressure gradient was experienced. This condition did not yield a separation point.

One should note that all analyses performed to date have assumed the flow to be laminar, providing a more accessible route to a solution. However, an assumption of turbulent flow is well worth considering. There are several basic reasons for assuming turbulent flow. First, Kestin and Maeder (10) found that the rate of local heat transfer in the region of the forward stagnation point may be doubled by increasing the free-stream turbulence intensity ϵ , defined by

$$\varepsilon = \frac{\sqrt{\frac{1}{3} (u'^2 + v'^2 + w'^2)}}{U_{\infty}}$$
 (1.2)

where u', v' and w' are nonsteady velocity disturbances in the flow field. This is especially true in single-phase flow if the initial intensity is less than one per cent. Another reason for considering turbulent flow is that separation of the boundary layer is changed in turbulent flow conditions. As an example, consider a flow Reynolds number of 1×10^4 . For laminar flow over a cylinder the separation point is approximately 80 degrees from the stagnation point. For turbulent flow and the same Reynolds number, the separation would shift behind the 90 degree point.

CHAPTER II

ANALYSIS

2.1 General Description and Objective

Let us restate the purpose of the investigation and then formulate two analytical models. The objective of this study is to investigate the transverse flow of a two-phase (air-water spray) mixture over a right circular cylinder for a range of gas Reynolds numbers of 1 × 10⁴ to 2 × 10⁵ and mass ratios of water to air less than 10 per cent. For single-phase flow this would be in the regime of subcritical flow and the phenomenon of flow separation would occur with separation forward of the 90-degree point. The particular area of investigation is the region of the flow field where the boundary-layer separates from the cylinder. A preliminary experimental investigation had established the fact that the boundary layer does indeed separate.

For both analytical models, the flow at a great distance upstream from the test specimen is assumed to be a homogeneous mixture of saturated air and water droplets. Both the velocity of the air and the velocity of the water droplets are assumed to be known, while only average droplet size distribution is obtainable.

Martinelli (3) classified two-phase flow in pipes into four possible modes of flow:

- 1. Liquid and gas in turbulent flow.
- 2. Liquid in laminar flow and gas in turbulent flow.

- 3. Liquid in turbulent flow and gas in laminar flow.
- 4. Both liquid and gas in laminar flow.

He considered two-phase pipe-flow regimes where the conduit can be divided into two distinct regions, the first region conveying liquid and the second gas. Separating the regions in a gas-liquid interface whose average surface is parallel to the direction of flow. He found for the case of pipe flow that the first mode was realized only with large liquid to gas mass ratios, and that third mode was impossible to achieve and the fourth possible only for the flow in a capillary tube. These conditions might be thought equally possible to exist for the external flow problem. With this as a guide the following models are presented: Section 2.2 presents the laminar gas boundary-layer model for both liquid and gas in laminar flow. Section 2.3 presents the gas boundary-layer model for liquid in laminar flow and gas in turbulent flow.

2.2 Gas Boundary-Layer Model for Both Liquid and

Gas in Laminar Flow

This mode of flow assumes that both the liquid film on the cylinder and the gas boundary layer on top of the liquid film are in laminar flow. This is a reasonable assumption when the droplet Reynolds number is in the neighborhood of unity, according to the results of Chiu (6) quoted in Section 1.2. We assume that the gas boundary layer will not separate from the cylinder before the liquid film separates, since preliminary experimental evidence indicates a single separation point.

For the complete laminar flow system the following assumptions are imposed on the solution:

- 1. The flow is taken to be two-dimensional, and laminar within the boundary layer.
- 2. On top of the liquid film a gas boundary layer forms, which joins the flow in the liquid film to the external flow field. The usual boundary-layer assumptions are assumed to apply in this region.
- 3. Surface-tension effects on the surface of the liquid film are neglected.
- 4. The effects of compressibility and of heat generated by dissipation can be ignored for the case of low-speed flow.
- 5. For that region of flow over a right circular cylinder, up to and including the point in the flow field where separation takes place, the effects of gravity are assumed negligible. This assumption is supported by the results, reported in Appendix A, of a study by the author of horizontal flow over a vertical cylinder. When dye was injected into the boundary layer, the mean flow of the dye followed a horizontal path up to the point of separation, indicating that the gravitational force was negligible in comparison to the other forces acting on the boundary layer.
- 6. All fluid properties will be taken as constant; e.g., the liquid and gas are separately assumed incompressible.
 - 7. No appreciable vaporization occurs.
- 8. Under certain conditions waves may be formed on the surface of the liquid film, and splashing or bouncing may occur at this surface. These effects are neglected.

9. The envelope formed by the liquid film which is developed on the cylinder produces essentially a circular cylindrical surface.

With these assumptions, the von Kármán integral equation and associated boundary conditions are formulated for the outer gas boundary layer from the elementary volume shown in Figure 1:

$$\rho \frac{d}{dx} \left(\int_{0}^{\ell} (U_{S}-U) U dy \right) - \rho \frac{dU_{S}}{dx} \int_{0}^{\ell} U dy = \tau_{0} + \ell \frac{dP}{dx}$$
 (2.1)

$$U = U_0$$
 at $y = 0$

$$U = U_s$$
 at $y = \ell$

where U_S and U are velocity components, x is the coordinate along the interface between the liquid film and the gas boundary layer while y is the coordinate normal to the interface and measured from the interface, ρ is the gas density, τ_0 the shear stress at the liquid-gas interface and ℓ is the constant distance from the liquid-gas interface to a layer arbitrarily selected in the external flow. From the well-known Prandtl boundary layer analysis, "there is negligible variation in pressure through the thickness of the boundary layer for regions not near the stagnation point." Hence the Bernoulli Equation can be put into the form

$$\frac{dP}{dx} = -\rho U_S \frac{dU_S}{dx}$$
 (2.2)

Substituting Equation (2.2) into Equation (2.1) results in

$$\rho \frac{d}{dx} \left(\int_0^{\ell} (U_s - U) U dy \right) + \rho \frac{dU_s}{dx} \int_0^{\ell} (U_s - U) dy = \tau_0$$
 (2.3)

The boundary-layer thickness δ is defined as the distance measured from the liquid-gas interface to the point where the external velocity prevails. This point is reached asymptotically. On the other hand, a practical definition of δ is that distance from the liquid-gas interface to a point where the velocity differs by one per cent from the external velocity. The integration limits in Equation (2.3) may now be changed, since in the range $\delta < y < \ell$ the term U_S -U in the integrands of the left side of the equation is equal to zero. The equation can further be written in a simpler form when the following definitions are used for the boundary layer <u>displacement thickness</u> δ * and the <u>momentum</u> thickness θ

$$\delta * = \int_0^{\delta} (1 - \frac{U}{U_s}) dy$$
 (2.4)

$$\theta = \int_0^{\delta} (1 - \frac{U}{U_S}) \frac{U}{U_S} dy \qquad (2.5)$$

First changing the integration limits of Equation (2.3) to run from 0 to δ and then utilizing the definitions of Equations (2.4) and (2.5) results in

$$\rho \frac{d}{dx} (U_s^2 \theta) + \rho U_s \delta^* \frac{dU_s}{dx} = \tau_0$$
 (2.6)

Equation (2.6) is a form of von Kármán's integral equation. The only new feature of the present treatment appears in the boundary conditions used in the evaluation of δ * and θ . Here, a boundary condition is no longer given by U=0 at y=0 but rather $U=U_0$ at y=0. Further it is not expected that δ * and θ would have the same typical values as found in single-phase flow.

The information desired from the above equation will, to some extent, dictate the most desirable method of solution and hence the form the equation takes on for this analysis. The major item of information of current interest is an estimate of the boundary layer separation point, and in particular the role of the film velocity $\rm U_0$ at y = 0 in altering the separation point. Curle 1962 (11) published a comparison of the approximate methods of solution for the incompressible laminar boundary-layer equations. Here one finds that any of the standard methods of solution provides an estimate of the separation point. Further, if detailed distribution of skin-friction is sought, any method is satisfactory, with the qualification that for flow which starts from a stagnation point rather than a sharp leading edge, the Stratford-Curle method is only used downstream of the pressure minimum.

The solution of Equation (2.6) requires knowledge of the velocity distribution in the gas boundary layer in order to evaluate δ * and θ . A velocity distribution as outlined by Pohlhausen (12) and cited by Curle (11) is assumed to exist. The velocity dependence on y at any given x is assumed to be of the form

$$\frac{U}{U_S} = f(\eta) \tag{2.7}$$

Now the boundary conditions to be satisfied by the local velocity $\ensuremath{\mathtt{U}}$ are

$$U = U_0(x), \rho U \frac{\partial U}{\partial x} = -\frac{\partial P}{\partial x} + \mu \left(\frac{\partial^2 U}{\partial x^2} + \frac{\partial^2 U}{\partial y^2} \right) \quad \text{at } y = 0$$
 (2.8)

and

$$U-U_S = 0$$
, $\frac{\partial U}{\partial y} = 0$, $\frac{\partial^2 U}{\partial y^2} = 0$ at $y = \delta$ (2.9)

The second boundary condition of Equation (2.8) is the Navier-Stokes equation of motion in the x direction evaluated at y equal zero (v and w are assumed zero at this point). The second boundary condition of Equation (2.9) is a result of vanishing shear stress at y equal δ and the third condition is arbitrary as in Pohlhausen (12). Since we have five independent boundary conditions, an approximation to the velocity profile may be assumed as a polynomial in η with five coefficients which are functions of x that can be determined from the boundary conditions:

$$\frac{U}{U_S} = a + b\eta + c\eta^2 + d\eta^3 + e\eta^4$$
 (2.10)

As will be seen in the discussion of initial conditions following Equation (2.15), the solution is obtained in two parts: a small neighborhood of the stagnation point where the flow is assumed to be the same as single-phase flow and the region outside this neighborhood. For analytical convenience $\rm U_0$ will be assumed independent of x in each part of the solution with a discontinuity between the two. As may be seen in Figures 38 to 40 there is actually a considerable variation in the experimentally observed values of $\rm U_0$. But it is found that the solution of Equation (2.15) is relatively insensitive to variations in $\rm U_0$.

The second boundary condition of Equation (2.8) and the Bernoulli Equation (2.2) then yield for the coefficient c of Equation (2.10)

$$c = -\frac{1}{2} \frac{\rho \delta^2}{\mu} \frac{dU_s}{dx}$$

$$= -\frac{1}{2} \lambda$$
(2.11)

where λ is a dimensionless parameter defined by

$$\lambda = \frac{\delta^2}{v} \frac{dU_s}{dx}$$
 (2.12)

After some algebra and utilizing the definition of Equation (2.12) one may obtain the velocity profile in the form

$$\frac{U}{U_{S}} = \frac{U_{0}}{U_{S}} + 2 \left(1 - \frac{U_{0}}{U_{S}} + \frac{\lambda}{12}\right) \eta - \frac{\lambda}{2} \eta^{2} + 2 \left(\frac{U_{0}}{U_{S}} - 1 + \frac{\lambda}{4}\right) \eta^{3} + \left(1 - \frac{U_{0}}{U_{S}} - \frac{\lambda}{6}\right) \eta^{4}$$
 (2.13)

Setting $1 - \frac{U_0}{U_s} = \beta$ one obtains

$$\frac{U}{U_{S}} = 1 - \beta + (\frac{\lambda}{6} + 2\beta) \eta - \frac{\lambda}{2} \eta^{2} + (\frac{\lambda}{2} - 2\beta) \eta^{3} + (\beta - \frac{\lambda}{6}) \eta^{4}$$
 (2.14)

It may be observed that the new parameter β characterizes the change in velocity across the gas boundary layer. Substituting Equation (2.14) into Equation (2.6), one obtains, after some algebra, the boundary-layer equation in the form

$$\frac{dY}{d\Phi} = \frac{0.8U_{\infty}}{U_{S}} \left[\frac{9072 + (295.2\beta - 1965.6)\lambda + (80.4 - 33\beta + 4.8 \frac{U_{S}U_{S}''}{(U_{S}')^{2}})\lambda^{2} + (1 + \frac{U_{S}U_{S}''}{(U_{S}')^{2}})\lambda^{3}}{544.32\beta - 331.2\beta^{2} + (36.6\beta - 45.36)\lambda - \lambda^{2}} \right]$$
(2.15)

where

$$Y = \left(\frac{\delta}{R}\right)^2 \frac{Re}{2}$$

$$\Phi = \frac{\mathbf{x}}{R}$$

 $Re = 2RU_{\infty}/v$

 U_S^{\prime} and $U_S^{\prime\prime}$ are derivatives with respect to x

It should be observed that for the case of flow over a dry cylinder U_0 vanishes and β is equal to unity. For this case Equation (2.15) reduces to the Pohlhausen Equation (12).

The initial value of Y at Φ = 0 is unknown, but may be determined as follows from the requirement that the right-hand side of Equation (2.15) remain finite as $\Phi \to 0$, where U_S and U_0 are zero, and the assumption that in a small neighborhood of the stagnation point the flow is the same as in single-phase flow so that β = 1 in this neighborhood. For dY/d Φ to be finite at the stagnation point the numerator must also vanish. The value of λ to force the numerator to vanish when U_S = 0 and β = 1 is obtained from the expression

$$9072 - 1670.4\lambda + 47.4\lambda^2 + \lambda^3 = 0$$
 (2.16)

For a physical solution to the problem, λ must be real and positive. The root which satisfies this condition is

$$\lambda = 7.052 \tag{2.17}$$

This then is the initial value of λ , which determines the initial value of Y as follows. Returning to the definition of λ and Y, we may write

$$Y = \left(\frac{\delta}{R}\right) \frac{Re}{2}$$

$$\lambda = \frac{\delta^2}{V} \frac{dU_S}{dx} = Y \frac{d}{dx} \frac{U_S}{dx}$$
(2.18)

Under the assumption of potential flow outside the boundary layer $U_{\rm S}$ is given by the expression

$$U_{S} = 2U_{\infty} \sin \Phi \qquad (2.19)$$

whence

$$\frac{d}{d\phi} \frac{U_{s}}{d\phi} = 2 \cos\phi \qquad (2.20)$$

Evaluating Equation (2.20) for Φ equal to zero and substituting the results into Equation (2.18) yields

$$\lambda = 2Y$$
or
 $Y = 3.526$
(2.21)

Equations (2.17) and (2.21) are now the initial conditions for Φ equal to zero. Two different procedures have been used to give U_S . The first procedure assumed that the external potential flow Equation (2.19) applies for all Φ , giving the required second derivative very accurately. The second procedure used a measured pressure profile

and calculated $U_{\rm S}$ from the Bernoulli Equation, requiring a second derivative from the numerical data, and did not successfully predict separation in the cases considered. For the studies of the effect of the choice of the constant $U_{\rm O}$ the first procedure was used.

If we assume, as in single-phase flow, that separation will take place when the shear stress at the interface vanishes, we may write from Equation (2.14)

$$\tau_0 = \mu \left. \frac{\partial U}{\partial y} \right|_{y=0} = \frac{\mu}{\delta} \left(\frac{\lambda}{6} + 2\beta \right) = 0 \tag{2.22}$$

or

$$\lambda = -12\beta = -12 \left(1 - \frac{U_0}{U_s}\right)$$
 (2.23)

at the separation point. (A more appropriate criterion might be the vanishing of the shear stress at the solid surface.)

The solution of Equation (2.15) to determine that value of Φ for which λ satisfies Equation (2.23) requires values of U_S and its first two derivatives.

All that remains is to patch the initial conditions, the value of U_0 and the flow properties at the edge of the boundary layer together. For this purpose the single-phase flow pattern is assumed to exist with U_0 = 0 and β = 1 in a small but finite neighborhood Φ < Φ_0 of the stagnation point. The neighborhood must be large enough that β will be positive for any values of U_0 used outside of the neighborhood. Solutions were obtained for the three cases of Φ_0 equal to 0.1, 0.2 and 0.3 radians in order to determine whether the solution

was sensitive to the choice of Φ_0 . It was found relatively insensitive in this range, and Φ_0 = 0.1 radian was used for the remainder of the investigation. Five solutions were then obtained with the constant value of U_0 in the region $\Phi > \Phi_0$ chosen to be 1, 2, 3, 4 or 5 per cent of U_∞ to test the effect of variations in U_0 on the location of the separation point. As the results given in Section 6.4 show, the separation point is quite insensitive to the value of U_0 chosen in the range considered. One now seeks values of Φ which would yield the location of the separation point for various values of U_0 . The results are presented in Section 6.4.

2.3 Turbulent Gas Boundary-Layer Model for Liquid in Laminar Flow and Gas in Turbulent Flow

The existence of a laminar gas boundary layer was based on the assumption that the droplet Reynolds number was of the order unity. This assumption required both a small droplet diameter and a small difference between the droplet and gas velocity. For the case of real processes this may be difficult to realize and thus Reynolds numbers outside the regime of Stokes flow (Schlichting (13), Figure 1.5) may occur. Under these conditions appreciable disturbances may be generated by the wake which is formed behind the droplet. From this an increased intensity of turbulence may be precipitated in the free stream.

The following assumptions are imposed on the solution of the turbulent gas boundary-layer model.

1. The gas boundary layer which joins the liquid film to the external flow is assumed turbulent.

- 2. Surface-tension effects on the surface of the liquid film are neglected.
- 3. The effects of compressibility and of heat generated by dissipation can be ignored.
- 4. The effects of gravity in the gas boundary layer are neglected.
 - 5. All fluid properties will be taken as constant.
 - 6. No appreciable vaporization occurs.
- 7. Under certain conditions waves may be formed on the liquid surface. Considering the case of a turbulent gas boundary-layer model it is assumed that such a phenomenon would only produce an increased intensity of turbulence.
- 8. The envelope formed by the liquid film produces essentially a cylindrical surface.
- 9. From the results of Section 2.2 given in Section 6.4 it was found that the presence of the velocity U_0 , which for that analysis of laminar flow was assumed constant, had little effect on the rate of growth of the boundary layer and the displacement of the separation point. It is assumed that U_0 will have negligible effect on the growth of the boundary layer and the location of the separation point for turbulent gas boundary layer. Under the limitations of these assumptions a turbulent gas boundary layer is investigated with the aid of a semi-empirical method to be discussed. The objective here is to investigate the relationship between the boundary-layer separation and parameters of the semi-empirical method.

From Schlichting the momentum integral equation for the turbulent model is obtained in the form

$$\frac{\tau_0}{\rho} = \frac{d}{dx} \left(U_s^2 \theta \right) + \delta * U_s \frac{dU_s}{dx}$$
 (2.24)

where δ^* and θ are defined by Equations (2.4) and (2.5) respectively. Equation (2.24) has the same form as Equation (2.6), since they apply to the laminar and turbulent boundary layer alike, as long as no statement is made concerning τ_0 . As in the case of laminar flow several methods exist for calculating the boundary-layer properties. The method best suited for a particular problem depends upon the information desired and the available experimental data. Currently the information pertaining to the separation point is desired.

For this problem we utilize an experimental pressure profile.

We also obtain a set of initial conditions by using the single-phase flow solution as in Section 2.2 for a neighborhood of the stagnation point. This would represent the minimum required information for a meaningful solution to Equation (2.24). Von Doenhoff and Tetervin (14) developed a method for the calculation of the turbulent boundary-layer characteristics, requiring as minimum information a set of initial conditions and the pressure profile. We assume that the method of calculation by von Doenhoff and Tetervin is adequate for this study.

A more detailed discussion of the methods of calculating the turbulent boundary-layer characteristics, which utilize either the momentum integral equation or the energy integral equation, can be found in the cited reference of Schlichting (13).

Von Doenhoff and Tetervin showed from analysis of experimental data that the boundary-layer profile was a function of a single parameter H (the ratio of the boundary-layer displacement thickness δ * to the

momentum thickness θ). They developed an empirical equation in terms of the rate of change of H

$$\theta \frac{dH}{dx} = e^{4.680(H-2.975)} \left[-\frac{\theta}{q} \frac{dq}{dx} \frac{2q}{\tau_0} - 2.035(H-1.286) \right]$$
 (2.25)

where q is the velocity pressure (q = $\frac{1}{2} \rho U_S^2$). Equation (2.24) can be put into a more convenient form for numerical calculations. The introduction of H and δ * into Equation (2.24) yields

$$\frac{\mathrm{d}\theta}{\mathrm{d}x} + \left(\frac{\mathrm{H}+2}{2}\right) \frac{\theta}{\mathrm{q}} \frac{\mathrm{d}q}{\mathrm{d}x} = \frac{\tau_0}{2\mathrm{q}} \tag{2.26}$$

Equation (2.25) and Equation (2.26) represent a system of semi-empirical equations for the turbulent boundary layer.

The shear stress is still unknown. In single-phase flow Squire and Young (15) have proposed the empirical formula

$$\frac{2q}{\tau_0} = \left[5.890 \log_{10} (4.075 \text{ Re}_{\theta})\right]^2$$
 (2.27)

where Re_{θ} is the Reynolds number based on the momentum thickness. In the absence of experimental data for two-phase flow, we tentatively assume that the same formula applies.

The turbulent boundary-layer properties can now be obtained from the simultaneous solution of Equations (2.25), (2.26) and (2.27). It should be observed that the empirical equation for dH/dx, Equation (2.25), and the momentum equation, Equation (2.26), represent a system of first-order differential equations, which can be solved numerically with a step-by-step calculation once the initial conditions

are known. The solution for the system of equations is completed once the separation point has been reached.

At this time a criterion for the establishment of the region of separation is required. In single-phase flow Gruschwitz (16) established a criterion that separation was imminent when H increased to a value of 1.85. Von Doenhoff and Tetervin found that single-phase flow separation would take place for the range of values of H between 1.8 and 2.6. For the first attempt at this analysis the range of values of H established by von Doenhoff and Tetervin was assumed adequate to establish the region of separation. In single-phase flow this range was not a large segment of the cylinder, since the rate of change of H with respect to x is large in the region near the separation point. Further, the separation point in turbulent flow is not well defined. As is reported in Section 6.4 it turns out that for the two-phase flows investigated experimentally separation occurs in the vicinity of H = 1.23, so that the single-phase flow criterion is not applicable.

For the case of two-phase flow systems, which are the gasliquid spray type, two models of the flow field have been considered. In these analyses a gas-liquid spray system is defined as that system where the gas is the primary fluid which is transporting a small amount of liquid in droplet form (mass ratio of liquid to gas less than 10 per cent).

The first model, Section 2.2, considered the liquid film to be laminar as well as the gas boundary layer. A model of the gas boundary layer was developed which permitted a finite velocity U_0 to prevail at the gas-liquid boundary layer interface. Two parameters λ and β

characterized the flow. The parameter λ , Equation (2.12), by virtue of being dependent on the pressure gradient assured one that separation would not take place in a region of a negative pressure gradient. The parameter β characterized the change in velocity across the gas boundary layer. The objective of the analysis was to determine, under the limitation that $dU_0/dx=0$, what effect U_0 had on the displacement of the separation point from that found in single-phase flow for the same gas Reynolds number.

The second model which represents the case of turbulent flow in the gas boundary layer was based on a semi-empirical model obtained from the literature. This was made possible by the assumption that U_0 did not affect the location of the separation point. Here, the objective of the investigation was to determine, under a condition of turbulent flow and assuming that U_0 may be neglected, if calculated values of H would predict separation.

The above two analytical models have as their common objective the prediction of the separation point for the case of two-phase flow over a circular cylinder. It would not be expected that both models would predict the same results, since they represent different types of flow structure. At the same time both models should provide a better understanding of the flow phenomenon. The results of the two analytical models are compared with each other and with experimental results in Section 6.5.

CHAPTER III

EXPERIMENTAL METHODS AND APPARATUS

3.1 General Description and Objective

The basic apparatus for the present investigation was developed specifically for this study. A schematic drawing of the apparatus is shown in Figure 2, and a series of general views of the test setup are shown in Figures 3 and 4.

The test apparatus is essentially a low-speed wind tunnel (0 to 185 feet per second), whose test section is located in a vertical position upstream of the fan. Both the air and the water spray pass vertically downward through the test section into the fan and on leaving the fan are exhausted to the atmosphere. This open wind tunnel is composed of the following components.

- 1. Inlet screens
- 2. Water spray assembly
- 3. Inlet diffuser
- 4. Test section and test specimen
- 5. By-pass spray assembly
- 6. Fan
- 7. Butterfly valve
- 8. Exhaust diffuser
- 9. Control panel

The objective of this experimental investigation is to perform the necessary diagnostic studies of the flow field, as well as perform visual, photographic and physical measurements of the boundary layers formed on a right circular cylinder. The results will be utilized to predict the behavior of the boundary layers in the region of the separation point.

3.2 The Quality of the Test Apparatus

Before passing to a discussion of components of the test apparatus, let us first consider the quality. For this evaluation we return to consideration of single-phase flow. The reason for this is to make it possible to compare performance data for this apparatus in single-phase flow with that which is published in the literature. Schmidt and Wenner (17) published the results of a comprehensive investigation for transverse flow of air over a circular cylinder under laminar flow conditions. Their paper included a plot of the average Nusselt number $\bar{N}u$ versus the flow Reynolds number,

$$\bar{N}u = \frac{\bar{h}D}{k}$$
 (3.1)

where

$$\bar{h} = \frac{Q}{A} \frac{1}{T_{W} - T_{\infty}}$$
 (3.2)

is the average heat transfer coefficient, Q/A the heat transfer per unit time per unit area, k the thermal conductivity, T_W the wall temperature and T_∞ the stream temperature at infinity. Also published was a graph of pressure coefficient Cp versus Φ measured from the stagnation point, for various Reynolds numbers. By definition C_P has the form

$$C_{P} = \frac{P - P_{S}}{Q_{\infty}} \tag{3.3}$$

where $P_{\mathbf{S}}$ is static pressure at infinity, q_{∞} velocity pressure at infinity and P local pressure.

Kestin (10) found that an increased turbulence level affected not only the separation point by shifting it downstream but also materially increased the overall heat transfer rate. For cases where results do not agree with those of Schmidt and Wenner (17) one may conclude that the intensity of turbulence is different than their value.

The pressure in the wake behind the cylinder is an index to tunnel blockage. Since the flow Reynolds number is directly proportional to the cylinder diameter, one would want to select the largest possible cylinder diameter as an aid to increasing the flow Reynolds number in order to investigate as wide a range of Reynolds numbers as possible.

The results of this tunnel evaluation experimental data and the conclusions drawn from a comparison of this data with that found in the cited literature are given in Section 6.2.

3.3 The Inlet Screens and Diffuser

The inlet screens and diffuser were salvaged from an abandoned low-turbulence wind tunnel. The screens were made in two sections, each composed of a 20-mesh hardware cloth covered with cheese cloth. The square inlet diffuser has a 30×30-inch inlet and reduces to a 10×10-inch outlet. This, it should be noted, determined the basic cross-sectional area of the test section.

3.4 The Water-Spray System

A full-cone impactor nozzle, number 2116 manufactured by the Spray Engineering Company, was employed to supply the water spray for this study. The nozzle was located on the centerline of the diffuser, between inlet screens and diffuser inlet, and directed toward the geometric center of the test specimen. Its installation permitted rotation in a plane including the axis of the test cylinder and also in the plane normal to the cylinder axis.

3.5 The Wind-Tunnel Test Section

The wind-tunnel test section was made of plexiglass and had internal cross-sectional dimensions of 10×10 inches. A series of .005-inch diameter thermocouple wires were installed in the test section to provide temperature histories along the test section.

The test cylinder was located 20 inches downstream from test section inlet. Distance was selected after analysis of velocity profiles taken with a standard Pitot tube at various stations along the test section revealed a variation of less than one per cent in free-stream velocity at this station. The test section wall boundary layer at this station was approximately one-half inch thick.

3.6 The Wind-Tunnel Fan and By-Pass Spray Nozzle Assembly

The wind tunnel was driven by a one-hundred-horse-power motor and two-stage fan assembly. Since performance characteristics of the fan strongly depend on the condition of air at the fan inlet, it was found that these conditions must remain constant if one desired to maintain the same test-section gas Reynolds number for both single and two-phase flow. This was accomplished by the installation of a

secondary spray system located downstream of the test section,
providing an air-water mixture to the fan for those runs when singlephase flow conditions were desired at the test section.

3.7 Butterfly Valve and Outlet Diffuser

A butterfly valve was located in the fan discharge duct. This permitted the test section velocity to be varied from 0 to 185 feet per second. The air-water mixture next passed through a straight duct (diffuser) and then exhausted to the atmosphere outside the laboratory.

3.8 Summary of Test Facility

In operation the test facility had both desirable and undesirable qualities. The major objection to the system was an excessive noise level of the apparatus. Some vibrations of the test section were also observed. On the plus side there was a condition such that the static pressure, in the test section and all duct work up to the fan, was below atmospheric pressure. Under this condition all leakage including water was inboard.

3.9 The Test Specimen and Control Panel

The calibration of the wind tunnel was based on the analysis of data collected for a right circular cylinder in single-phase flow.

The average heat transfer coefficient and the pressure coefficient for the cylinder were analyzed.

The determination of the average heat-transfer coefficient required a test cylinder capable of being maintained at some constant wall temperature above the free-stream temperature. A 1.5-inch

diameter test cylinder was fabricated; it is shown in schematic form in Figure 5, and in a photograph in Figure 6. The cylinder is composed of five basic sections: a copper test section, two copper guard sections and two bakelite end sections. The test section was provided with six heating elements on 60-degree centers, six thermocouples similarly spaced, and three pressure taps. Each of the two copper guard sections were also provided with six heating elements and equally spaced thermocouples. The two bakelite end sections serve a dual purpose: first, to reduce the conduction of heat to the tunnel walls; second, to provide facilities for mounting the test cylinder in the wind tunnel.

The maintenance of a constant wall temperature for the test cylinder was accomplished by providing each heater with a regulated power supply to control the power input to each of the six heaters in the test specimen and the twelve heaters in the two guard sections. The regulated power supply consisted of a variac for each heater and a master variac for each of the three cylinder sections. A 24-point recording potentiometer was utilized to measure the output of the 18 thermocouples. The power input to each of the 18 heaters was measured by a wattmeter through a switching arrangement. Pressure profile for the cylinder in the case of single phase flow was determined by rotating the cylinder through two-degree increments and observing pressure on an inclined manometer.

For the case of single-phase forced flow, Schlichting (13) shows that under the assumption of incompressible flow and constant properties (i.e., properties independent of temperature) the velocity field is independent of the temperature field. This assumption was

utilized in the analysis by Tifford (8), and in that by Goldstein,
Yang and Clark (9). For the case where the free-stream Mach number is
equal to or less than 0.1 and the difference between the cylinder wall
temperature and the free-stream temperature is less than 50 degrees F,
the properties of the hydrodynamic boundary layer can, without serious
error, be determined in the absence of a temperature gradient. Under
this assumption a second copper cylinder, Figure 6 was fabricated.
This test cylinder was made from a section of copper tubing with
mounting sections fitted at each end of the tube. The cylinder was
provided with six pressure taps and provisions to rotate the cylinder
in order to make a complete pressure survey. Grid lines were
inscribed into the cylinder surface and filled with epoxy. These
lines were located every five degrees and utilized in the measurements
of the liquid film velocity.

CHAPTER IV

EXPERIMENTAL PROCEDURE

4.1 Determination of the Pressure Profile

Fundamental to all experimental boundary-layer investigation is a detailed knowledge of the pressure gradient along the surface in question. This not only represents the key to the study, but also the minimum information that one must gather for a meaningful boundary-layer investigation in the absence of heat transfer.

The pressure impressed on the two hydrodynamic boundary layers is assumed constant through these boundary layers. This is equivalent to the assumption of zero pressure gradient normal to the surface.

Thus, only the pressure gradient along the surface is to be determined. Introduction of the information from this pressure profile into the Bernoulli Equation yields the velocity at the location where the boundary layer joins the external flow field.

For the required pressure measurements a system of pressure taps 0.025 inches in diameter and associated pressure lines were selected. This tap size is approximately the size of a number 71 drill, and represented two degrees of cylinder arc on the 1.5-inch diameter test cylinder. This now places a limit on both the concept of local pressure measurements and the arc length between pressure measurements. In order to develop the pressure profile the cylinder was rotated through two or five degree increments. The pressure was measured

every two degrees of cylinder rotation in the region where the boundary layer separation takes place, and at five-degree intervals for rest of the profile.

For the case of single-phase flow the pressure determination would present no challenge, and data would be collected with the use of standard manometers or electrical pressure transducers, depending on the particular application.

For the case of two-phase flow a search of the literature (References 18, 19 and 20) revealed two basic approaches to the measurement of pressure drop in pipe flow.

The first system was one where the transducer lines were filled with the same liquid as that flowing in the duct. This was successful for those cases where the flowing film thickness in the pipe was approximately an order of magnitude larger than the pressure tap diameter. This system, as one would anticipate, would not function adequately for the external flow problem, since the film thickness of the boundary layer was of the same order of magnitude or less than the pressure tap diameter.

The second method was found to be more promising; it again utilized liquid-filled transducer lines, but employed a technique whereby the lines were externally pressurized. This caused a small amount of secondary fluid to be injected through the pressure tap into the pipe. Those cases in which the injected liquid was a small fraction of the total liquid flow proved acceptable. This second system was investigated and found to be a practical method of pressure measurement along the surface of the cylinder.

A schematic diagram and a picture of the pressure-measuring system is shown in Figures 7 and 8. The system is composed of two essential parts. First a standard differential pressure transducer with a range of * 0.7 psi was employed; this transducer was a straingage type requiring a 14-volt source. The transducer output was measured with a portable potentiometer. The second essential item of the system was a 0.030 * 0.0001 inch internal diameter capillary tube 34 inches long, used to meter the secondary fluid being injected into the boundary layer. In order to make the system function two reservoirs were employed. One supplied the distilled water to the capillary tube, while the other was used to flush the system with distilled water to remove any air bubbles. A wetting agent was added to the distilled water to yield a mixture of approximately one part in ten thousand.

In order to test the system the pressure profile for single-phase flow was obtained. If one is successful in obtaining an acceptable pressure profile by injecting water (whose density is three orders of magnitude greater than air) into an air boundary layer, one would expect favorable results for the case of two-phase flow. This should be a conservative approximation to the problem, since less error would be anticipated from the injection of water into a water boundary layer. The results of pressure measurements taken in single-phase flow and compared to data collected by conventional methods are given in Section 6.3.

The development of the system required the solution of the following problems.

- 1. The control of the rate of water injection.
- 2. Determination of the optimum rate of water injection.
- 3. Elimination of hysteresis effects.

A capillary tube was selected to meter the injected water for the injection rate in the range of one to one and a half milliliters of water per minute. This gave an injection velocity less than 0.1 feet per second normal to the surface and a pressure drop through the pressure tap of 0.01 inches of water. A suitable injection rate was determined experimentally by observing pressure at the stagnation point, and at a location ninety degrees from this point, where the gravity vector was first normal to the surface and then parallel to the surface. For the case of single-phase flow, insufficient water yielded pressure measurements less than the conventionally observed values, while large rates of water injection yielded excess pressure measurements. It is believed that insufficient water injection permitted the pressure tap to be exposed to the primary fluid flow, so that capillary action at the pressure tap produced a reduction in pressure at the transducer. In the case of excess fluid injection, a disturbance to the external flow field was experienced to an extent that the gas velocity was reduced, with a corresponding pressure rise.

In order to maintain a constant water injection rate the differential pressure across the capillary tube must remain constant. In order to accomplish this a preliminary survey was made, providing an approximate pressure profile. The reservoir for the capillary tube was then raised or lowered in order to maintain a constant differential pressure across the capillary tube.

It was observed that the capillary tube had a memory of past pressure excursions impressed upon it. This was erased by installing a shutoff valve between the pressure tap and the capillary tube. After each measurement the valve was closed to bring the fluid to rest in the entire system. Next, a small amount of fluid from the secondary reservoir was injected into the boundary layer in order to replace the liquid at the pressure tap, since it was observed that during the shutoff period the fluid was eroded. Figure 9 is the calibration curve for the pressure transducer.

One is now ready to measure the pressure along the surface of the cylinder. Since the cylinder is in a horizontal position, a correction must be made for the relative height between the pressure transducer and the pressure tap when the cylinder is rotated. This correction is a simple function of the cosine of the angle of rotation from the stagnation point, the radius of the cylinder, and the calibration of the pressure transducer. Figure 10 is the graph employed for this required correction.

4.2 Determination of the Water Droplet Velocity and Droplet-Size Distribution

For a first-order approximation to the problem at hand one could assume that the difference between the gas velocity and droplet velocity approaches zero at a great distance upstream from the test section. For this case the droplet Reynolds number would be of the order of unity, which was a basic assumption for the laminar flow model. The difference between gas velocity and liquid velocity and also the droplet diameter are required for the droplet Reynolds

number. These values were determined experimentally by a high-speed photographic system capable of taking pictures up to 7000 frames per second and of so tagging the pictures that the local film speed may be determined.

The droplet velocity used a grid of wires parallel to the cylinder axis, installed directly upstream from the stagnation point. The wire size and grid pattern are indicated in Figure 11.

The droplet velocity was determined by counting the number of frames (consecutive pictures) required for a droplet to advance from one grid wire to the next. The droplet velocity $U_{\rm d}$ in feet per second was then determined from the expression:

$$U_{d} = \frac{n}{m} \left(\frac{s}{12} \right) \tag{4.1}$$

where n is the number of frames per second and m is the number of elapsed frames for a droplet to travel a distance s inches. For ease of calculations the grid-wire spacing was one inch, and the picture frames were tagged every one-hundreth of a second. In order to obtain a meaningful average velocity a large number of droplets must be observed and samples taken from various sections of the roll of film.

The determination of the droplet-size distribution was also made with the aid of high-speed photography, using the same photographs as for the velocity determination. The drops observed on a single frame, which were located between adjacent grid wires, were classified into four basic sizes. The four sizes selected were 1/4, 3/16, 1/8 and 1/16 inches when projected on a screen. The distance from the projector to the screen was adjusted to yield a magnification factor of

four, so that the actual droplet sizes were one fourth the size observed on the screen.

The number of drops for a given size classification and the total number observed per frame varied considerably from one sample to the next. Thus in order to obtain a representative size distribution a large number of observations must be made and the results analyzed statistically. A large number of observations may now be defined as that number N that would yield 68 per cent of the observations possessing residuals α within the limits of plus or minus one standard deviation σ , where α is the difference between the arithmetic mean value and the observed value, and σ is determined from the expression:

$$\sigma = \sqrt{\frac{\sum_{1}^{N} \frac{\alpha^2}{N}}{1}}$$
 (4.2)

4.3 Measurement of the Liquid-Film Thickness

The measurement of the liquid-film thickness used a system similar to that employed by McManus (5), who measured the liquid-film thickness for the case of two-phase flow in a duct. The system, Figure 12, is essentially a microscope traversing mechanism employing an electrical circuit. An open circuit is experienced until the probe comes into contact with the liquid film, and a change in resistance for the circuit is indicated later when the probe makes contact with the cylinder.

A suitable value for the potential applied between the probe and the cylinder was determined experimentally by measuring the film thickness at a location 90 degrees from the stagnation point, where the gravity vector was normal to the probe. A range of voltages were investigated, and it was found that the indicated film thickness was the same for the voltage range of 5 to 7 volts. When the voltage was in excess of 7 volts the indicated film thickness was increased, possibly because the film was distorted by the higher voltage, or a droplet could have been captured and retained between the probe and cylinder. The failure of the lower voltage to indicate the same film thickness, as say 6 volts indicates, could be caused by lack of sensitivity of the oscilloscope employed for the project. Figure 13 is a plot of film thickness versus applied probe voltage. A value of six volts was chosen for the film-thickness investigation.

The film thickness was measured over a range of angles (measured from the stagnation point) from 60 to 90 degrees. Angles less than 60 degrees did not yield acceptable results because droplets impinging on the probe caused water to run down the probe and make contact with the cylinder.

In order to reduce the error produced by droplets striking the probe and causing a film to run on it, a paraffin coating was painted on the probe. A film could not form over the paraffin surface, and the droplets which came in contact with the probe would form very small particles and be swept away by the air. This served satisfactorily for angles equal to or greater than 60 degrees.

The Determination of the Ratio of the Mass of Water Flow to Mass of Air Flow

The determination of the mass of air flow per unit of time was accomplished by the utilization of the continuity equation (ρ AU = constant). The density ρ was determined from the equation of state,

W.

se.

in:

sec

a c wer

Eor . Lea

to ·

tub. air

bac;

When ti.e

Figure Capt

Wàs s

which required both the static pressure and temperature at the test section. The velocity was determined with a standard Pitot tube.

The discussion of the determination of the mass of water flow per unit of time and per unit cross-sectional area will be divided into two parts: first, the actual measuring technique; and second, the development of a so-called uniform spray pattern over the test section.

The mass of water flowing per unit time was determined by placing a capture tube, Figures 14 and 15, in the flow field. Arrangements were provided to receive the collected water in a graduated cylinder. For the flow profile a one-half-inch capture tube was used, with the leading edge of the tube tapered on the inside to present a knife edge to the flow and minimize the deflection of the streamlines around the tube. The graduated cylinder was vented to the tunnel; in this way air passed through the capture tube into the graduated cylinder and back into the tunnel.

Two basic capture-tube assemblies were evaluated. First, a straight tube 0.503 inch OD and 0.485 inch ID at the knife-edge entrance was employed. Because one may question such a large tube when considering the amount of liquid which may be deflected around the tube opening, a 0.366 inch OD and 0.350 inch ID capture tube, Figure 15, was also evaluated. After it was determined that the capture rate per unit area and per unit of time for the two capture tubes showed a difference of less than one per cent, the larger tube was selected for the experimental investigation.

The test section at the cylinder location was traversed, and sufficient data collected to determine the average water-flow rate and the repeatability of the observation. The results are given in Section 6.4.

The major problem encountered in this phase of the program was the development of a uniform spray field. For the development of a uniform spray field, two basic spray nozzles were considered. First, a series of nozzles similar to the one designated in Section 3.4, and a series of internal mixing nozzles were evaluated. These nozzles may be characterized by the production of large drops for the solid cone nozzle and much smaller droplets for the internal mixing nozzle. It has already been stated that the larger drops have a greater probability of impinging on the cylinder and thus enhancing the heat-transfer rate. There are other phenomena to be considered in the selection of the nozzle: Does the particle bounce from the cylinder before it has arrived at the cylinder temperature, or does the particle splash other fluid from the cylinder?

The final nozzle selection was a compromise between several variables. Finally it should be noted that most nozzle specifications are based on a spray system in a quiescent atmosphere.

4.5 Measurement of the Liquid-Film Velocity

The determination of the velocity at the outer edge of the liquid film was accomplished by injecting dye (safranin bluish) into the liquid film through a pressure tap. The test cylinder had lines inscribed every five degrees on the surface starting at one of the pressure taps and extending for 110 degrees. The dye when injected

into the film would disperse throughout the fluid. That part which arrives at the film surface is swept around the cylinder at the greatest velocity. It is the time history of this interface that is of interest. Here high-speed color photography was utilized to observe the progress of the interface. It was determined experimentally that a camera speed of four thousand frames per second was required for an adequate definition of the flow field. It was assumed for this experiment that the maximum velocity occurs at the outer edge of the liquid film.

4.6 The Determination of the Boundary-Layer Separation Point

For the case of single-phase flow a schlieren apparatus, Figure 16, was utilized to observe and photograph the boundary-layer separation point. A photograph of the separation point is given in Figure 17 for a flow Reynolds number of 5.64×10^4 .

For the case of two-phase flow the disturbance produced by the water droplets made it impossible to observe the boundary-layer separation point with the aid of the schlieren apparatus. A simple and direct method was developed. A mixture of distilled water and wetting agent was injected into the liquid film (boundary layer) through a pressure tap. For example, in Figure 44 the mixture is injected at the upper tap shown in the figure, four and a half inches from the right wall and approximately 30 degrees from stagnation. The separation point could then be observed visually. It was noted that small bubbles were produced by the turbulence in the region of separation. These bubbles were observed to move both upstream and

downstream in the separated liquid film downstream of the separation point. The point where the upstream movement of the bubbles reversed and returned in a streamwise direction was considered to be the separation point. By this technique the separation point may be located with an accuracy estimated to be ± 2 degrees. The separation point was also visible due to reflection of light from the cylinder, under proper lighting conditions, since the air space under the separated liquid film altered the characteristics of the reflected light.

CHAPTER V

NUMERICAL PROCEDURES

5.1 The Scope of the Numerical Procedures

The solution of Equation (2.15) and the solution of the system of Equations (2.24) and (2.25) were obtained by the Runge-Kutta method with the aid of a digital computer. The solutions also required functional relationships which were derived from experimental data. The functions were obtained by fitting a polynomial to the experimental data by the technique of least squares.

5.2 Polynomial Fitted to Experimental Data

An IBM Library Program No. 7.0.002 was used to obtain a polynomial fitted to the experimental data. This program determines by the least squares technique the coefficients of a polynomial up to and including a fifteenth order polynomial. The program, in Fortran language for an IBM 1620 computer, accommodates up to 100 data points.

5.3 The Runge-Kutta Numerical Procedure

The Runge-Kutta numerical procedure is a numerical method of obtaining a solution to a system of first order differential equations when certain initial conditions are obtainable. Equation (2.15) and the system of Equations (2.24) and (2.25) meet these requirements; i.e., they are first order differential equations of the initial value type. Before a solution can be obtained, the differential equations

must first be put into standard form

$$\frac{dy}{dx}\Big|_{j} = f_{j}(x,y_{1},y_{2}, \dots, y_{N}); j = 1,2, \dots, N$$
 (5.1)

where N is the number of first order differential equations. For the case of N = 1 and the value y_i at the left end of the i^{th} interval is known, the value y_{i+1} at the right end is calculated by the following set of formulas.

$$k_{1} = f(x_{i}, y_{i})$$

$$k_{2} = f(x_{i} + \frac{1}{2}h, y_{i} + \frac{1}{2}hk_{1})$$

$$k_{3} = f(x_{i} + \frac{1}{2}h, y_{i} + \frac{1}{2}hk_{2})$$

$$k_{4} = f(x_{i} + h, y_{i} + hk_{3})$$

$$y = y_{i} + \frac{h}{6}(k_{1} + 2k_{2} + 2k_{3} + k_{4})$$
(5.2)

where h is the width of the ith integration interval.

If there are N first order equations

$$\frac{dy}{dx}\Big|_{j} = f_{j}(x,y_{1},y_{2}, \dots, y_{N}); j = 1,2, \dots, N$$

there will be N solution values, one for each of the N equations. Let the solution function of the jth equation (j = 1,2, \cdots , N) at the left end of the ith integration interval be y_j. Then the above set of formulas become

$$k_{j1} = f_{j}(x, y_{1}, y_{2}, \dots, y_{N})$$
 (a)

$$k_{j_2} = f_j(x + \frac{h}{2}, y_1 + \frac{hk_{11}}{2}, y_2 + \frac{hk_{21}}{2}, \dots, y_N + \frac{hk_{N1}}{2})$$
 (b)

$$k_{j3} = f_j(x + \frac{h}{2}, y_1 + \frac{hk_{12}}{2}, y_2 + \frac{hk_{22}}{2}, \dots, y_N + \frac{hk_{N2}}{2})$$
 (c) (5.3)

$$k_{j_4} = f_j(x + h, y_1 + hk_{13}, y_2 + hk_{23}, \dots, y_N + hk_{N3})$$
 (d)

$$y_{j}^{*} = y_{j} + \frac{h}{6} (k_{j1} + 2k_{j2} + 2k_{j3} + k_{j4})$$
 (e)

Here $1 \le j \le N$ and y_j^* is the new value of the y, i.e., $y_{j,i+1}$. The set of Equations (5.3) can be evaluated in sequence in such a way that only one value of k need be used for each of the equations, say k_j , since k_{j1} computed in (a) is used only in (b), k_{j2} computed in (b) is used only in (c), and so on. This assumes that the term $(k_{j1} + 2k_{j2} + 2k_{j3} + k_{j4})$ in (e) is computed by accumulating the partial sum as each new k_{ji} is determined. The entire system of difference equations can then be solved by a multi-pass procedure described below.

Pass 1:

1. Compute the derivative F(J) ($J=1,2,\cdots,N$) for each of the N equations, using the current X and Y(J) values. These are the values of the $k_{j1}=f_j(x,y_1,y_2,y_3,\cdots,y_N)$ of Equation (5.3a).

$$F(J) = f_{j}(X,Y(1),Y(2), \dots, Y(N)); J = j = 1,2,\dots, N$$

Pass 2:

2. Save all the current Y(J) values (i.e., the initial values of the solution $y_{j\,i}$ at the left edge of the integration step) in another array called OLDY.

$$OLDY = Y(J)$$
; $J = 1, 2, \dots, N$

3. Begin accumulation of the $k_{
m ji}$ terms in Equation (5.3e) in an array called PHI

$$PHI(J) = F(J)$$
; $J = 1,2, \dots, N$

4. Compute the next y value, $(y_j + \frac{hk_{j1}}{2})$, needed for Equation (5.3b).

$$Y(J) = OLDY(J) + .5*F(J) ; J = 1,2, ..., N$$

where H = h

5. Compute the next x value needed for Equation (5.3b), $x + \frac{h}{2}$

$$X = X + .5$$
*H

6. Compute the derivative values F(J) ($J = 1, 2, \dots, N$) for each of the N equations, using the current X and Y(J) values. These F(J) are the k_{j2} of Equation (5.3b).

$$F(J) = f_j(X,Y(1),Y(2), \dots, Y(N)); J = 1,2, \dots, N$$

Pass 3:

7. Add the contribution of k_{j2} = F(J) to PHI(J)

$$PHI(J) = PHI(J) + 2.*F(J); J = 1,2, ..., N$$

8. Compute the next y value $(y_j + \frac{hk_{j2}}{2})$ needed for Equation (5.3c)

$$Y(J) = OLDY(J) + .5*H*F(J); J = 1,2, ..., N$$

Note that x already has the proper value from step 5.

9. Compute the derivative values F(J) ($J = 1, 2, \dots, N$) for each of the N equations, using the current X and Y(J) values. These F(J) values are the k_{13} of Equation (5.3c).

$$F(J) = f_{j}(X,Y(1),Y(2), \dots, Y(N)); J = 1,2, \dots, N$$

Pass 4:

10. Add the contribution of k_{13} = F(J) to PHI(J)

$$PHI(J) = PHI(J) + 2.*F(J); J = 1,2, ..., N$$

11. Compute the next y value, $(y_j + hk_{j3})$ needed for Equation (5.3d)

$$Y(J) = OLDY(J) + H*F(J); J = 1,2, ..., N$$

12. Compute the next x value, (x + h), needed for Equation (5.3d). Since the original x was incremented by h/2 in step 5 only h/2 need be added to the current x.

$$X = X + .5$$

13. Compute the derivative values F(J) ($J = 1, 2, \dots, N$) for each of the N equations, using the current X and Y(J) values. These F(J) values are the k_{j4} of Equation (5.3d).

$$F(J) = f_{j}(X,Y(1),Y(2), \dots, Y(N)); J = 1,2, \dots, N$$

Pass 5:

14. Add the contribution of $k_{j4} = F(J)$ to PHI(J)

$$PHI(J) = PHI(J) + F(J); J = 1,2, \dots, N$$

15. Compute y_j *, the new value of y_j , for all N equations, and put results into the solution array y.

$$Y(J) = OLDY(J) + PHI(J)*H/6; J = 1,2, ..., N$$

At this point all computed solution functions for N equations, at the right end of the integration step, are in location Y(1), Y(2), ..., Y(N). Also, X has been incremented by H from its value before step 1. The procedure can be repeated if integration is required across another interval of width H (H can be changed if desired). Note that steps 1, 6, 9 and 13 are identical and of the form

$$F(J) = f_{j}(X,Y(1), Y(2), \dots, Y(N)); J = 1,2, \dots, N$$

These steps are the only ones in which the N different equations are specifically mentioned. Hence it is possible to write a very general integration subroutine for an arbitrary set of N first order differential equations which implement all steps in the sequence except 1, 6, 9 and 13. A possible communication sequence between a calling program, which contains the definition statements for any specific set of N equations (the f_j 's) and subroutine RUNGE and accompanying flow chart is given in Figure 20 or Figure 21. Steps 1, 6, 9, 13 and any other essential steps such as the setting of initial

values, the punching of results, etc., are incorporated into the calling program.

5.4 Numerical Procedures for the Laminar Gas

Boundary-Layer Model

The computer program for the laminar gas boundary-layer model is listed in Figures 18 and 20, where Figure 18 is the Runge-Kutta subroutine. Listed below is the correspondence between nomenclature in the computer program and nomenclature used in text.

Computer Nomenclature	Text Nomenclature
N	l (number of equations)
DB	U ₀
XL	λ
x	$x/R = \Phi$
Y (1)	Y
Q	U _s /U _∞
QPR	Us'/U∞
Q2PR	U <mark>"</mark> /U∞
FUDU	U _s U <mark>"</mark> /(U's) ²
A (5)	coefficients of polynomial for U_{S}/U_{∞}
СС	the upper limit on X for which A (5) are valid
ICNT	the number of computations for each output
Н	h

The results of the computer program are reported in Section 6.4.

5.5 Numerical Procedure for the Turbulent Gas

Boundary-Layer Model

The computer program for the turbulent gas boundary-layer model, Equations (2.25), (2.26) and (2.27), is listed in Figures 18 and 21, where Figure 18 is the Runge-Kutta subroutine. Listed below is the correspondence between nomenclature used in computer program and nomenclature used in text.

Computer Nomenclature	Text Nomenclature
N	2 (number of equations)
Т	2q/τ ₀
RE	Re ₀
Y (1)	θ/R
Y (2)	Н
х	$x/R = \Phi$
Q	q
QPR	dq/d x
DR	$\frac{\text{Re}}{2U_{\infty}} \sqrt{\frac{\rho_{\mathbf{w}}}{\rho_{\mathbf{a}}} \frac{2g_{\mathbf{c}}}{12}}$
ICNT	the number of computations for each output
A (5)	coefficients of polynomial for q
С	the upper limit on Φ for which the coefficients A (5) are valid
Н	h
CONS=1./LOG(10)	conversion of log from the base 10 to the base e

The results of the computer program are reported in Section 6.4.

CHAPTER VI

RESULTS

6.1 Preliminary Remarks

The objective of this experimental investigation is to perform the necessary diagnostic studies of the flow field and perform visual, photographic, and physical measurements of the boundary layer formed on a right circular cylinder. The results will be utilized to predict the behavior of boundary layers in the region of the separation point.

The investigation was divided into three sets of experiments. The first set of experiments provided the data for an evaluation of the wind tunnel under the conditions of single-phase flow. The second set of experiments was conducted with the gas Reynolds number held in the neighborhood of 5.6×10^4 . The objectives of this second set of experiments were:

- 1. To develop a pressure-measuring technique for the case of two-phase flow.
- 2. To locate the region of boundary-layer separation and investigate the flow properties in this region.
- 3. To collect experimental data required for the solutions of the analytical models.

The third set of experiments was conducted with the mass flow of water from the spray nozzle held constant, while the gas Reynolds number was varied from 3.55×10^4 to 1.04×10^5 . The objective of this third set

of experiments was to determine the effect of variations in gas Reynolds number on the region of flow separation.

The results of these investigations are reported in the following three sections: Section 6.2 contains the results of the wind-tunnel evaluation in single-phase flow. Section 6.3 contains the results of the experimental investigation. The results of the analytical investigations are reported in Section 6.4.

6.2 Wind-Tunnel Evaluation in Single-Phase Flow

An evaluation of the system under the conditions of single-phase flow was made prior to the two-phase flow investigation. The evaluation included:

- 1. Determining the average Nusselt number over a range of Reynolds numbers for the case of transverse flow of air over a heated cylinder.
- 2. Measuring profiles for a range of velocities in the test section.
 - 3. Determining a pressure profile for a test cylinder.

The results of the heat-transfer studies are tabulated in Table 1 and plotted in Figure 22, where the curve is from Hilpert (21), based on a large number of experiments. The points marked with a plus sign are from the present investigation. The range of Reynolds number based on cylinder diameter was from 3.24 × 10⁴ to 1.1 × 10⁵. Runs one through five yielded an average Nusselt number (Equation (3.1)) less than the average experimental values reported by Hilpert (21) for corresponding Reynolds number. Runs six and seven yielded values in excess of Hilpert's measurements. The measurements of Schmidt and

Wenner (17) for a 50mm diameter cylinder (1.965 inch diameter) are also included in Figure 22 by solid circles. The data spreads for Schmidt and Wenner and for the present investigation are similar, and in the same range of values reported by Hilpert. Kestin (10) estimated that the intensity of turbulence ε for Hilpert's measurements was in the range of 0.85 to 0.90 per cent where ε (in per cent) is given by $\varepsilon = 100 \sqrt{\frac{1}{3}(u'^2+v'^2+w'^2}/U_{\infty}$, u', v' and w' are nonsteady velocity disturbances in the flow field. Since the heat-transfer data of the present investigation is in the range of Hilpert's, it is concluded that the intensity of turbulence for the system utilized for this investigation is also in the same range as Hilpert's, and therefore less than one per cent for single-phase flow.

The test cylinder was located at a point in the test section where the variation of the free-stream velocity from the average free-stream velocity was found to be less than one per cent. Table 2 contains the tabulated results of velocity measurements which met this specification. These measurements were made in a plane normal to the free-stream velocity and twenty inches downstream from the test section inlet in the manner described in Section 3.5. Table 2 gives the maximum and minimum values of the free-stream velocity for a series of tests in which the maximum ranged from 42 to 176 feet per second. In run number four the maximum per cent variation in free-stream velocity occurred. Here, it varied from 137.5 to 139 feet per second or * 0.6 per cent from the average. Tables 3 through 7 are coordinate plots of the velocity pressure measurements summarized in Table 2. It was observed that all velocity measurements taken at least one inch from the tunnel walls were in the free-stream velocity

field. Measurements taken one-half inch from the tunnel walls were observed to be (in most cases) inside the wall boundary layer. The maximum reduction of velocity at the one-half inch station occurred in run number four. A reduction of six per cent was observed.

The pressure profile for a Reynolds number of 1.15×10^5 is plotted in Figure 23. For comparison, pressure profiles by Giedt (22) for Reynolds numbers of 1.01×10^5 and 1.4×10^5 are plotted on the same figure. It was observed that the separation took place at the anticipated location, while the pressure on the downstream side of the cylinder was less than the value obtained by Giedt.

The principal cause for the pressure reduction was believed to be tunnel blockage. From Kestin the free-stream velocity is subject to two principal corrections, namely those due to "solid blocking" and to "wake blocking". The solid-blocking correction for a cylinder as given by Kestin is

$$\beta_{SD} = \frac{\pi^2}{12} \left(\frac{S}{A}\right)^2$$
$$= \frac{\pi^2}{12} \left(\frac{15}{100}\right)^2$$
$$= 0.0185$$

where A denotes the area of the test section and s is the frontal area of the cylinder. The wake-blocking correction as given by Kestin is

$$\beta_{\text{wb}} = -\frac{1}{4} C_{\text{D}} \frac{\text{s}}{\text{A}}$$
$$= -\frac{1}{4} (1.18) \left(\frac{15}{100}\right)$$
$$= -0.0434$$

where C_D denotes the drag coefficient for a cylinder (C_D = 1.18 for cylinder with a range of Reynolds numbers of 1 × 10⁴ to 2 × 10⁵, Schlichting, page 16). Consequently

$$U_{\infty} = u' (1 + \beta_{Sb} + \beta_{Wb})$$

$$= u' (0.974)$$

$$= 0.974 u'$$

where u' is the measured free-stream velocity and U_{∞} denotes the corrected free-stream velocity. Adopting no correction introduces an error of approximately 2.5 per cent in Reynolds number. Applying this correction to the heat-transfer data of Figure 22 and comparing the new results to Hilpert's curve (21) would yield the following results: Runs one through five would show a slight improvement. Six and seven would yield an increased divergence.

In single-phase flow, the average Nusselt number for the range of Reynolds numbers considered was found to be in the same range of values as those published in the cited references (References 10, 17, 21 and 22). The boundary-layer separation point agreed with that reported in Reference 22. From this it may be concluded that two sets of meaningful comparisons may be formulated: First, the result of the two-phase flow studies may be compared to those for single-phase flow. Second, the results of this investigation may be compared to the findings of other investigators whose test facilities perform similarly in single-phase flow.

6.3 Experimental Results in Two-Phase Flow

In order that we may arrive at some definite conclusions as to the boundary-layer behavior in two-phase flow, the separation point and pressure profile for single-phase flow are required for the same gas Reynolds number.

For the case of single-phase flow the phenomenon of boundary-layer separation was photographed with the aid of a schlieren apparatus. Figure 17 is a photograph of the separation region for a Reynolds number of 5.64 x 10⁴. The photograph is an axial view of the test cylinder with the forward stagnation point located at the top of the cylinder. Flow was observed to separate from the cylinder at an angle of 78 ± 2 degrees from the forward stagnation point. In Figure 17 separation is observed as a light line tangent to the cylinder at the 78-degree point and extending downstream. The quality of the photograph is not typical of that obtained when optical glass windows are utilized on a wind tunnel as part of the schlieren optical system.

Figure 24 is a plot of the pressure coefficient for a gas Reynolds number of 5.64 x 10⁴. The separation point was indicated by the inflection in the pressure coefficient curve. This occurred in a region approximately 78 ± 2 degrees from the forward stagnation point, which agreed well with the results in the schlieren photograph, Figure 17.

The results of calibration of the pressure transducer and evaluation of pressure measuring technique utilizing water injection are given in Figures 9, 25, 26, and 27. Figure 9 is a plot of the millivolt output of the pressure transducer versus pressure impressed on the transducer in inches of water. For an applied voltage of 14 volts

the calibration constant was 1.840 millivolts per inch of water pressure. The linearity of the transducer through the pressure range of interest was good. Over a range of ten inches of water pressure the maximum deviation was ± 0.005 millivolts per inch of water. For a pressure measurement utilizing a standard inclined manometer with a least scale graduation of 0.02 inches of water pressure (estimating the measurement to the hundreth inch of water) would require, for equal accuracy, that the output of the transducer be read to the nearest 0.018 millivolt. The results of the hysteresis studies of the pressure measuring system are given in Figure 25. The pressure profiles were obtained for the case of single-phase flow with a gas Reynolds number of 5.64 × 104. A pressure profile determined with an inclined manometer and gas-filled pressure lines was assumed to be the actual pressure profile for comparison with the measured profile. The measured pressure profile utilized a pressure transducer, liquid filled pressure lines and a water injection rate of 1.4 milliliters per minute into the gas boundary layer. The measured profile took the 90-degree point as the initial point, and measurements were made every two degrees over the range of 90 to 0 degrees and 90 to 110 degrees. Operating the system without taking the necessary precautions to reduce hysteresis effects resulted in a maximum error of 13.5 per cent. This occurred at a point 50 degrees from the forward stagnation point. The same error was observed at the forward stagnation point.

The pressure profile for a case where the water injection into the gas boundary layer was turned off between each pressure measurement to remove the hysteresis effect is given in Figure 26. Variations between the measured pressure and actual pressure are given in Figure 27. The data was obtained for a single-phase gas Reynolds number of 5.64 × 10⁴ and a water injection rate of 1.4 milliliters per minute. Pressure measurements were made every five degrees starting at the forward stagnation point and extending 110 degrees around the test cylinder. Similar measurements were made at the 110-degree point and returning to the stagnation point. A maximum error of 5.2 per cent was observed at 75 degrees. This occurred in the region of the pressure minimum which is also the region of maximum free-stream velocity. A 1.4 per cent error was observed at the forward stagnation point.

The performance characteristics of the pressure-measuring technique for the case of two-phase flow are exhibited in Figure 28. Here, the difference between local pressure on the cylinder and the atmospheric pressure is plotted against the angle (distance) measured from the forward stagnation point. The system was operated at gas Reynolds number of 5.64×10^4 . Water-nozzle pressure was maintained at 20 psig and a water-injection rate of 1.4 milliliters per minute was employed.

The curve of Figure 28 represents two sets of data. The first set of data was collected by starting at the forward stagnation point and making pressure measurements every four degrees until the pressure at the 140-degree point had been measured. The rotation of the cylinder was reversed and each pressure measurement repeated. The second set of data was collected by observing the pressure at the forward stagnation point and then indexing to 2 degrees. From this location on around the cylinder pressure measurements were made every

four degrees until the pressure had been measured at the 138-degree point. The direction of cylinder rotation was again reversed and all measurements repeated. The general scatter of data was small, with the largest variations in pressure occurring at 26, 46 and 86 degrees. The average difference for these three points was 0.14 inch of water pressure. After reviewing the method of reading angle of cylinder rotation and analyzing the data, it was concluded that at these three stations an incorrect angle was observed for cylinder rotation. Excluding those three data points, an average pressure variation (at a repeated data point) of 0.02 inches of water was observed. This represents the estimated accuracy of pressure measurements. The pressure at the forward stagnation point was -0.714 inches of water. For the case of single-phase flow a pressure of -0.72 inches of water was observed when employing the water injection technique. The actual pressure at the forward stagnation point for single-phase flow was -0.73 inches of water. This represents a 2 per cent increase in pressure at the forward stagnation point.

For the case of two-phase flow the pressure coefficients for a constant gas Reynolds number of 5.64 × 10⁴ are plotted in Figures 29, 30 and 31. Nozzle water pressures for the above curves were 15, 20 and 25 psig respectively with the 20 psig curve taken as the base value. In each case the pressure at the forward stagnation point was higher than the pressure observed at the corresponding point for single-phase flow with the same gas Reynolds number. The magnitude of pressure coefficient at the point of minimum value (which is the region of maximum free-stream velocity) was in all cases less than the corresponding value in single-phase flow. The location of the

region where the pressure coefficient passes through its minimum value was observed, in all cases, to have shifted downstream approximately 6 degrees. Also, the slope of the pressure coefficient curve downstream from the point of its minimum value is less than the corresponding slope for the case of single-phase flow. As a result of these two effects the separation point was observed to have shifted downstream approximately 14 degrees. The distance along the cylinder between the separation point and the region where the wake pressure approaches constant value has increased in all three cases, with the 15 psig case indicating the greatest disturbance.

The determination of the droplet Reynolds number $\left(\text{Re}_{d} = \frac{d(U_{\infty}-U_{d})}{v}\right)$ requires an estimate of the droplet diameter d and the droplet velocity U_{d} . High-speed photography (4000 frames per second) was utilized to obtain a gross value of the droplet diameter, and an average value for the velocity. It should be observed that the study included only those droplets the camera could see.

The droplet velocity, the average velocity of the water leaving the nozzle, the air velocity at infinity and the volumetric flow rate of the nozzle are given in Table 8 for a constant gas Reynolds number of 5.64×10^4 and nozzle water pressures of 15, 20 and 25 psig.

From Table 8 it is observed that an increase in water nozzle pressure increases the volumetric flow rate and the average liquid velocity at the nozzle. Accompanying this increase in water pressure an additional decrease in the difference between the air velocity and the droplet velocity is observed. This suggests that the droplet size is also decreasing as nozzle pressure increases. All this tends

to decrease the droplet Reynolds number for increased water nozzle pressures.

The scatter in droplet velocity data was ± 5 per cent without establishing correlation between droplet size and droplet velocity. The range of droplet diameters observed was 0.015 to 0.0625 inches.

In order to determine a representative size distribution of those droplets which were photographed it was found necessary to take 40 photographic samples for each flow condition. This provided approximately 68 per cent of the film samples with a variation in total number of drops per observation less than one standard deviation. Figures 32, 33 and 34 are plots of per cent of observations versus fraction of standard deviation. The nozzle pressures were 15, 20 and 25 psig respectively and the gas Reynolds number was 5.64×10^4 for each run. The above figures are similar and indicate a large fluctuation in droplet population. The droplets were classified into four size groups (1/16, 3/64, 1/32 and 1/64 of an inch) and an equivalent droplet diameter was calculated. The equivalent diameter is a droplet diameter that would provide the same mass flow and same total number of drops. Table 9 is a summary of the results of the survey. The important result of the survey was the determination of the droplet Reynolds number. The droplet Reynolds number decreased as the nozzle pressure increased. This was brought about by a reduction in droplet size and decrease in the velocity difference that exists between the gas and the droplet as the water pressure was increased. This is in agreement with the pressure coefficient curves of Figures 29, 30 and 31. These curves were ordered with the 15 psig curve indicating the maximum disturbance.

The variation in the measured liquid boundary-layer thickness versus probe voltage is given in Figure 13, all measured at 90 degrees from the stagnation point. The measured boundary-layer thickness appeared to be independent of probe voltage in the range of 4.5 to 7 volts. Here a 3 per cent variation in liquid boundary-layer thickness was observed. For a probe voltage of 10 volts there was a 12 per cent increase in thickness. A probe voltage of 4 volts indicated a 20 per cent reduction in liquid boundary-layer thickness. For all subsequent boundary-layer measurements a probe voltage of 6 volts was employed.

Curves of liquid boundary-layer thickness versus angle (distance) measured from the forward stagnation point are plotted in Figures 35, 36 and 37 for water nozzle pressures of 15, 20 and 25 psig respectively. For the above curves, the gas Reynolds number was held at 5.64 × 10⁴ and each data point represents an average of twenty or more observations. For a typical data point a scatter in the measurements of 0.002 inches was observed. This apparent large scatter in the measurements was attributed to two major factors. The first of these was the presence of vibrations in the system. Coupled with this it was found by observing the liquid boundary layer with the aid of high-speed photography, that waves were formed on the liquid surface as a result of droplets striking the surface. As a result of the vibrations and the presence of waves it was difficult to determine the exact location of the film surface.

For angles less than 60 degrees an added complication was the problem of water running down the probe and making contact with the cylinder. Boundary-layer thickness measurements less than 0.002 inches,

which are typical values for angles less than 60 degrees, would be subject to serious error. It is doubtful if the present technique of measurement could be employed in that region.

The three curves of Figures 35, 36 and 37 are all similar, indicating a rapid growth of the liquid boundary layer in the regions of the pressure minimum and the separation points.

The velocity U_0 at the outer edge of the liquid boundary layer was determined with the aid of high-speed color photography. A filming speed of 4000 frames per second was required to adequately define the flow field. Plots of the velocity U_0 versus angle (distance) measured from the forward stagnation point are given in Figures 38, 39 and 40. The gas Reynolds number of 5.64×10^4 was maintained for the three runs and the water nozzle pressure was 15, 20 and 25 psig respectively.

The above curves are all similar and a reduction in the velocity U₀ was observed for all cases in the region of the separation point. Two significant observations were made during the evaluation of the photographic film. It was observed that waves were formed on the cylinder and traveled around the cylinder at a constant velocity. The range of velocity of the waves was from 1.82 to 3.40 feet per second. These waves were generated by droplets striking the surface of the liquid film. When the droplets would strike the liquid surface it was also observed that part of the liquid film would splash from the cylinder. This fact was established by the presence of dye in the fluid leaving the cylinder.

The phenomenon of boundary-layer separation can be observed in the photograph of Figure 41, for Reynolds number 5.64×10^4 and water

nozzle pressure 20 psig. The region of boundary-layer separation was made visible by the injection of a mixture of distilled water and wetting agent into the liquid boundary layer at the upper pressure tap shown in Figure 41. The presence of the wetting agent promoted the formation of gas bubbles in the separated liquid film. Within the separated liquid film in a region downstream of the separation point some of these bubbles are observed to move in a direction parallel to the axis of the cylinder, while some of the bubbles were observed to move upstream and some downstream in the liquid film. The point where the upstream movement of the bubbles reversed and returned in a streamwise direction was considered to be the separation point. This location was in agreement with the pressure profiles of Figures 29, 30 and 31. Both of these techniques yielded separation point with an accuracy estimated to be ± 2 degrees. Three important pieces of information were obtained from this photograph.

The line forming the separation region spans the wetted length of the cylinder and was located between 90 and 95 degrees from the forward stagnation point. The water spray flow distribution along the axis of the cylinder is plotted in Figure 42, and the water spray distribution over the test segment of the cylinder is shown in the coordinate plot of Figure 43. The first important observation can now be made by considering water spray flow distribution and the line of separation. The observation is that the separation region is not strongly affected by the water spray distribution for mass ratios of liquid to gas less than 8 per cent. Further it was observed that a liquid film would not form on the cylinder in a region near the end of the cylinder for the case of low rate of water spray, particularly

if the surface was contaminated with oil or wax film. This may be observed at the right end of the cylinder.

The second important observation was the ability of the liquid film to transport the mixture of distilled water and wetting agent laterally along the cylinder. This was characterized by the appearance of soap bubbles along the complete length of the cylinder when the mixture was injected through a pressure tap located four and one half inch from the right wall of the tunnel, approximately 30 degrees from stagnation point. The rotation in the liquid boundary layer was indicated by the shedding of streamwise vortices. There was no set pattern for the shedding of the vortices even though a pair was observed to be leaving the cylinder in Figure 41. The vortex in Figure 44 can be observed to be rotating so that fluid on the air side of the liquid film is moving from the wall toward the center of the cylinder. The rotation of the fluid in the region of separation can be observed in Figure 45 as a series of vortices whose axis of rotation is in the streamwise direction. The vortices may be similar to the Taylor-Goertler vortices (23) which are caused by threedimensional disturbances in the flow along a concave wall. Such a shedding of vortices was not observed in horizontal flow over a vertical cylinder (Appendix A).

The last observation was the existence of a bubble of water located downstream of the separation line Figure 41. The bubble extended the length of the wetted portion of the cylinder and appeared as a raised section on the cylinder. From this bubble vortices were shed in random order. Presence of the water bubble and the relatively thick liquid boundary layer in the region of the separation point

provided a contoured surface for the gas boundary layer to flow over. The contoured surface presented an opportunity for the gas stream to flow against a reduced pressure hill. This was reflected in the decreased slope (as compared to single-phase flow) for the pressure curve of Figures 29, 30 and 31, for that region downstream of the pressure minimum.

The third set of experiments was conducted in order to determine the effect that a change of gas Reynolds number would have on the separation region. A photograph of the boundary-layer separation region for a gas Reynolds number of 3.55 × 10⁴ and a constant water nozzle pressure of 20 psig is given in Figure 46. The boundary layer is similar to those of Figures 41 and 45. A vortex was observed to have removed the turbulent fluid downstream of the separation point in the foreground of the photograph. The low gas velocity (48 feet per second) permitted a liquid film to be formed along the complete length of the cylinder. This was a result of droplets crossing the gas streamlines upstream of the cylinder, thus covering the complete cross section of the test area. At higher velocities this did not occur and only the central core of the test section was under the condition of two-phase flow.

A photograph of the boundary-layer separation region for a gas Reynolds number of 1.04×10^5 and a constant water nozzle pressure of 20 psig is given in Figure 47. At this gas velocity of 140 feet per second only the central section of the cylinder was wetted. The boundary-layer separation region has shifted downstream approximately 5 degrees, and the bubble of the liquid film has shifted downstream

from the region of separation. This gave an appearance of an irregular separation line.

6.4 Results of Analytical Investigation

The laminar gas boundary-layer investigation of Section 2.2 was to determine what effect the velocity U_0 had in altering the separation point (U_0 is the interface velocity between the gas and the liquid boundary layer, which for this analysis was assumed to be constant). Equation (2.15) was first solved numerically with U_0 = 0 and β = 1 with the external velocity expressed by U_S = $2U_\infty \sin \Phi$. This was accomplished with the aid of an IBM 1620 computer utilizing a modified form of the program listed in Figures 18 and 20. This provided a check for the computer program, since the separation point for single-phase flow over a cylinder is well established for this external velocity. The solution also provided initial data for the turbulent gas boundary-layer analysis.

Equation (2.15) was then solved with the same flow assumed to prevail in the external flow field for a range of values of U_0 up to and including 5 per cent of U_∞ except in a small neighborhood of the forward stagnation point where U_0 was kept zero and β unity as explained at the end of Section 2.2. The results are listed in Table 10.

For a value of U_0 equal to 5 per cent of U_∞ , which corresponds to the maximum observed value of U_0 , the calculated separation point shifted downstream approximately one degree. The observed separation point shifted downstream 14 degrees for a gas Reynolds number of 5.64 \times 10⁴. The analysis only accounted for 7 per cent of the total

displacement of the separation point. It was observed that U_0 had very little effect on the boundary-layer properties upstream of the pressure minimum. For the external flow used, given by Equation (2.19), λ is zero at Φ equal to 90 degrees, while at the point Φ = 1.5 radians (86 degrees) the maximum variation in Y from the single-phase flow value was 0.1 per cent for the range of values of U_0 considered. It may be concluded from the results shown in Table 10 that the solution of Equation (2.15) is not sensitive to U_0 upstream of the point of pressure minimum, while it is somewhat sensitive to \mathbf{U}_{0} downstream of the point of pressure minimum. For two-phase flow and a gas Reynolds number of 5.64 \times 10 4 the distance between the observed point of pressure minimum and the observed separation point was increased 8 degrees over that of single-phase flow. Thus Equation (2.15) predicted only 12.5 per cent of the observed increase in the distance of the separation point from the point of pressure minimum.

The turbulent boundary-layer investigation was to determine whether the region of boundary-layer separation could be predicted by the use of Equations (2.25), (2.26) and (2.27). The equations required for solution the input of actual velocity pressure information, viz., the derivative of the velocity pressure with respect to Φ , and initial conditions.

The pressure information contained in Figures 29, 30 and 31 was plotted in terms of the velocity pressure $q=\frac{1}{2}\rho U_S^2$. The plots of q versus the angle (distance) measured from the forward stagnation point are given in Figures 48, 49 and 50 for nozzle water pressures of 15, 20 and 25 psig respectively. The velocity pressure for

single-phase flow at the same gas Reynolds number is plotted as a broken line. The plots for two-phase flow show negative values of q near the stagnation point. Since $q = \frac{1}{2} \rho U_S^2$ and only real velocities are permitted, this restricts q to positive values. To accomplish this, single-phase flow was assumed in the region of the stagnation point. Each of the curves were divided into sections as indicated in the above figures. A polynomial fitted to the section of data along with an overlap of sections was accomplished with a Fortran computer program as referred to in Section 5.2.

Coefficients of the polynomials become the coefficients of the array A (5) of the computer program Figure 21 and C represents the maximum value of Φ for which a given set of coefficients was valid. In order to calculate the initial value of the momentum thickness 0 and the momentum Reynolds number (Re $_{\theta}$), single-phase flow was assumed to exist for values of Φ less than 0.2 radians, with the external flow given by Equation (2.19) in this region only. A numerical solution for the above equation was obtained with the aid of an IBM 1620 computer utilizing the computer program of Figures 18 and 21 for a range of Φ from 0.2 radians to 1.96 radians. The results are summarized in Table 11.

The range of values of θ , Re_{θ} and $\tau_{0}/2q$ are in agreement with results that would be predictable from analysis of data by Squire and Young (15), which indicates the computed data is reasonable. But the value of H did not increase to a value in the range 1.8 to 2.6 that would predict separation according to the criterion that von Doenhoff and Tetervin established for single-phase flow. The calculated values of H in the experimentally-established separation

region were near 1.23 ($^{\pm}$ 0.01 in the cases observed). The results of the computer solution of Equations (2.25) and (2.26) are reasonable for values of q less than the maximum q, where H decreases with increasing Φ because first term in Equation (2.25) is negative. Beyond the point of maximum q this term becomes positive so that H increases again. But because of the decreased slope of the pressure curve observed in two-phase flow as compared to single-phase flow (see Section 6.3), the contribution of the first term of Equation (2.25) in the region downstream of the pressure minimum is small, so that the calculated H does not increase as much as in single-phase flow. This discussion is all in the confines of the assumption that U0 (the velocity at the outer edge of the liquid film) did not materially affect the region of separation.

6.5 Summary of Results

As a result of an evaluation of the experimental apparatus under the conditions of single-phase flow, it was found that the average Nusselt number for the range of Reynolds numbers considered was in the same range of values as those published in the cited references (References 10, 17, 21 and 22). The boundary-layer separation point agreed with that reported in Reference 22. From this study it was concluded that the intensity of turbulence ε for the case of single-phase flow was less than one per cent for the range of Reynolds numbers considered. As a result of determining the system characteristics in single-phase flow it may now be possible to compare the findings in the two-phase flow studies with those of single-phase flow and also with the findings of other investigators whose system possesses similar characteristics in single-phase flow.

A system for measuring the pressure distribution around the test cylinder was developed. The system was evaluated in single-phase flow with a gas Reynolds number of 5.64 × 10⁴ by comparison with a standard system, which was assumed to be correct. An error of 1.4 per cent in pressure measurement at the stagnation point was observed while the maximum error of 5.2 per cent occurred at the point of pressure minimum. These results were considered acceptable, since this represented a severe test of the system, because of the injection of water (whose density is three orders of magnitude greater than air) into the air boundary layer.

Three pressure profiles were measured under conditions of two-phase flow with a fixed gas Reynolds number of 5.64 × 10⁴ and water pressures of 15, 20 and 25 psig respectively, at the spray nozzle. The following observations were made in regards to these profiles: The droplet Reynolds numbers were found to be 522, 450 and 380 for the respective water nozzle pressures. It was observed that the pressure profile for the 15 psig water pressure and droplet Reynolds number of 522 (which was the maximum observed droplet Reynolds number) experienced the greatest deviation from single-phase flow. The maximum excursion in pressure occurred (i.e., the least pressure at the point of pressure minimum) for this profile. The same profile required the greatest distance of travel from the point of pressure minimum to the point where the near constant wake pressure was observed. For all three pressure profiles the point of minimum pressure shifted downstream approximately 6 degrees from that observed in single-phase flow, while the separation point shifted downstream approximately 14 degrees. The three pressure profiles experienced a reduction in slope as compared

to single-phase flow, at the same gas Reynolds number, between the point of pressure minimum and the point where the near constant wake pressure was observed. Possibly this is a result of the observed rapid growth in the liquid boundary-layer thickness from the point of pressure minimum to the separation point and the presence of a bubble of water which was observed just downstream of the separation point. These two conditions could well have presented a new contour for the external flow field. This would be observed in the pressure measurements since it is coupled to the external velocity U_s through the Bernoulli Equation. The velocity U_0 (at the outer edge of the liquid boundary layer) presented somewhat similar profiles for the three pressure measurements. The important feature here was the observation that the maximum value occurred in the neighborhood of 50 degrees from the stagnation point. This was well upstream from the point of maximum value of $U_{\rm s}$. The average value of U_0 at its maximum point was 2.8 feet per second and decreased to approximately 1.7 feet per second at the 90 degree point, the nominal separation point.

The boundary-layer separation point was made visible by the injection of a mixture of distilled water and wetting agent into the liquid boundary layer. The separation point observed in this manner agreed with that interpreted from the pressure profiles. For the vertical downflow of a two-phase mixture over a horizontal cylinder a bubble of water was observed downstream of the separation point.

Water was shed from this bubble in the form of vortices. The location of the point of boundary-layer separation was found to be insensitive to the water spray distribution for ratio of mass of water to air less than 0.08. For the case where the gas Reynolds number was varied from

 3.55×10^4 to 1.04×10^5 the point of boundary-layer separation experienced a displacement similar to that found in single-phase flow for the same range of gas Reynolds numbers.

The first analytical model, which assumed a laminar boundary-layer system, where the interface velocity U_0 was assumed constant outside the neighborhood of the forward stagnation point, had as its objective the determination of the separation point. It was found that the calculated boundary-layer thickness from a point in the neighborhood of the stagnation point up to the point of pressure minimum was insensitive to U_0 which was assumed constant for a range of values of U_0/U_∞ up to and including 0.05. However, it was found that the calculated boundary-layer thickness from the point of pressure minimum to the separation point was somewhat sensitive to U_0 and for a value of $U_0/U_\infty = 0.05$ the separation point shifted downstream approximately 1 degree. This only accounted for 12.5 per cent of the change in distance between the point of pressure minimum and the separation point when compared to single-phase flow.

The second model, which assumed a turbulent gas boundary layer and U_0 = 0, was intended to predict that separation would occur for a value of the parameter H between 1.8 and 2.6, the range of H established empirically by von Doenhoff and Tetervin for separation in single-phase flow. But with the experimentally observed pressure profile, this range of H was not attained, and separation actually occurred at a point where the value of H was 1.23 (\pm 0.01 for those cases observed).

The result of a non-zero $\partial U_0/\partial x$ was not investigated in either model.

CHAPTER VII

SUMMARY AND CONCLUSIONS

For the case of two-phase flow (air-water spray) a technique for measuring the pressure profile was developed. The two-phase flow pressure-measuring system was evaluated in single-phase (air) flow with a gas Reynolds number of 5.64 × 10⁴ by comparison with a standard system, which was assumed correct. An error of 1.4 per cent in the pressure measurement was observed at the stagnation point while the maximum error of 5.2 per cent occurred at the point of pressure minimum. These results were considered acceptable, since this represented a severe test of the system, because of the injection of water (whose density is three orders of magnitude greater than air) into the air boundary layer.

Pressure profiles for two-phase flow with a gas Reynolds number of 5.64 × 10⁴ were measured. As a result of addition of water spray to the air flow, the separation point was observed to have shifted downstream approximately 14 degrees for the same gas Reynolds number. The minimum pressure was reduced and its location shifted downstream approximately 6 degrees. The slope of the pressure coefficient curve in the region between the point of minimum value and the location of the wake pressure was less than the slope for the corresponding region in single-phase flow with the same gas Reynolds number. This reduction

in slope permits a greater distance of flow against a positive pressure gradient before separation takes place.

The region of liquid boundary-layer separation was made visible by the injection of a wetting agent into the liquid boundary layer. The region of separation observed in this manner falls within the region predicted by the inflection points on the pressure profiles. It was observed that the point of separation for a given gas Reynolds number was not strongly affected by variations in water spray distribution (mass ratio of water to air less than 8 per cent). The region of separation moved with changes in gas Reynolds number. This response to change in Reynolds number was similar to that experienced in single-phase flow.

Photographs of the region of separation revealed the presence of vortices in the separated liquid flow layer for the cases of vertical downflow over a horizontal cylinder. The vortices were observed to have an axis of rotation in the streamwise direction. The shedding of vortices from the region of separated liquid flow was observed to occur in random order. No such vortices were observed in horizontal flow over a vertical cylinder.

In the closing remarks of Section 2.3 it was indicated that the two analytical models would not be expected to predict the same results, since they represent different types of flow structure. The first analytical model failed to predict a sufficient displacement of the separation point. The observed displacement occurred eight degrees further downstream from the point of pressure minimum as compared to single-phase flow for the same gas Reynolds number. The analytical model only predicted 12.5 per cent of this value $U_0/U_\infty = 0.05$, which

was found to be a reasonable value of U_0 for those cases considered. The second analytical model failed to predict separation under the assumption that separation would occur when H was bounded between 1.8 and 2.6. The observed separation occurred when H increased to a value of 1.23 ($^{\pm}$ 0.01 in those cases observed). The first analytical model predicted separation prior to the observed condition while the second analytical model did not indicate the fulfillment of the assumed separation criterion.

As a result of the experimental investigation a successful technique was developed for measuring the pressure profile of a surface in two-phase flow. A system employing liquid-filled pressure lines and injection of a small amount of liquid into the liquid boundary layer gave reasonable repeatability and a minimum of hysteresis effect. It was found that the pressure at a given point would vary $^{\pm}$ 0.01 inch of water when measured from ascending values and then descending values of $^{\Phi}$. These results compare favorably to similar observations made in single-phase flow with an inclined manometer utilizing air filled pressure lines. The rate of water injection, which was determined experimentally, was 1.4 milliliters per minute. The flow rate should be determined experimentally for each new application or range of gas Reynolds numbers.

A system for the visual observation of the region of boundary-layer separation was developed. This was accomplished by the injection of a small amount of mixture, consisting of distilled water and wetting agent, into the liquid boundary layer from one of the pressure taps. The point of boundary-layer separation and some of the properties of the separated liquid flow were made visible by the injection process.

The separation point observed by this process agreed with that interpreted from the observed pressure profiles.

The observed pressure profile and the observed thickening of the liquid boundary layer in the region between the point of pressure minimum and the separation point indicate that the external flow field sees an object of shape sufficiently different from the cylinder that neither of the analyses based on a circular cylinder gives a reasonable prediction of separation.

It is concluded that for the case of vertical downflow of a two-phase (air-water spray) mixture over a circular cylinder one may expect the point of boundary-layer separation for the range of Reynolds numbers considered (3.55 \times 10⁴ to 1.04 \times 10⁵) to be approximately 14 degrees downstream from the point of separation in single-phase flow at the same Reynolds number.

Further studies are suggested along several lines: (a) obtain the boundary-layer properties in the region of the forward stagnation point, (b) determine the effect of droplet size on the boundary-layer properties, (c) investigate the phenomenon of droplet bouncing and fluid splashing from the liquid film, (d) study the origin and properties of the vortices, (e) determine what effect the addition of a streamline section to the back side of the cylinder would have on separation and (f) investigate the properties of the liquid bubble located downstream of the separation point. An investigation including an analysis of the liquid boundary layer is recommended as this might yield improved separation prediction.

APPENDIX A

GRAVITATIONAL EFFECTS

The experimental apparatus was so designed that the test cylinder was in a horizontal plane and experiencing downward flow of a two-phase mixture; under these conditions the gravitational force was in the free-stream direction. The objective of the phase of the investigation reported in this appendix was to determine if the gravitational force may be neglected when considering the behavior of the boundary layer up to the point of flow separation.

The boundary-layer separation point was first observed and photographed for the vertical downflow over a horizontal cylinder (Figure 41). A test cylinder was then installed in a vertical position in a horizontal wind tunnel. The free-stream velocity was adjusted to give the same gas Reynolds number (5.64 x 10⁴) used in the vertical wind tunnel and the mass ratio of water to air was adjusted to the same range of values (approximately 0.05). Under these test conditions two sets of observations were made. The first utilized the technique of injecting a mixture of distilled water and wetting agent into the liquid boundary layer and the second required the use of dye injection into the boundary layer.

The results of the injection of the distilled water and wetting agent are shown in Figure 51. The injection was at the middle of the cylinder and 10 degrees downstream from the forward stagnation point.

Separation was observed to take place in the same neighborhood as that of the horizontal cylinder and vertical downflow. The significant change here was the shedding of water from the region of separated flow. A water bubble similar to that observed for the horizontal cylinder but located at the separation point was present and it was from this bubble that water left the cylinder. For the vertical cylinder it was observed that the primary method of water shedding was by gravity flow down the bubble, which was parallel to the cylinder axis. There was some evidence of water leaving the cylinder in the gas streamwise direction, but this was only a small fraction of the water flow.

The second set of experiments utilized a dye injected into the liquid boundary layer using the same pressure tap for the dye injection. It was observed that the dye on entering the liquid boundary layer would diffuse in a radial direction from the pressure tap, which meant that some of the dye was transported upward and some in a downward direction. The mixture of dye and water would then flow around the cylinder in a nearly horizontal plane to the separation point (Figure 52 is a typical photograph of the process), and the mixture then would turn and flow down the cylinder within the liquid bubble.

From these two experiments one concludes that the effect of gravity is negligible in the boundary-layer flow and has negligible effect on the location of the separation point, but once the flow separates from the cylinder gravitational forces are not negligible. The investigation did not consider the possible case of the vertical upflow of a two-phase mixture.

APPENDIX B

FIGURES

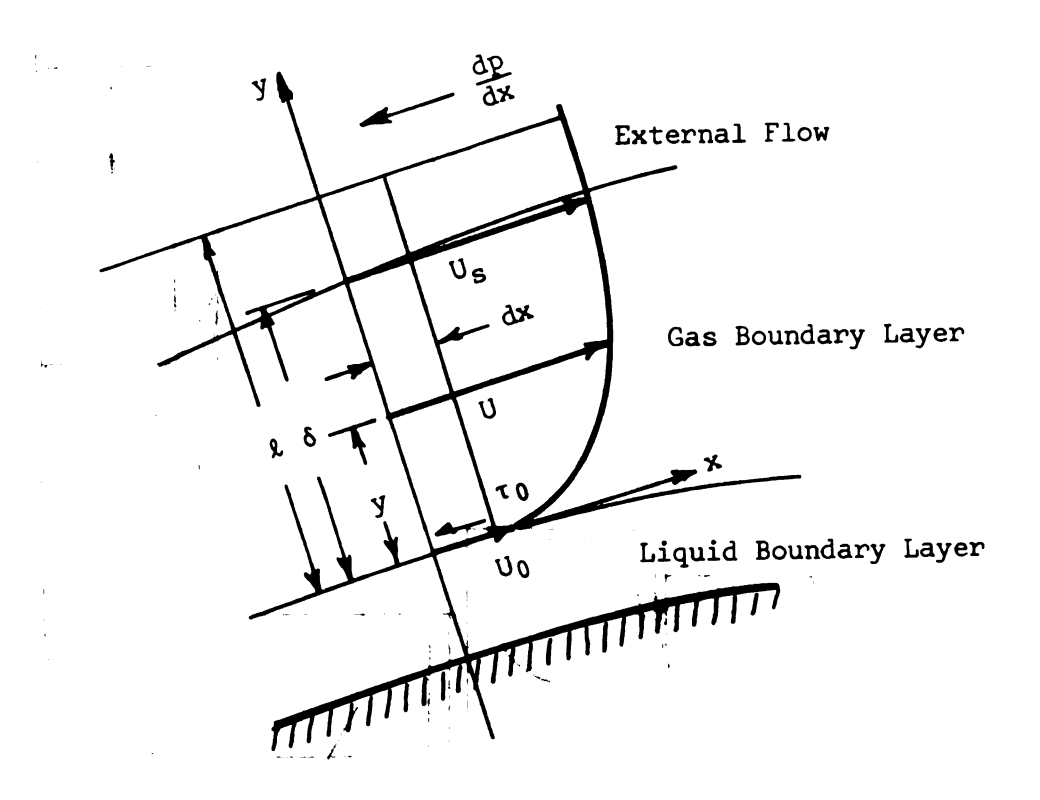
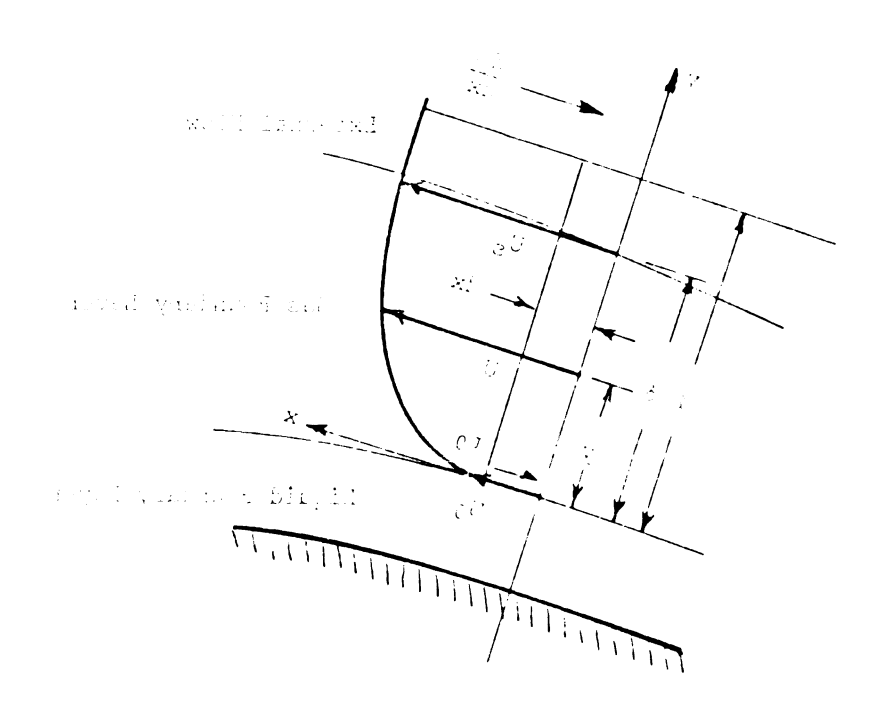
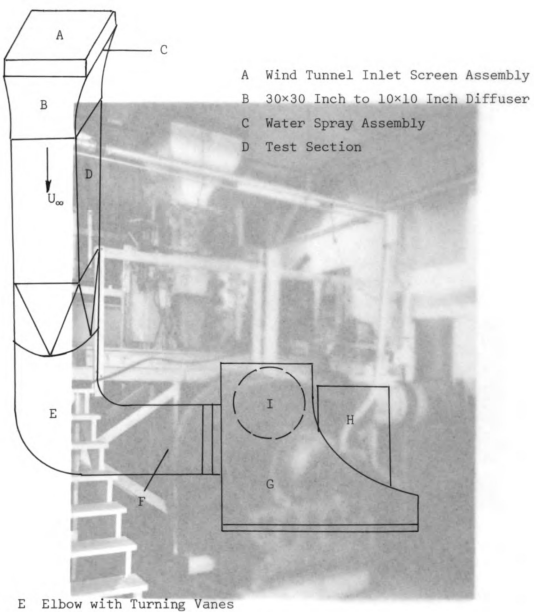


FIGURE 1 Boundary Layer Quantities for Gas Boundary Layer

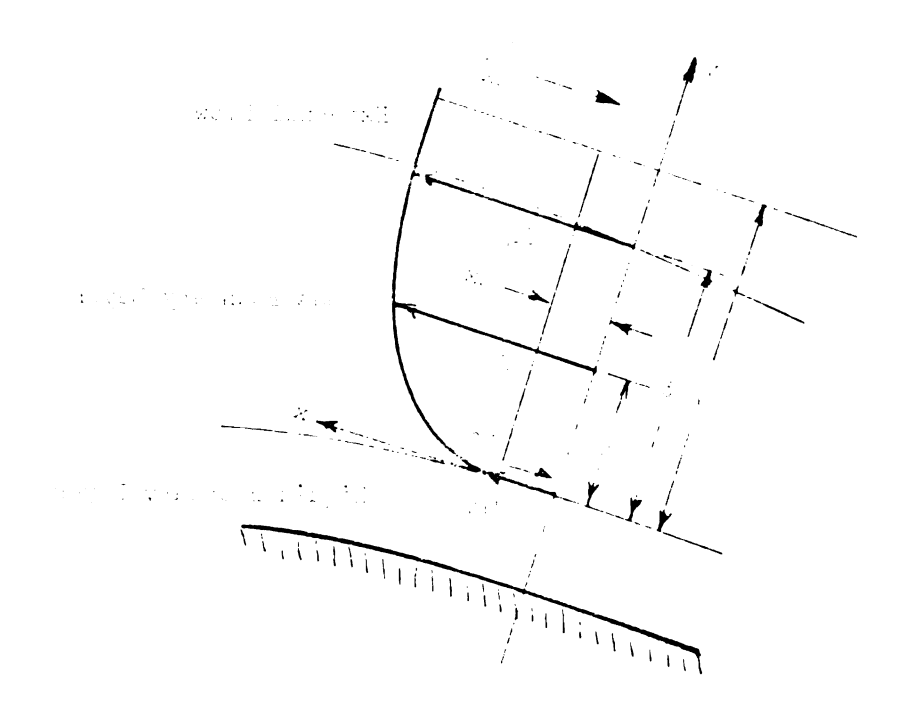


83



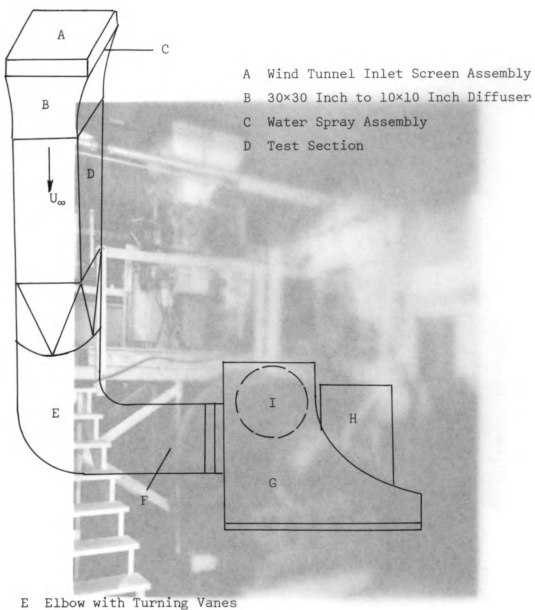
- F Auxiliary Water Spray Assembly
- G Two-Stage Fan
- H Electric Motor
- I Fan Outlet Duct and Butterfly Valve Assembly

FIGURE 2 Schematic Drawing of AFIT 10"×10" Wind Tunnel



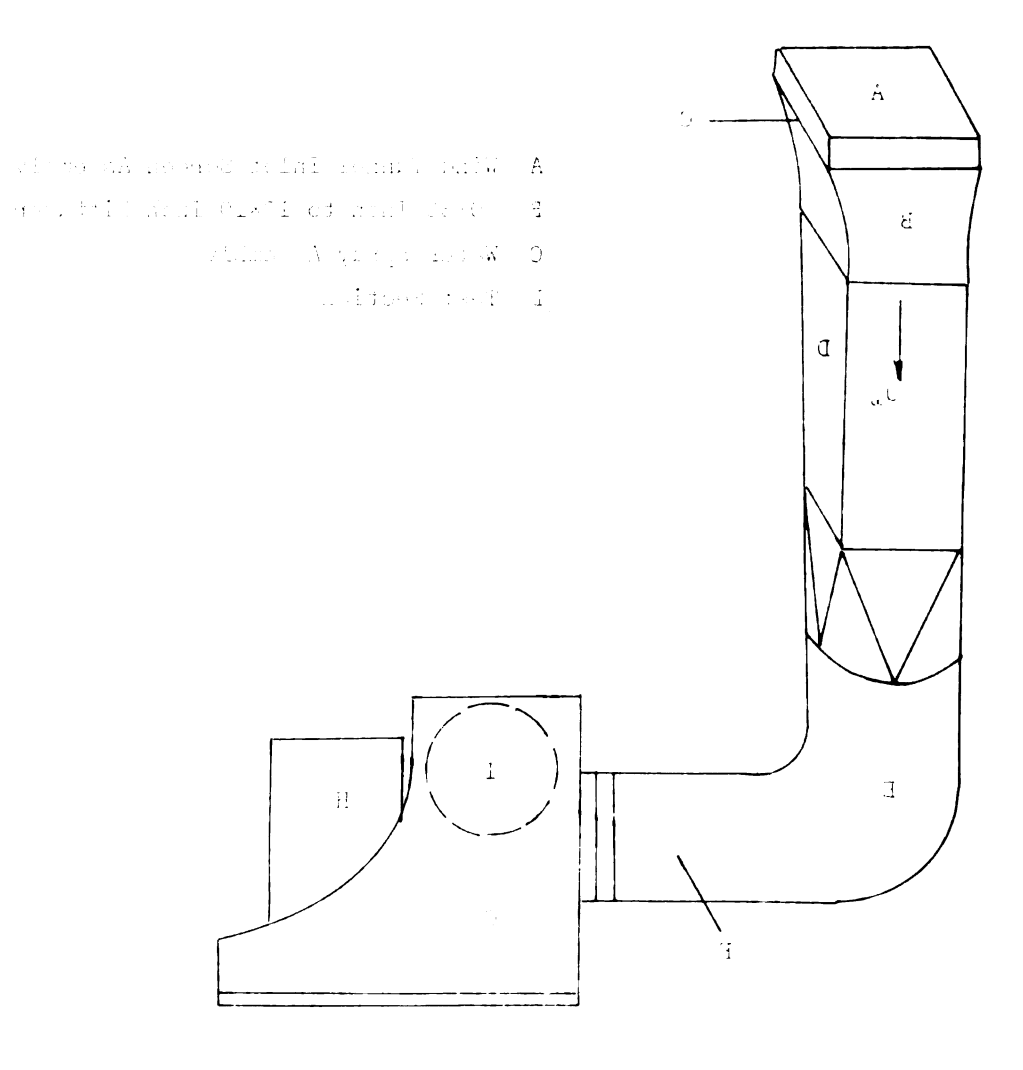
Plant 1 - Boardary Layer Coast the state of boardary land

83



- F Auxiliary Water Spray Assembly
- G Two-Stage Fan
- H Electric Motor
- I Fan Outlet Duct and Butterfly Valve Assembly

FIGURE 2 Schematic Drawing of AFIT 10"×10" Wind Tunnel



€ક

- E Ellow with Turnian Vance
- F Admiliary Water Sprey Arms over
 - G Two-State Path
 - H Electric Motor
- I Fam Outlet Dast and Suttently Valve Associng

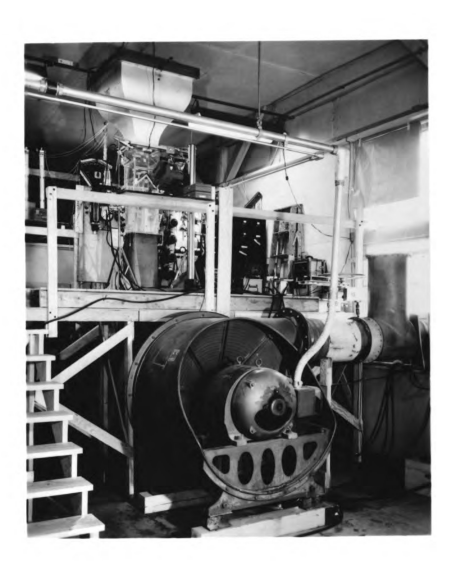


FIGURE 3 AFIT 10" × 10" Wind Tunnel

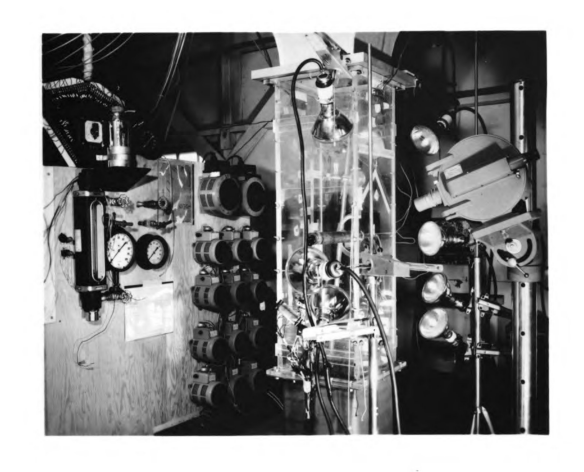


FIGURE 4 Test Section of AFIT 10" × 10" Wind Tunnel

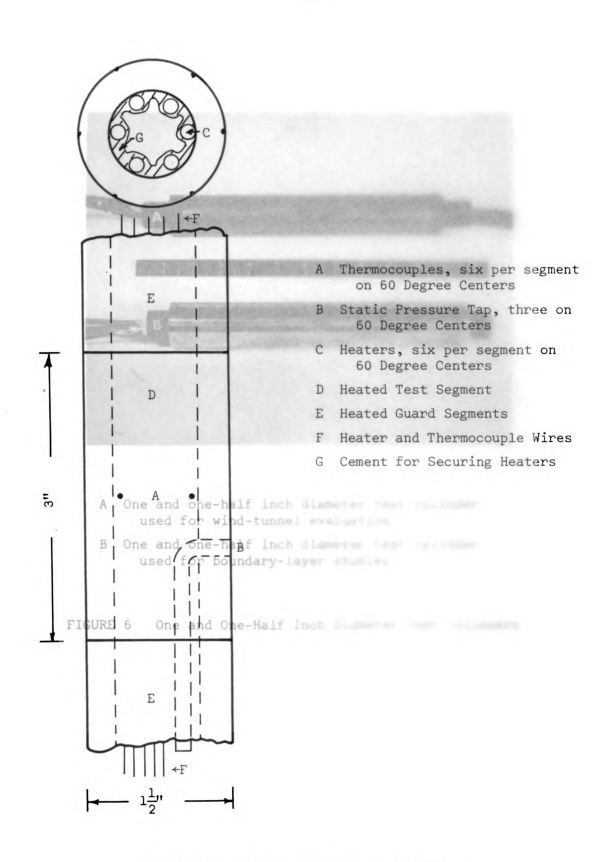
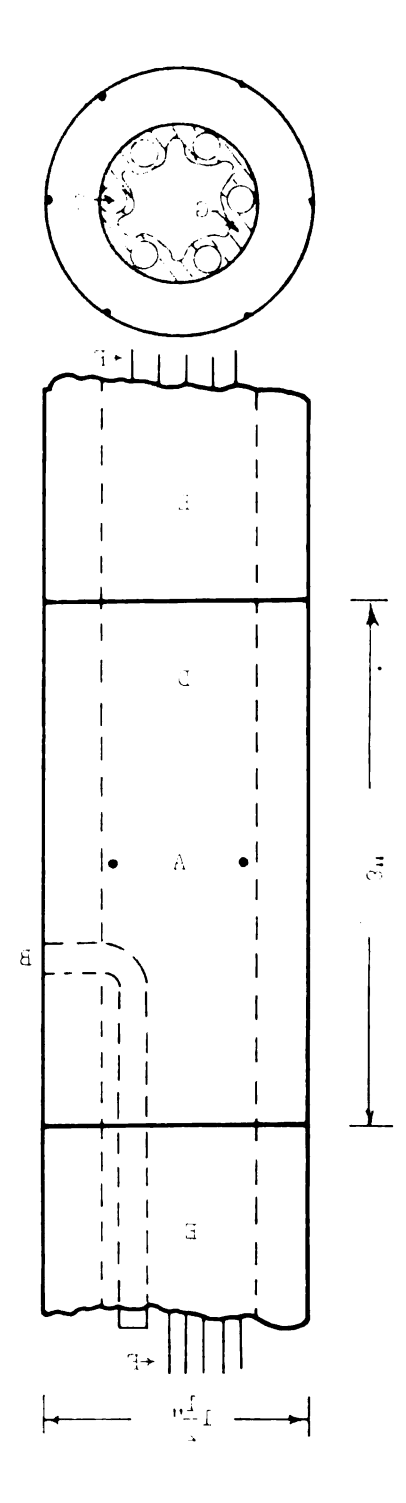
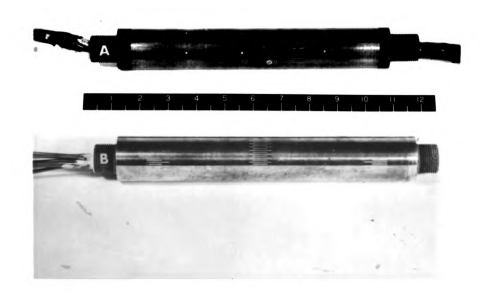


FIGURE 5 Schematic of Test Cylinder



- A Thermore is a six person of the separate of the same of the same
- no esnir .ur" endemil (1777) d proteste esnir (3
 - C Heatens, six per distriction 60 February Contents
 - object;od dod betodi G
 - E isabel soor servicets
- P. Sarter and Theregorouses wires.
 - G Patratical Socuring that to



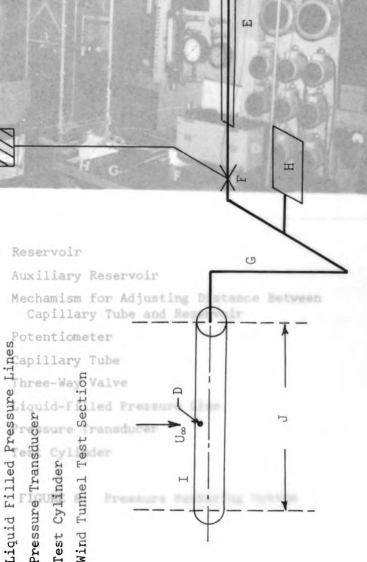
- A One and one-half inch diameter test cylinder used for wind-tunnel evaluation
- B One and one-half inch diameter test cylinder used for boundary-layer studies

FIGURE 6 One and One-Half Inch Diameter Test Cylinders

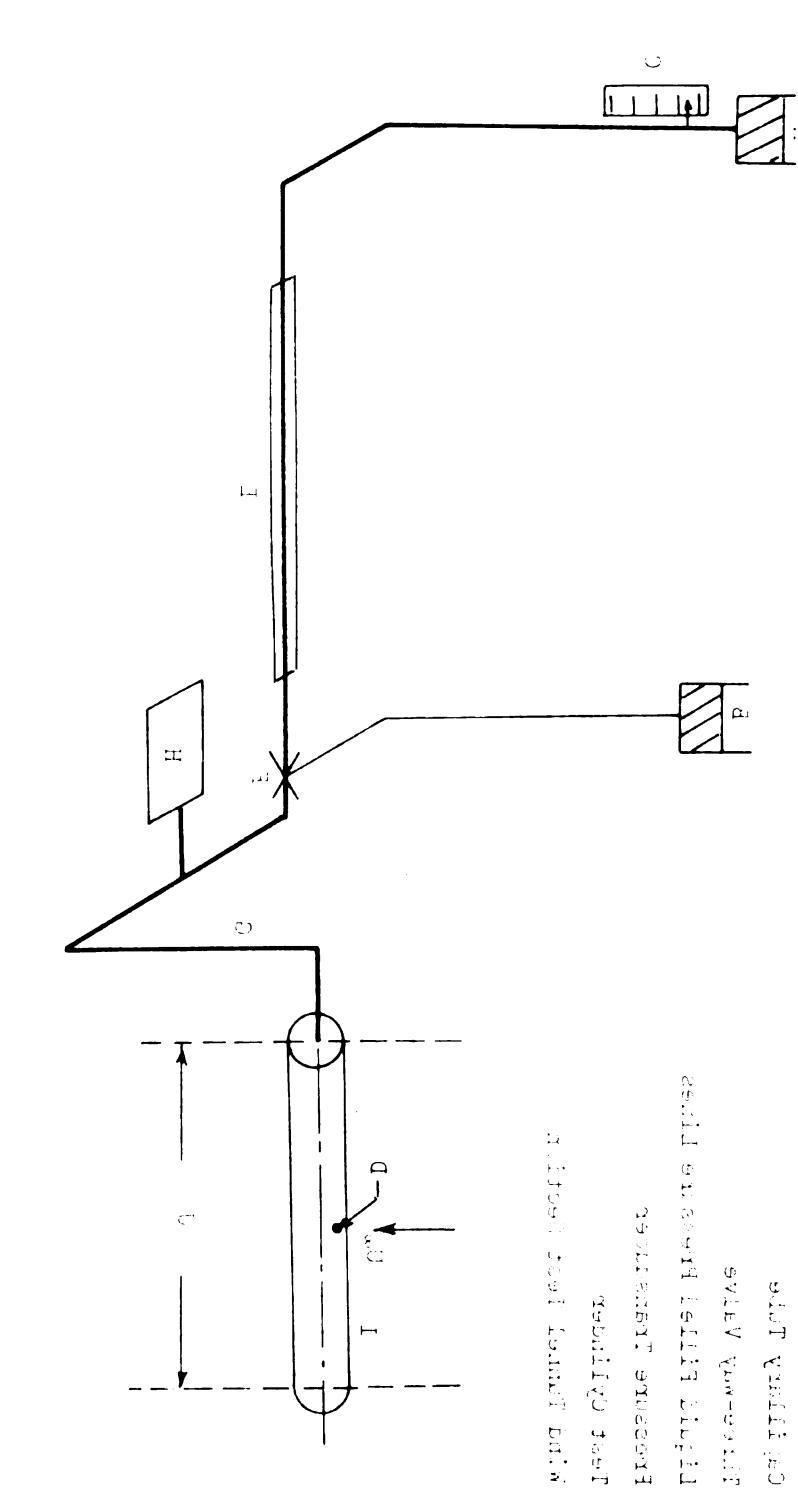




- Auxiliary Reservoir
- Scale & Reservoir Support
- Pressure Tap
- Capillary Tube
- Three-Way Valve
- Liquid Filled Pressur
- Pressure Transducer



Schematic Drawing of Pressure Measuring System FIGURE 7



Section and a new Heavise will be golden to bit mendes

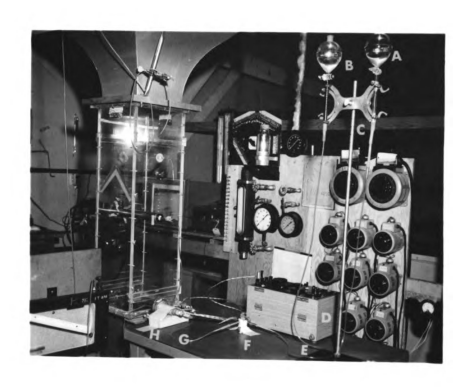
Adxified Reservoin

Soule & Paseutoju počious

Frecente 1et

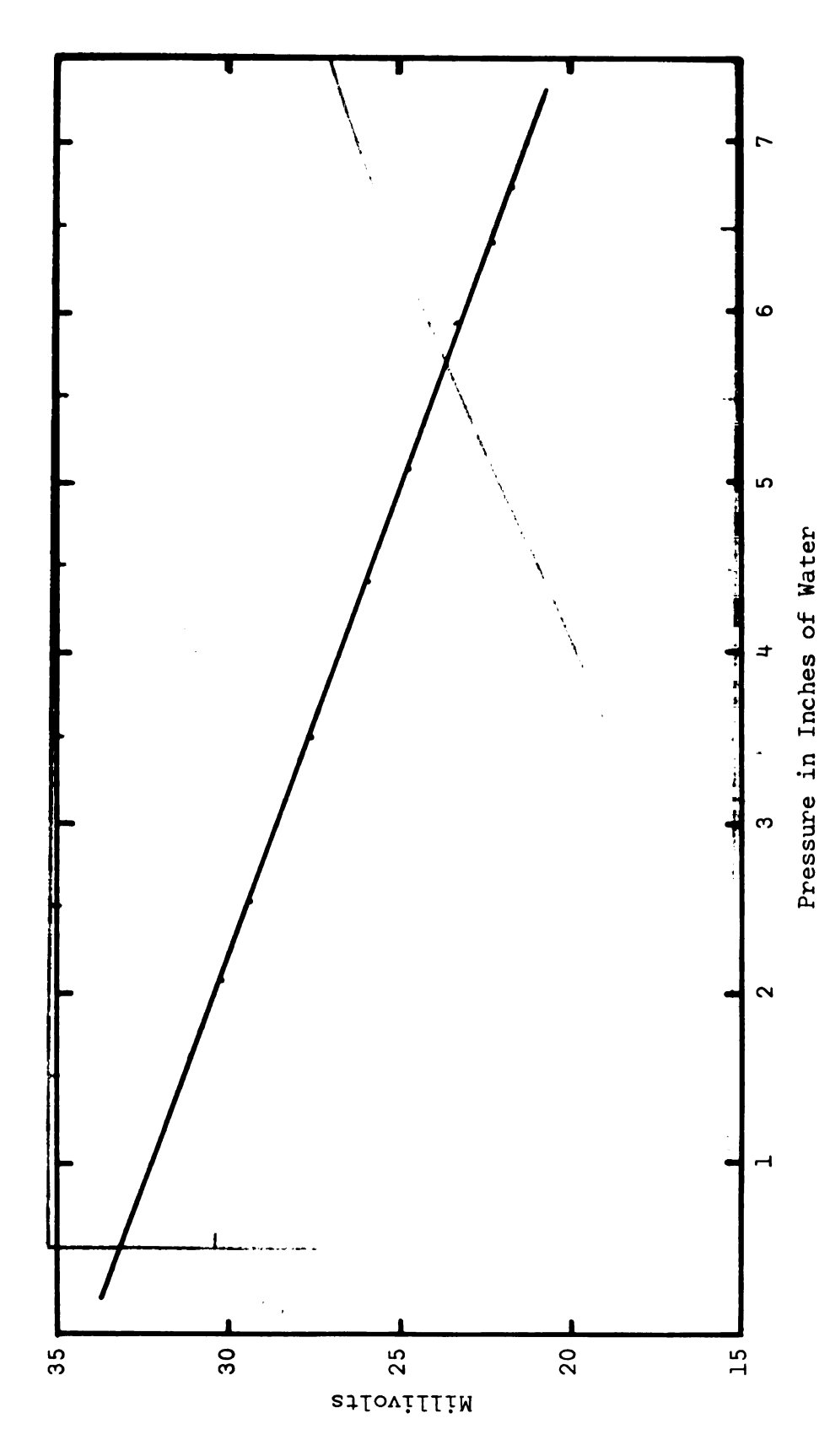
۲. ن

<u>piovresok</u>

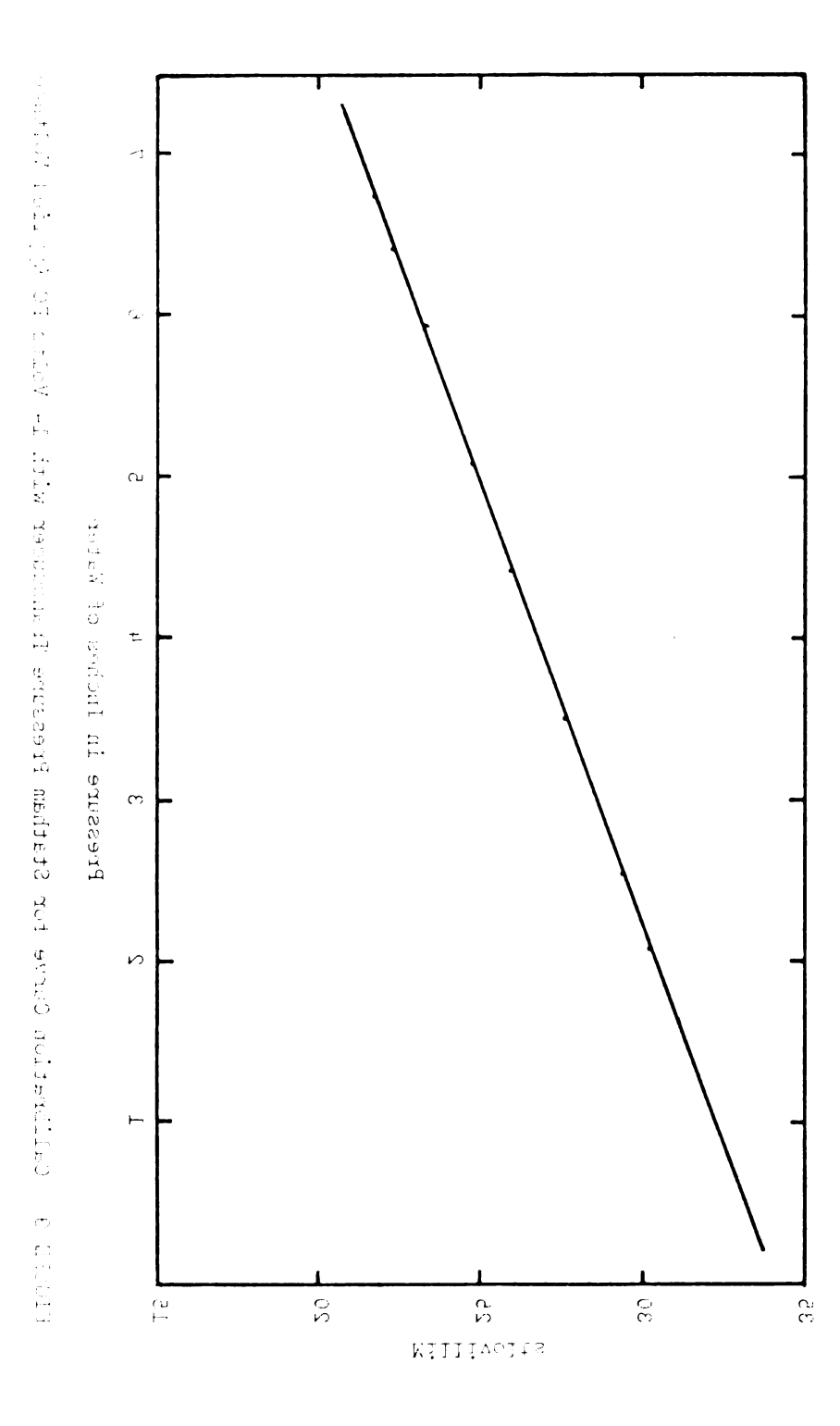


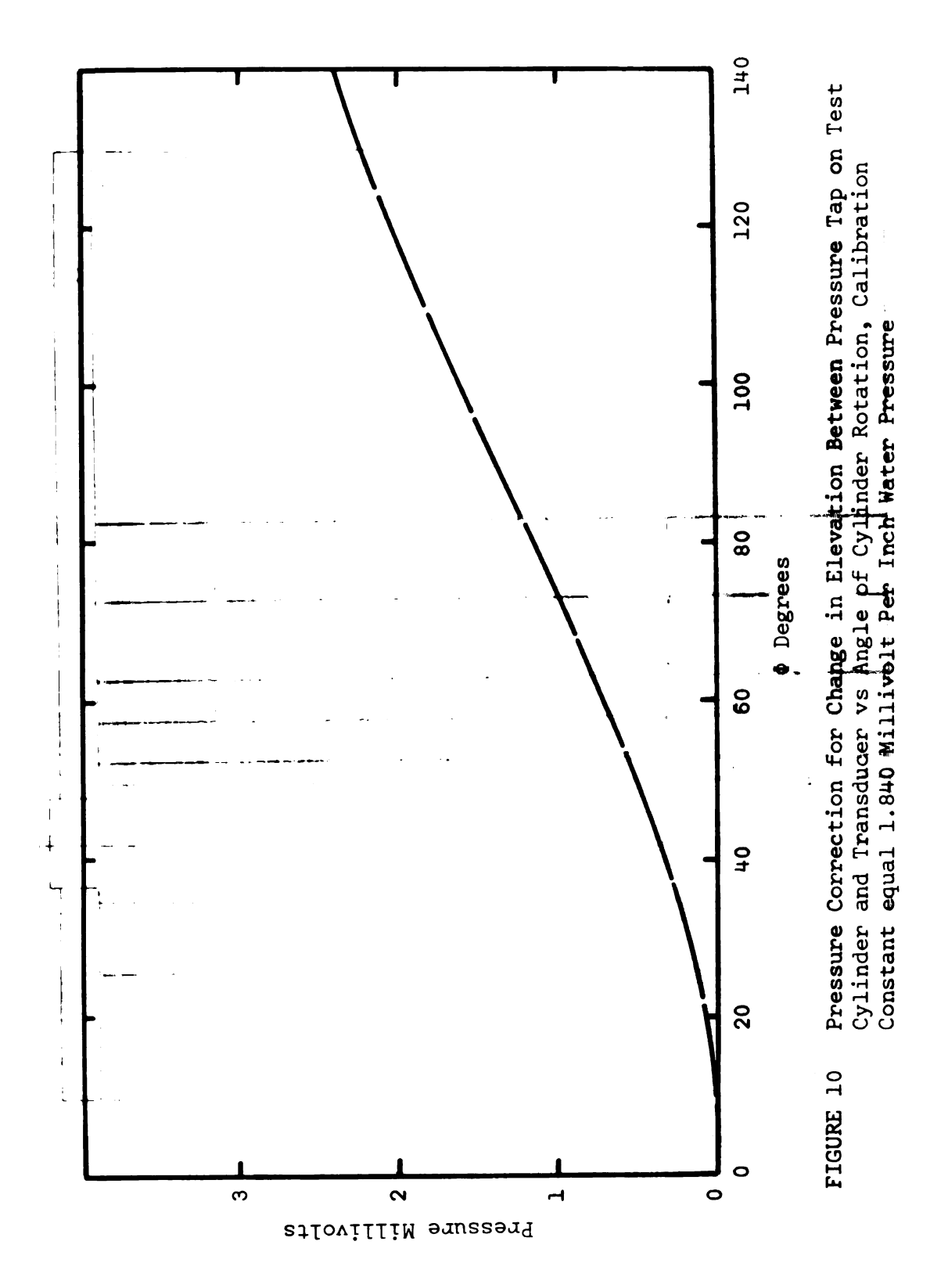
- A Reservoir
- B Auxiliary Reservoir
- C Mechamism for Adjusting Distance Between Capillary Tube and Reservoir
- D Potentiometer
- E Capillary Tube
- F Three-Way Valve
- G Liquid-Filled Pressure Line
- H Pressure Transducer
- I Test Cylinder

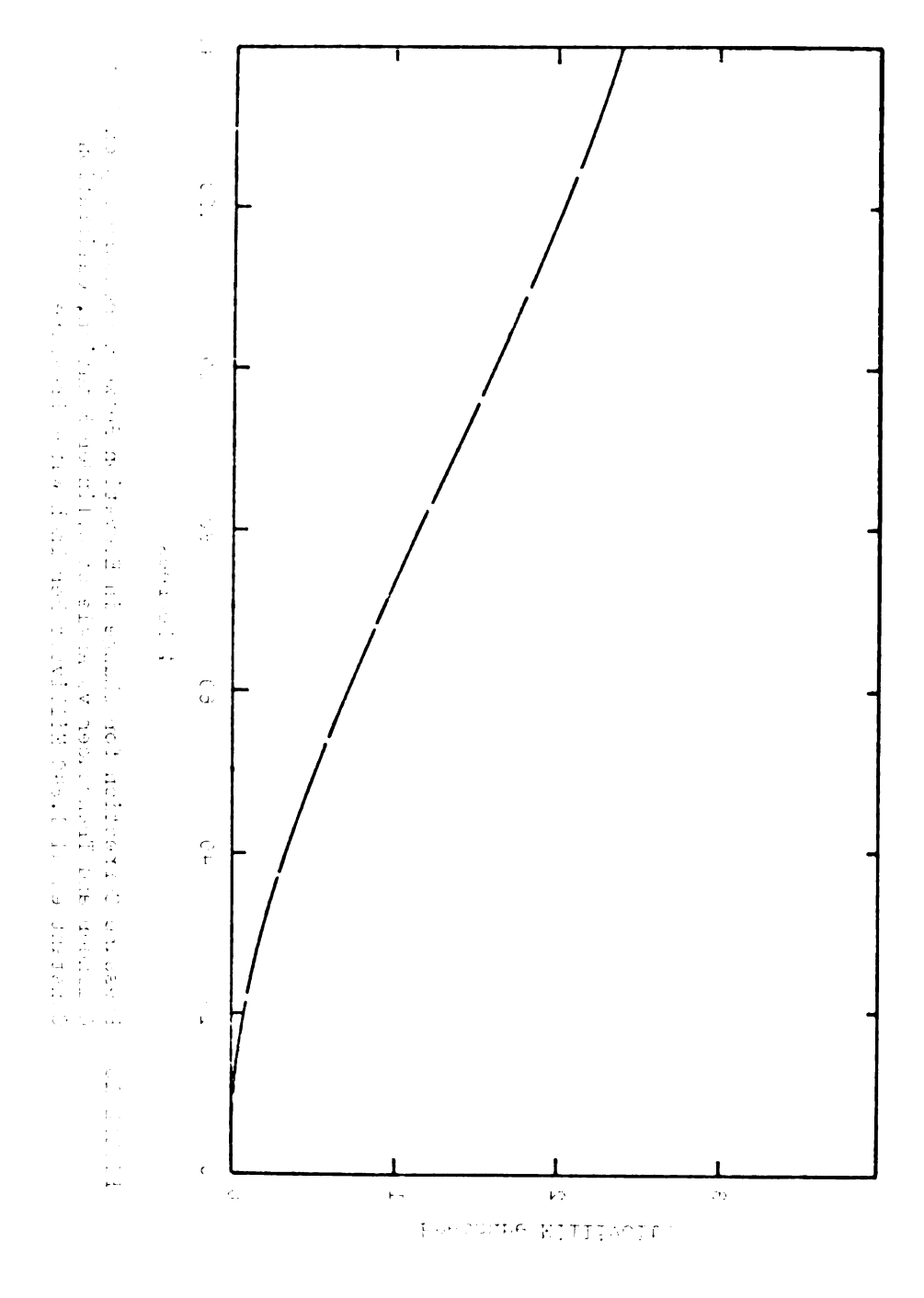
FIGURE 8 Pressure Measuring System



Calibration Curve for Statham Pressure Transducer with 14 Volts DC Applied Voltage FIGURE 9







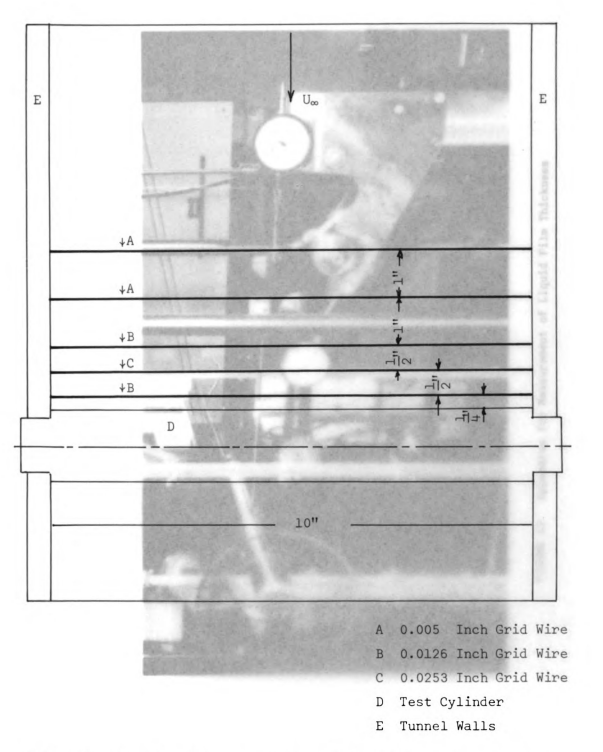


FIGURE 11 $\,$ Grid Wire Layout for Droplet Velocity \mathbf{U}_{d} Measurement

A 0.005 Inch 7:13 Wins

estW sink domi std.0.0 g

eath find must dark a be

 $\sigma_{2} = \{1, \dots, 0\} = \{1, \dots, 1\} = \{1, \dots, 1\}$

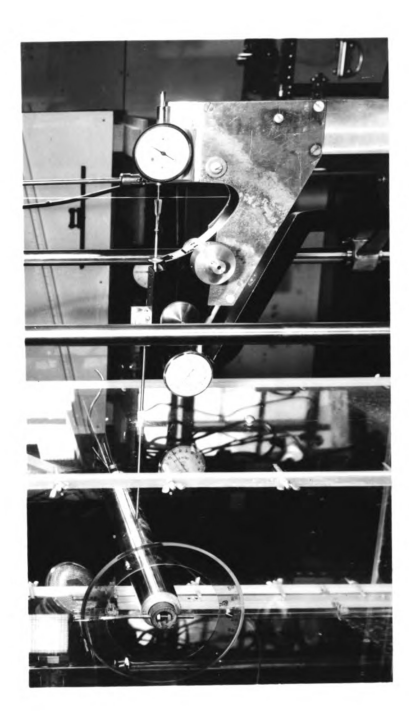


FIGURE 12 Apparatus for Measurement of Liquid Film Thickness

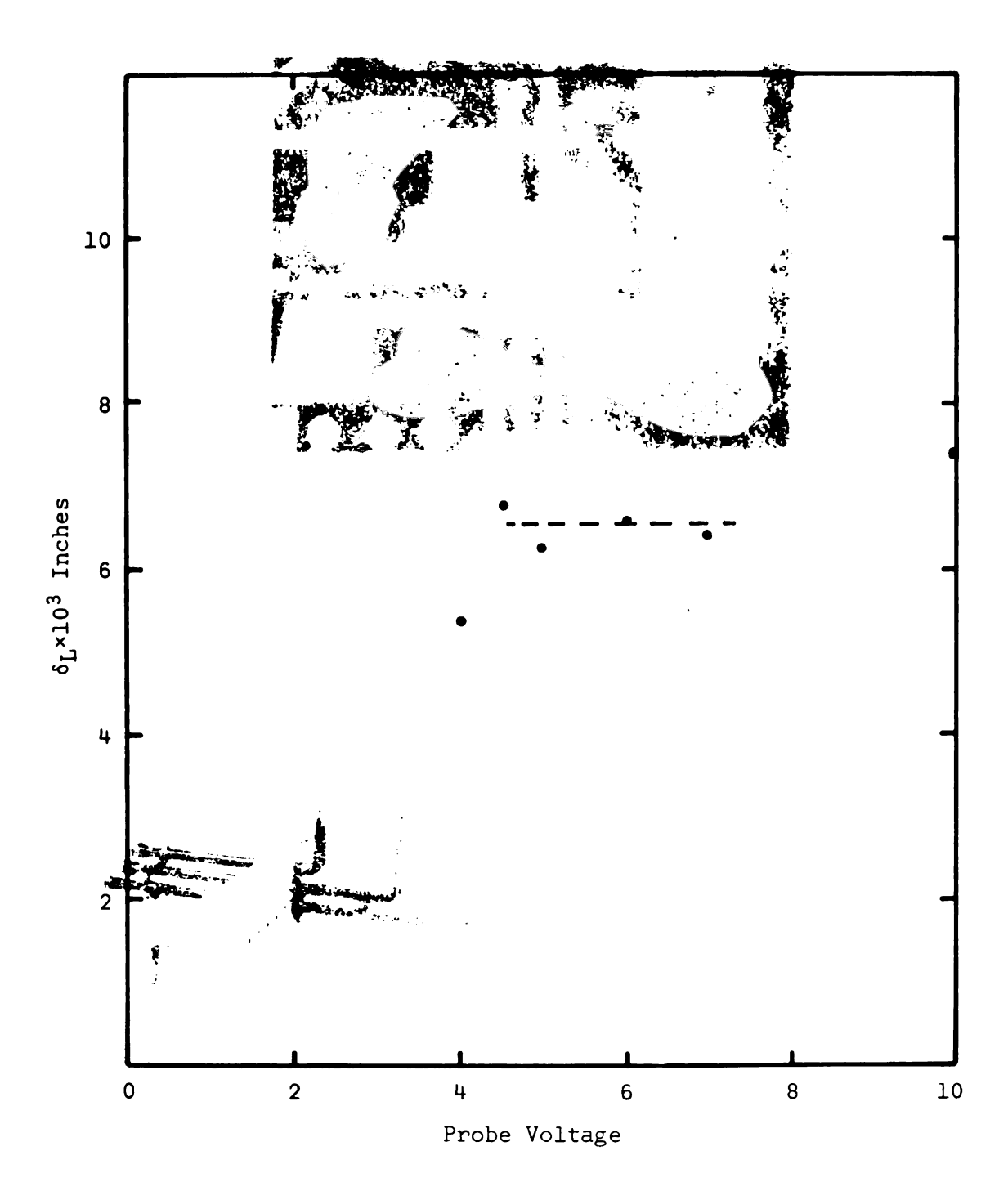


FIGURE 13 Liquid Film Thickness vs Probe Voltage, Φ = 90°, P_{W} = 20 psig

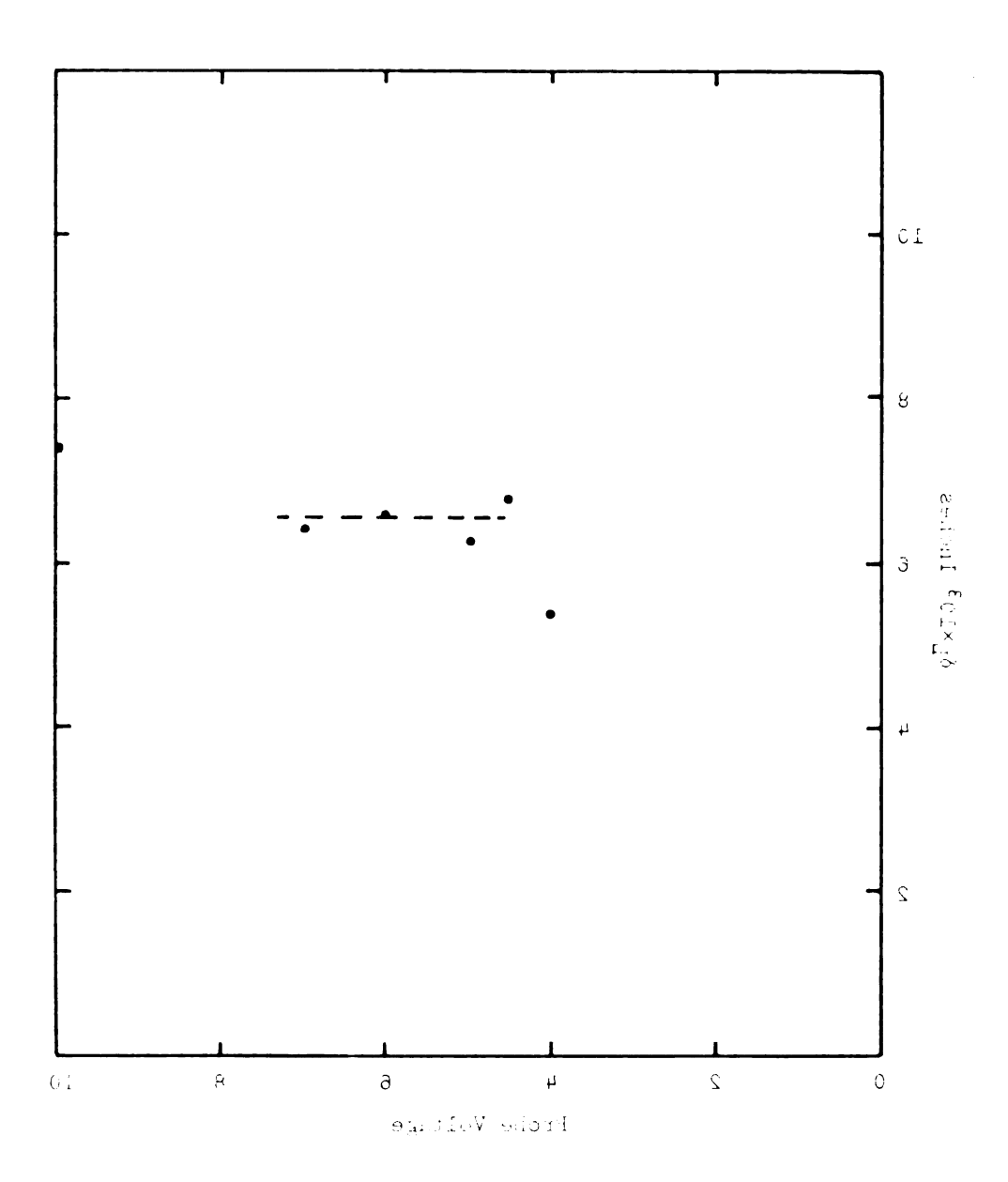


FIGURE 13 — Liquid Film Taichness vs Prole Volcage, $\phi = 60^\circ$, $P_W = 20$ psig

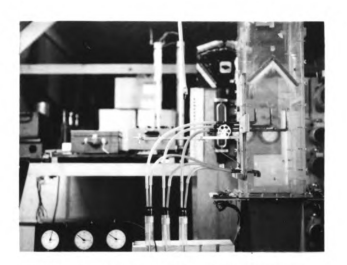


FIGURE 14 Droplet Capture Tube Apparatus



FIGURE 15 (a) One-Half Inch Capture Tube

(b) Three-Eighths Inch Capture Tube

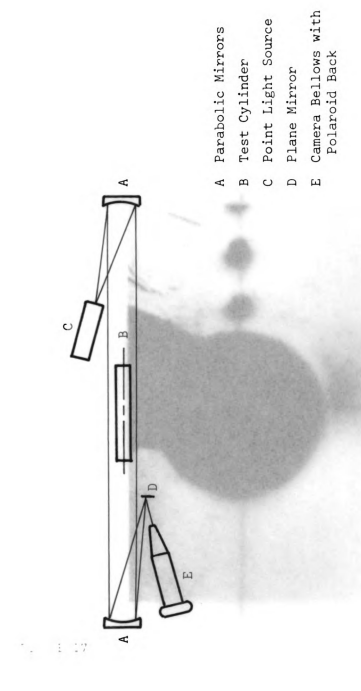


FIGURE 16 Schematic Drawing of Schlieren Apparatus

Parabolic Winners

Test Cylinea

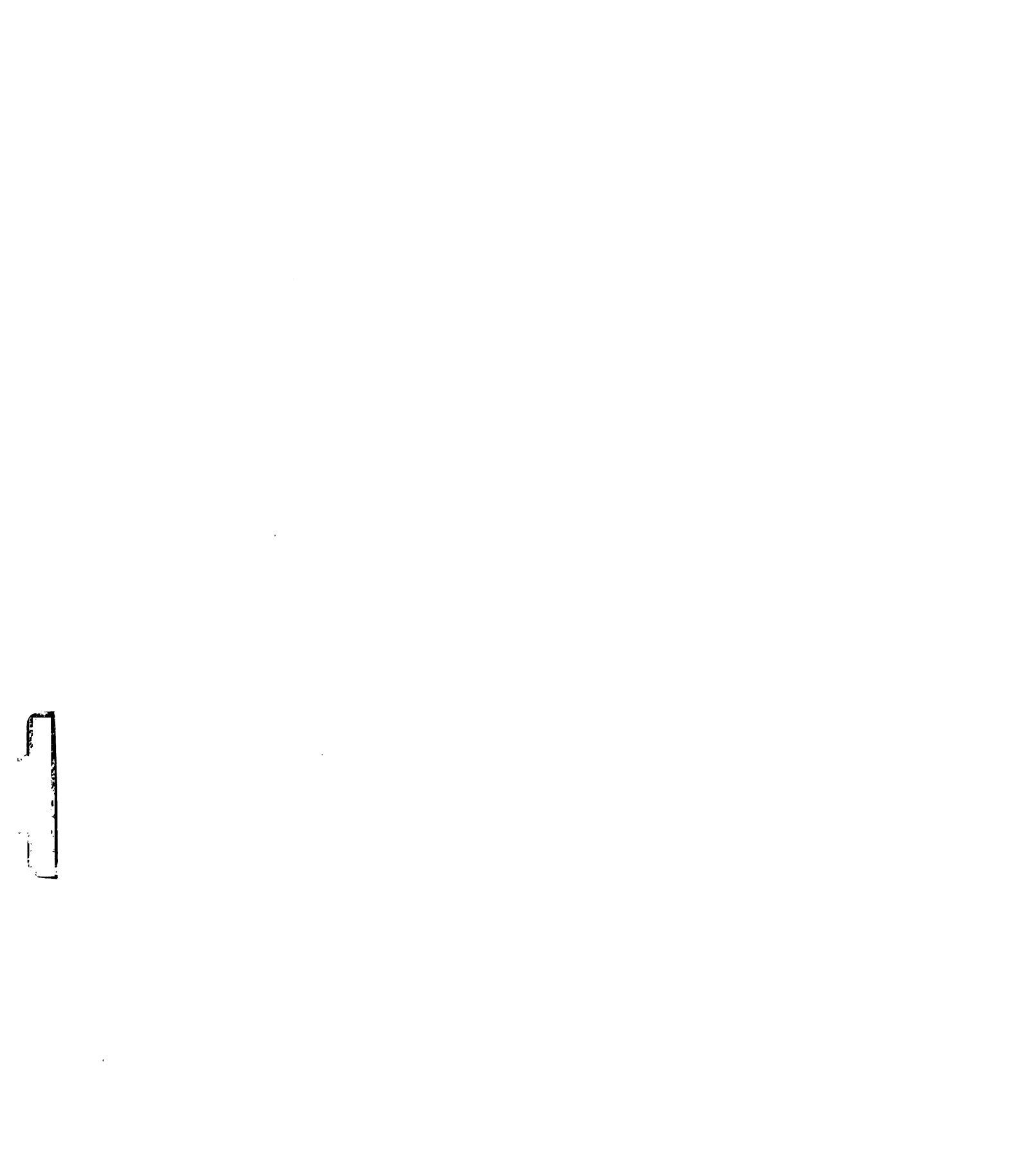
som of disil duion) # p.

Fulstord From Alth. Commens Religions Alth.

esten in dereited to spike dicitemento? al Islanda



FIGURE 17 Boundary-Layer Separation in Single-Phase Flow with Forward Stagnation Point at Top of Cylinder, Reynolds Number equal 5.64×10*



```
SUBROUTINE RUNGA
      M=M+1
      GO TO (10,11,12,13,14),M
10
      RETURN
11
      DO 20 J=1,N
20
      OLDY(J)=Y(J)
      DO 21 J=1,N
21
      PHI(J)=F(J)
      DO 22 J=1,N
      Y(J)=OLDY(J)+.5*H*F(J)
22
      X=X+.5*H
      RETURN
12
      DO 23 J=1,N
23
      PHI(J)=PHI(J)+2.*F(J)
      DO 24 J=1,N
24
      Y(J)=OLDY(J)+.5*H*F(J)
      RETURN
13
      DO 25 J=1,N
25
      PHI(J)=PHI(J)+2.*F(J)
      DO 26 J=1,N
26
      Y(J)=OLDY(J)+H*F(J)
      X=X+.5*H
      RETURN
14
      DO 27 J=1,N
27
      PHI(J)=PHI(J)+F(J)
      DO 28 J=1,N
      Y(J)=OLDY(J)+PHI(J)*H/6.
28
      M=0
      RETURN
      END
```

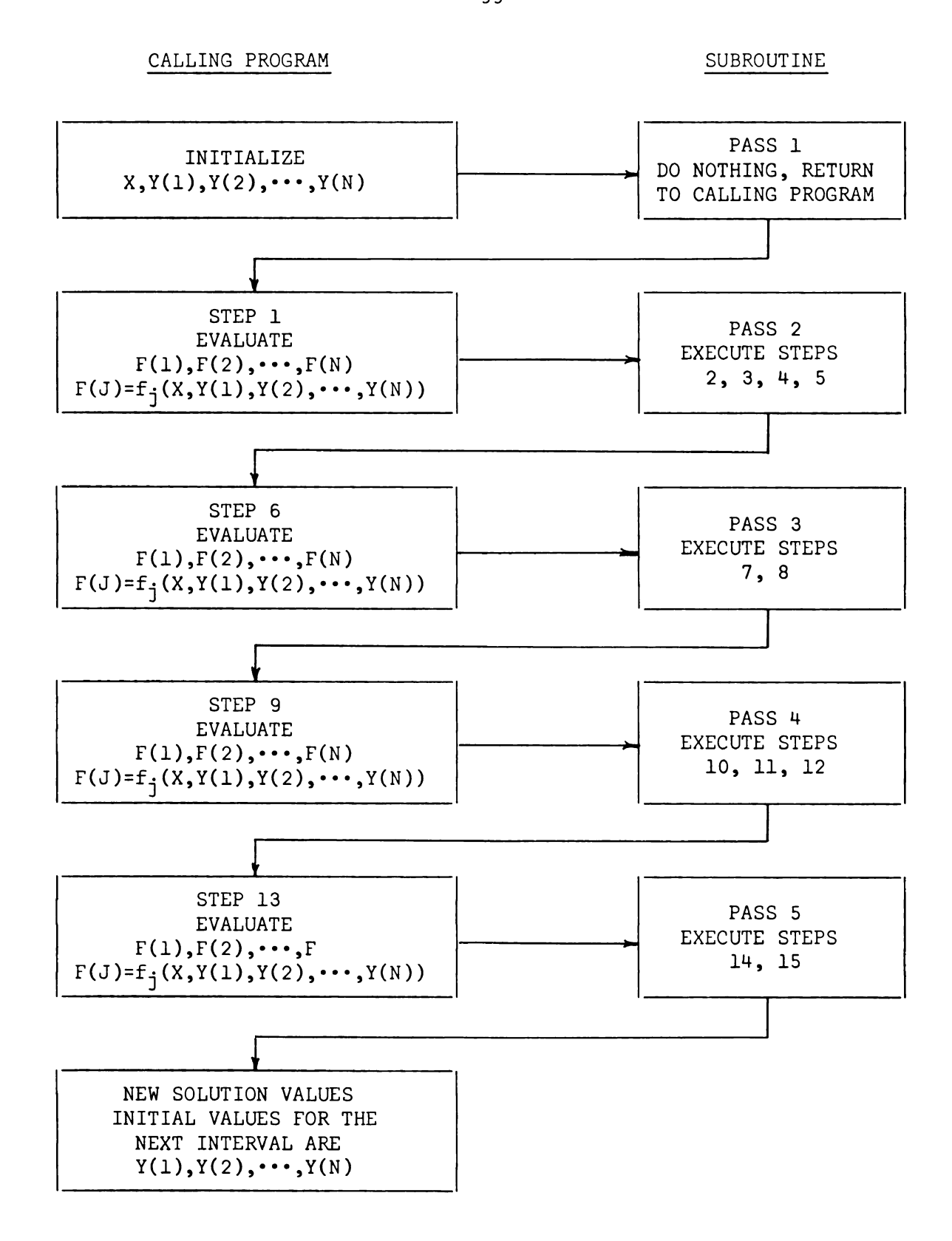


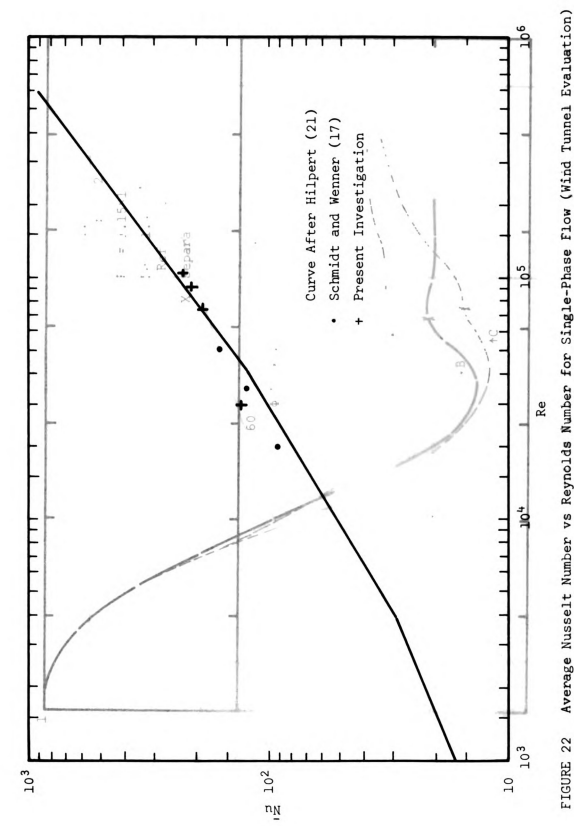
FIGURE 19 Computer Flow Chart for Runge-Kutta Subroutine

```
C C RUNGA-KUTTA SOLUTION OFR DIFF EQNS WRIGHT
      DIMENSION Y(5),F(5),OLD(5),PHI(5),OLDY(5),A(5)
      READ, N
6
      READ, H, XMAS, ICNT
      PUNCH 100, H, XMAX, ICNT
100
      FORMAT(2HH=,F5.3,4X,5HXMAX=,F6.3,4X,4HINT=I2)
      READ, X, Y(1), XL, DB, CC
      PUNCH 101, X, Y(1), XL, DB, CC
101
      FORMAT(5E14.6)
      M = 0
44
      K=ICNT
33
      IF(X-XMAX)3,6,6
3
      CALL RUNGA
      IF(M)1,2,1
52
      READ, CC, (A(L), L=1,5)
1
      IF(X-CC)51,51,52
51
      Q=A(1)+(((A(5))*X+A(4))*X+A(3))*X+A(2))*X
      QPR=A(2)+(((4.*A(5))*X+3.*A(4))*X+2.*A(3))*X
      Q2PR=2.*A(3)+(12.*A(5)*X+6.*A(4))*X
      XL=Y(1)*QPR
      B= 1. - DB/Q
      FUDU=Q*Q2PR/(QPR*QPR)
      BB=9072.+(292.5*B-1965.6)*XL
      C=(80.4-33.*B+4.8*FUDU)*XL*XL
      D=(1.+FUDU)*XL*XL*XL
      AA=(((-XL+39.6*B-45.36)*XL+B*(544.32-331.2*B))*Q)
      F(1)=.8*(BB+C+D)/AA
      GO TO 33
2
      K=K-1
      IF(K)3,4,3
4
      PUNCH 102,X,Y(1),XL
      FORMAT(F6.3,2(E15.8))
102
      GO TO 44
```

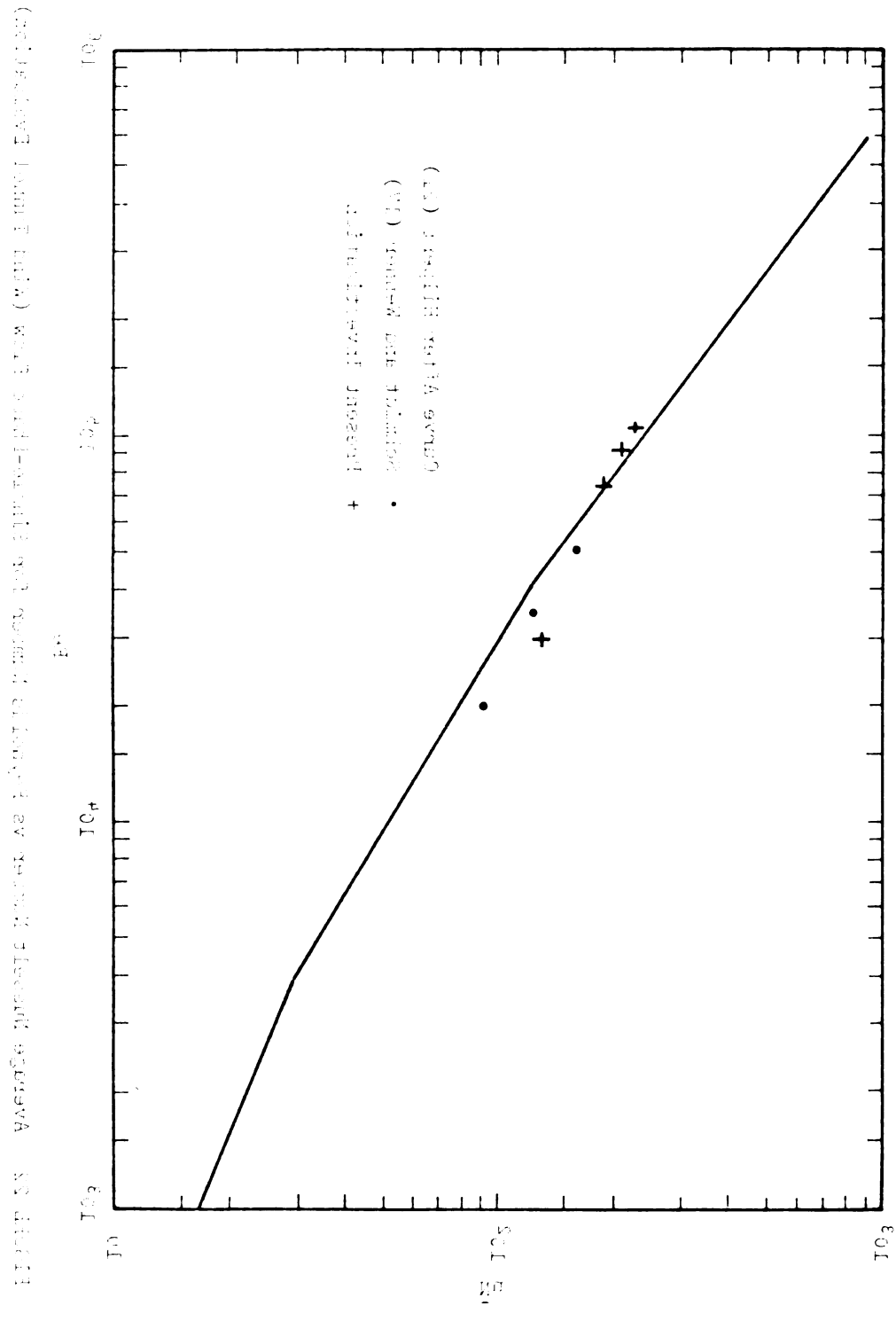
100

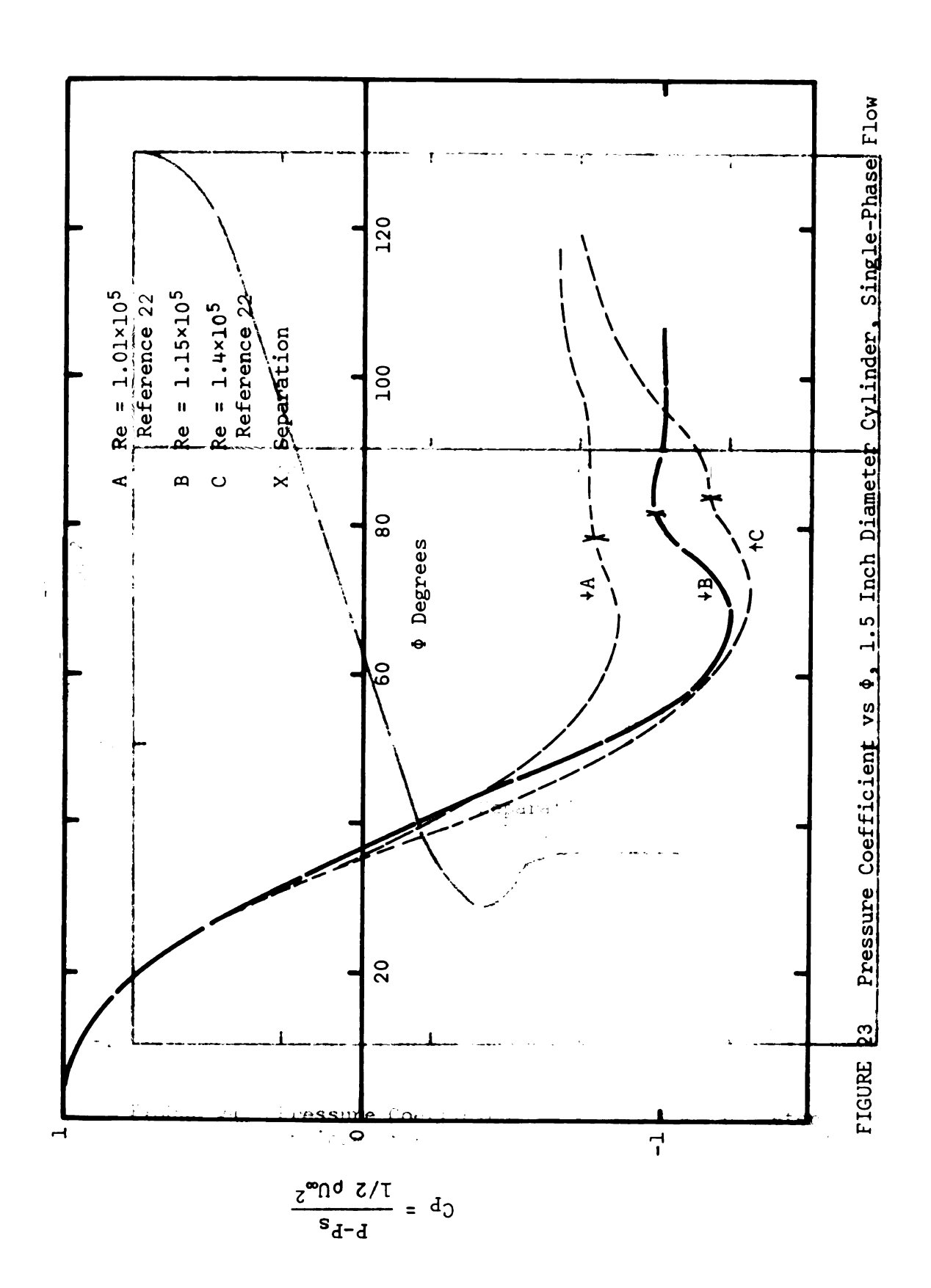
101

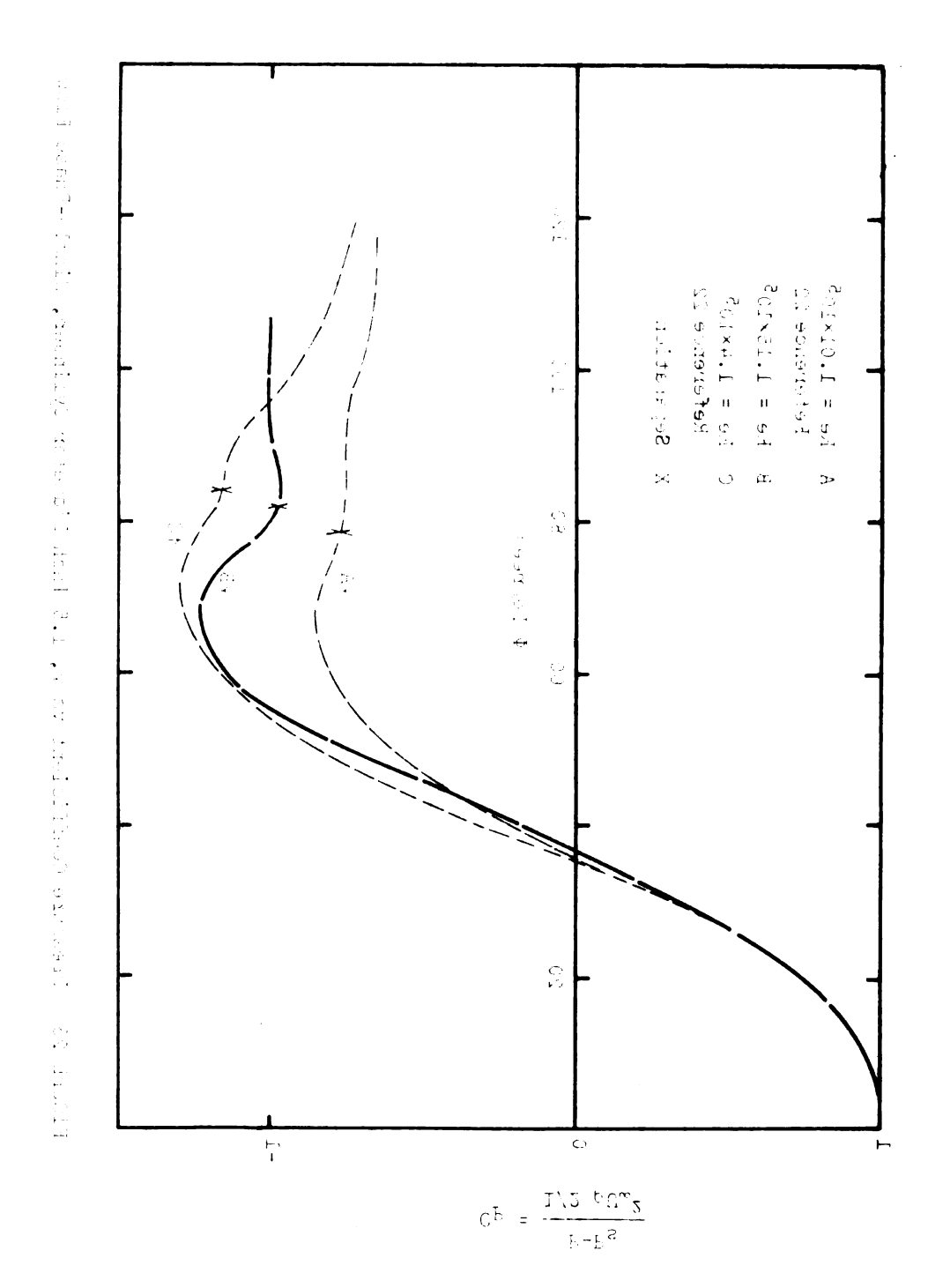
```
C C RUNGA-KUTTA SOLUTION OFR DIFF EQNS WRIGHT
      DIMENSION Y(5), F(5), OLD(5), PHI(5), OLDY(5), A(5)
      CONS=1./LOG(10.)
      I=0
      READ, N
6
      READ, H, XMAX, ICNT
      PUNCH 100, H, XMAX, ICNT
100
      FORMAT(2HH=,F5.3,4X,5HXMAX=,F6.3,4X,4HINT=I2)
      READ,X,Y(1),Y(2),DR,C
      PUNCH 101, X, Y(1), Y(2), DR, C
101
      FORMAT(5E14.6)
      M = 0
44
      K=ICNT
      IF(X-XMAX)3,6,6
33
      CALL RUNGA
3
      IF(M)1,2,1
52
      READ, C, (A(L), L=1,5)
1
      IF(X-C)51,51,52
51
      Q=A(1)+(((A(5))*X+A(4))*X+A(3))*X+A(2))*X
      QPR=A(2)+(((4.*A(5))*X+3.*A(4))*X+2.*A(3))*X
      RE=Y(1)*DR*SQRT(Q)
      I=I+1
      IF(RE)55,55,56
55
      PUNCH 103, RE, I
103
      FORMAT(E15.8, 14)
56
      T=(5.89*CONS*LOG(4.075*RE))**2
      F(1)=-((.5*Y(2)+1.)*Y(1)/Q)*QPR+1./T
      F(2)=EXP(4.68*(Y(2)-2.975))*(-QPR*T/Q-2.035*(Y(2)
     1-1.286)/Y(1)
      GO TO 33
2
      K=K-1
      IF(K)3,4,3
      PUNCH 102, X, Y(1), Y(2), RE, T
102
      FORMAT(F6.3,4(E15.8))
      GO TO 44
```

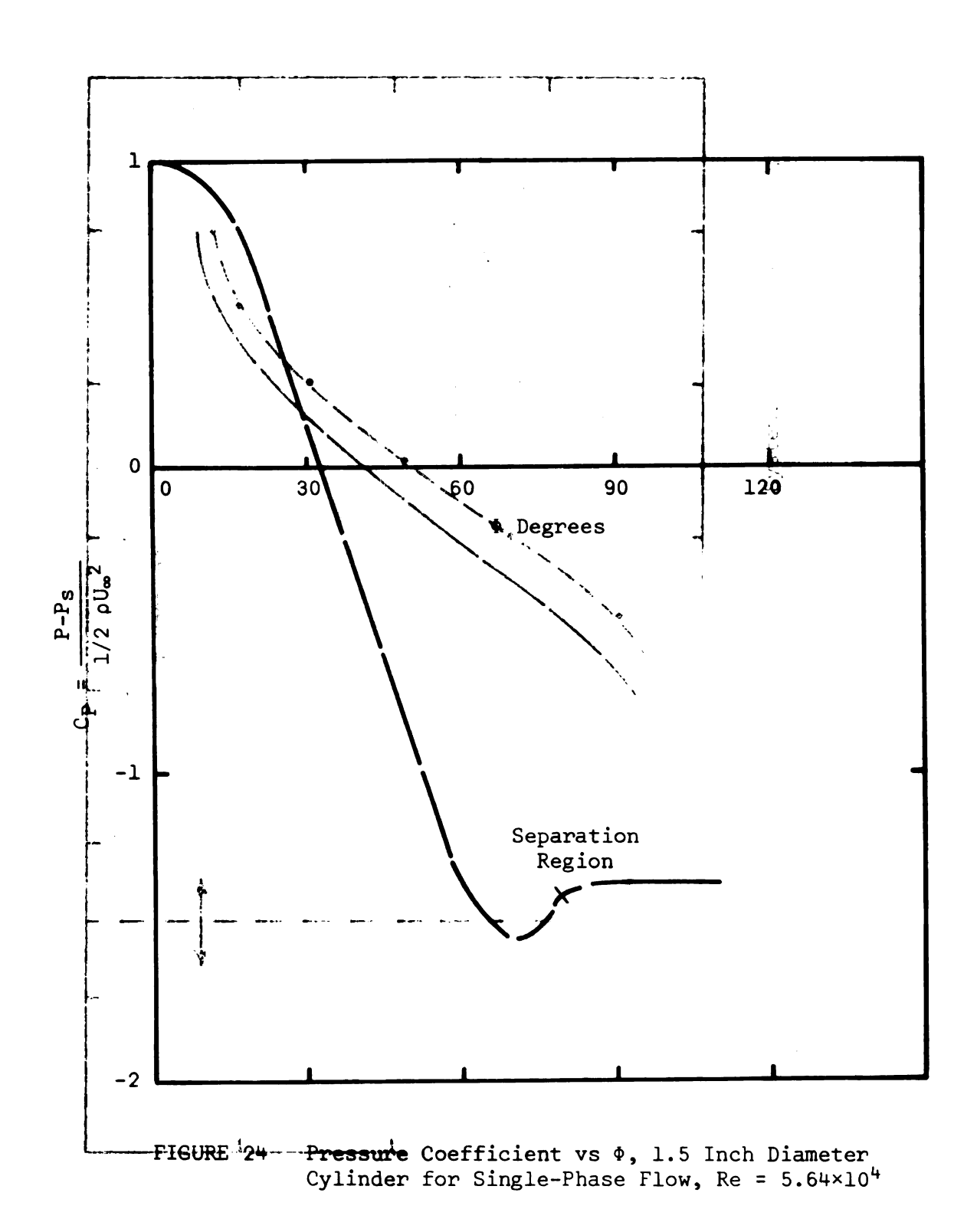


Average Nusselt Number vs Reynolds Number for Single-Phase Flow (Wind Tunnel Evaluation)









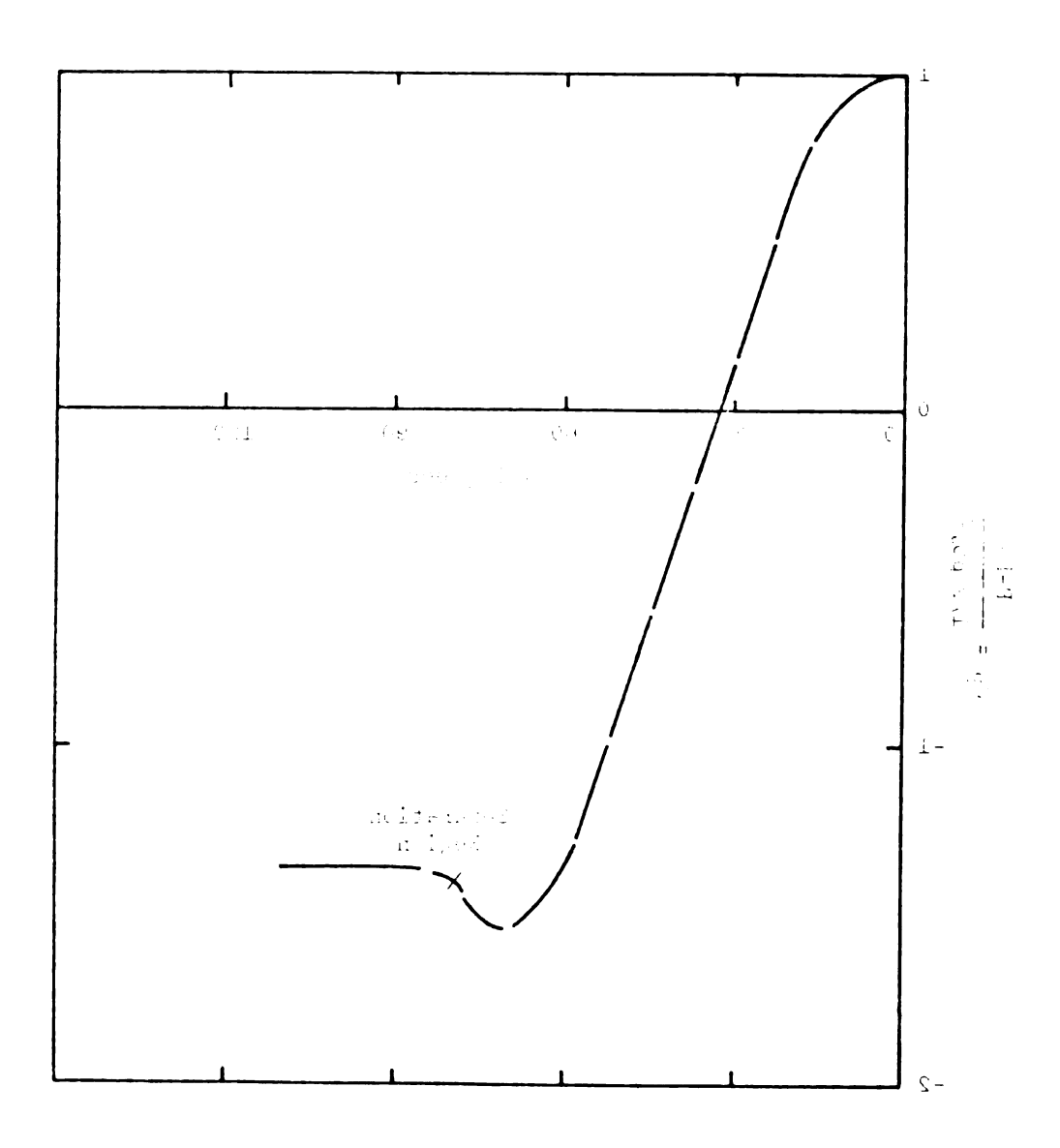
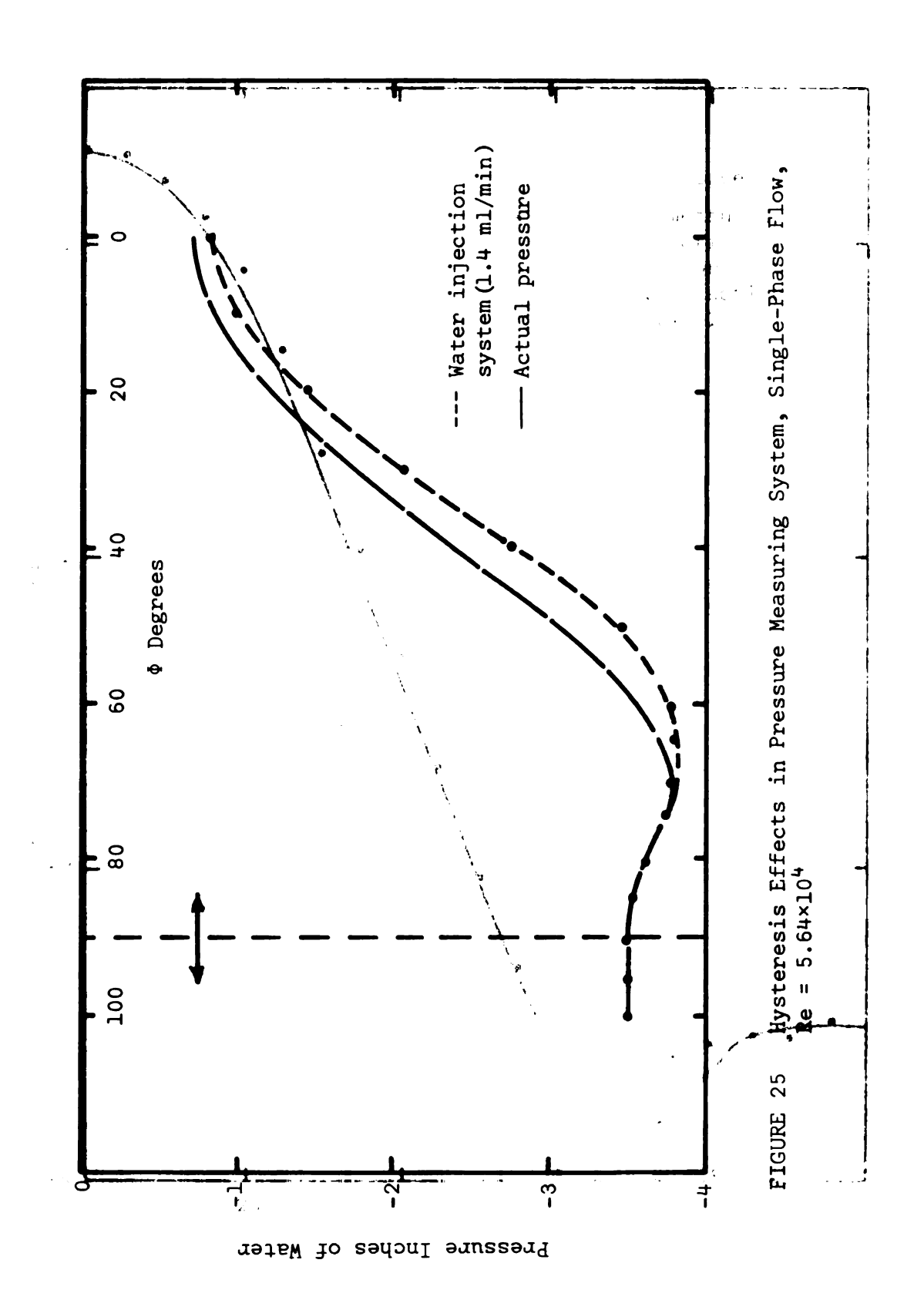
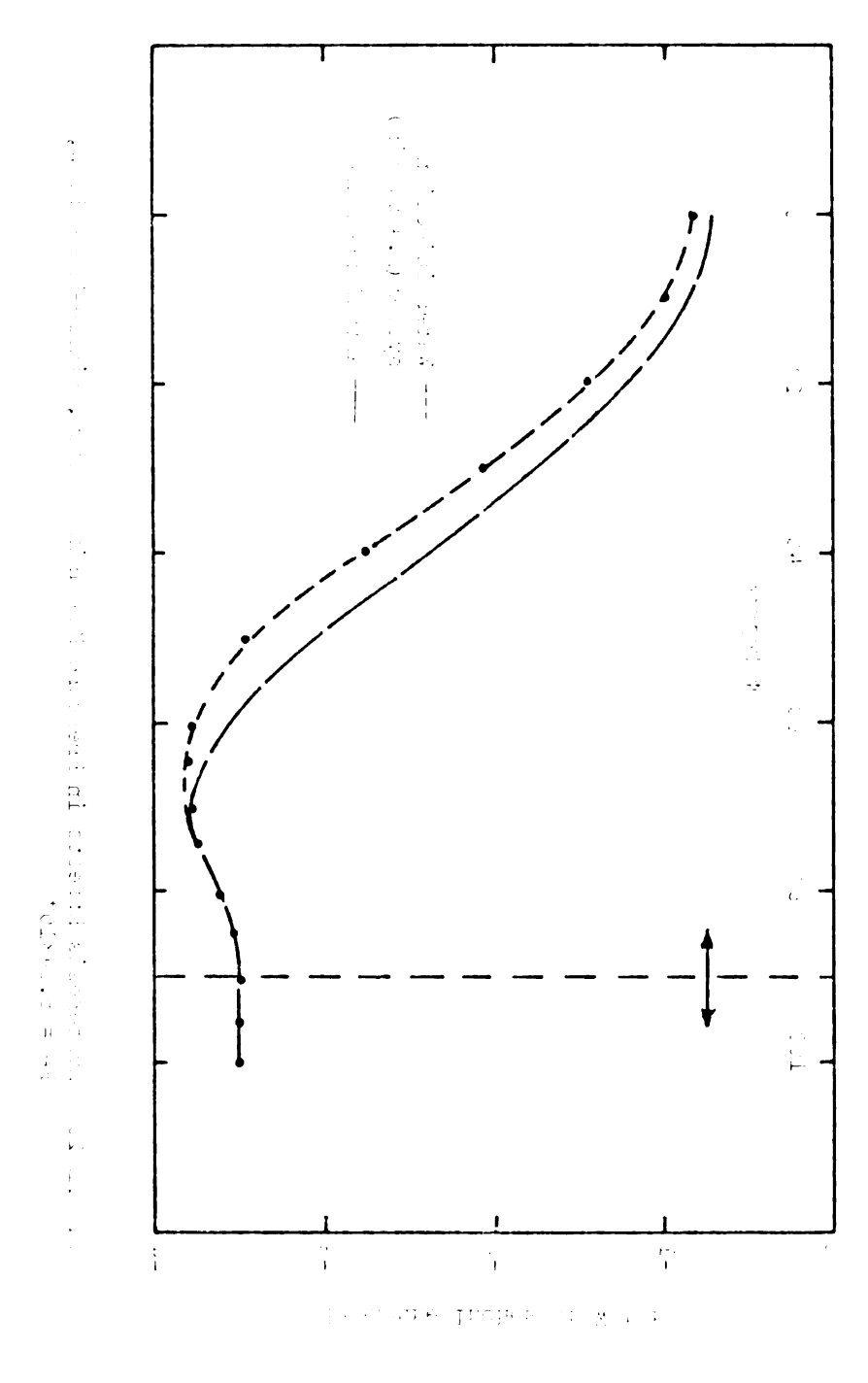


Figure 14 cases to Coefficient vs 4, 1.5 incm Displays Coefficient for Dimper-Passe Picture From $^{\rm th}$





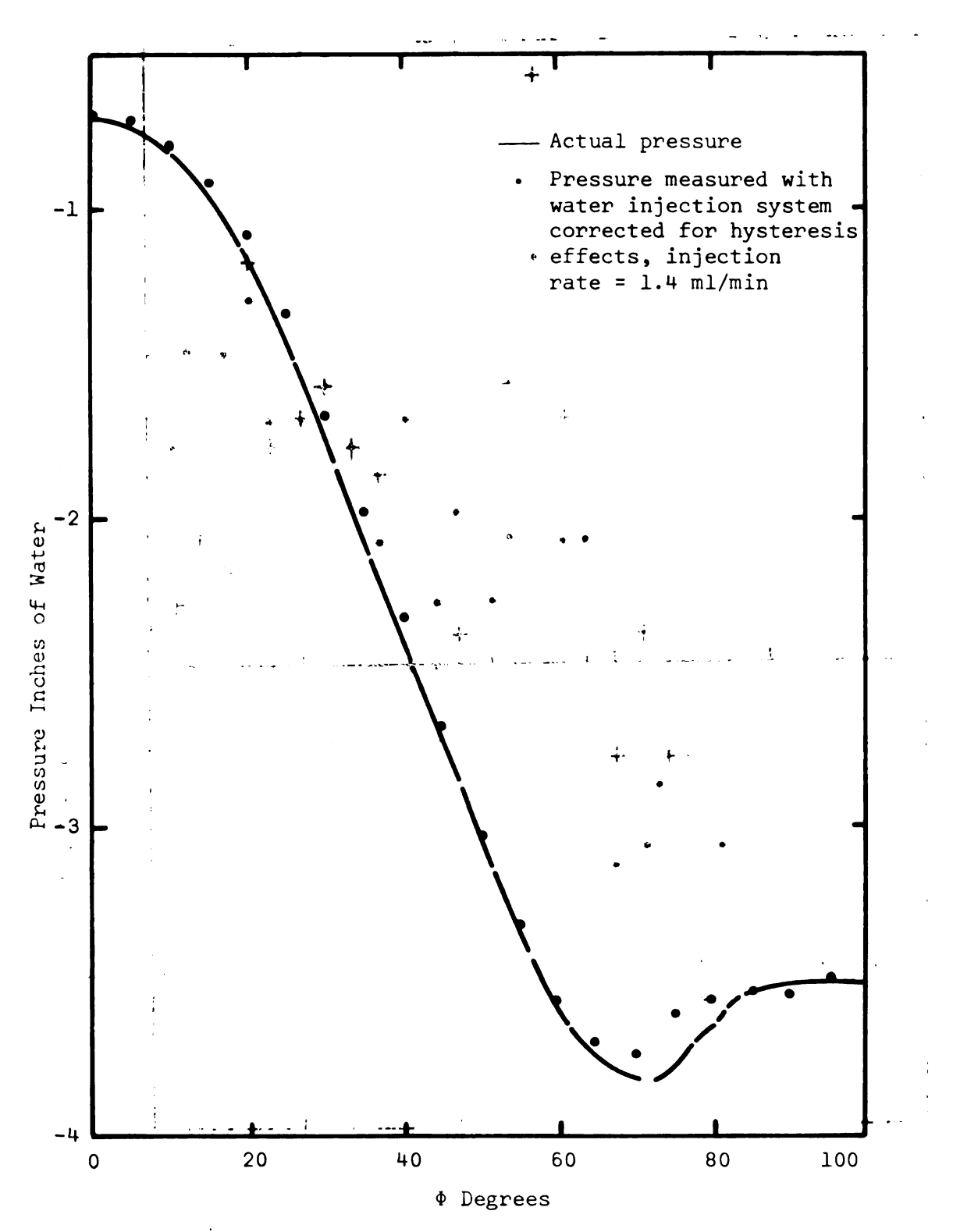
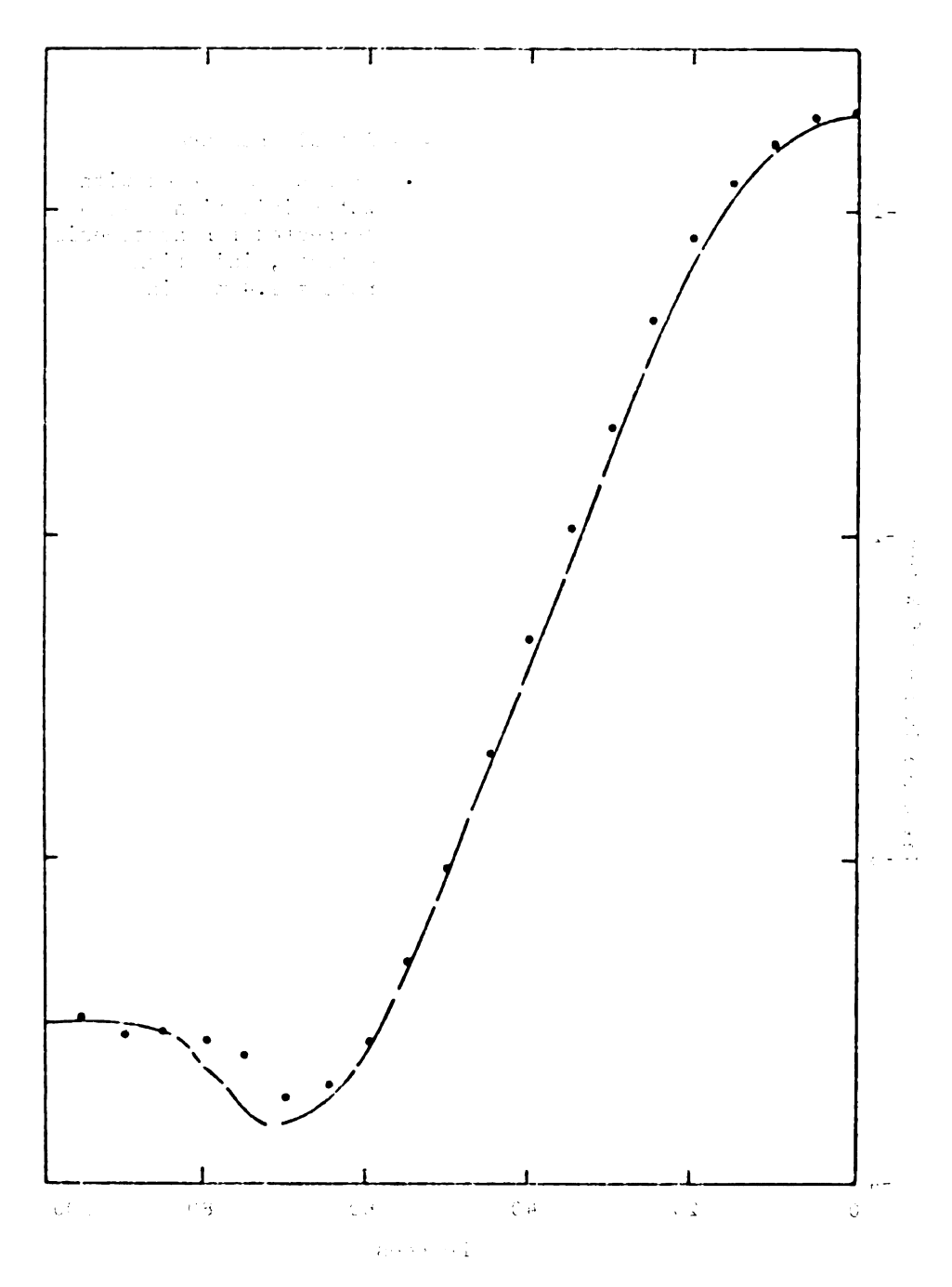


FIGURE 26 Pressure on Cylinder vs Φ for 1.5 Inch Diameter Cylinder Single-Phase Flow, Re = 5.64×10^4



Fill to 26 Figure as on Chathar val 4 top 1.5 Inch if each con C. Haller on Single-House From, i.e. = 5.04×iof

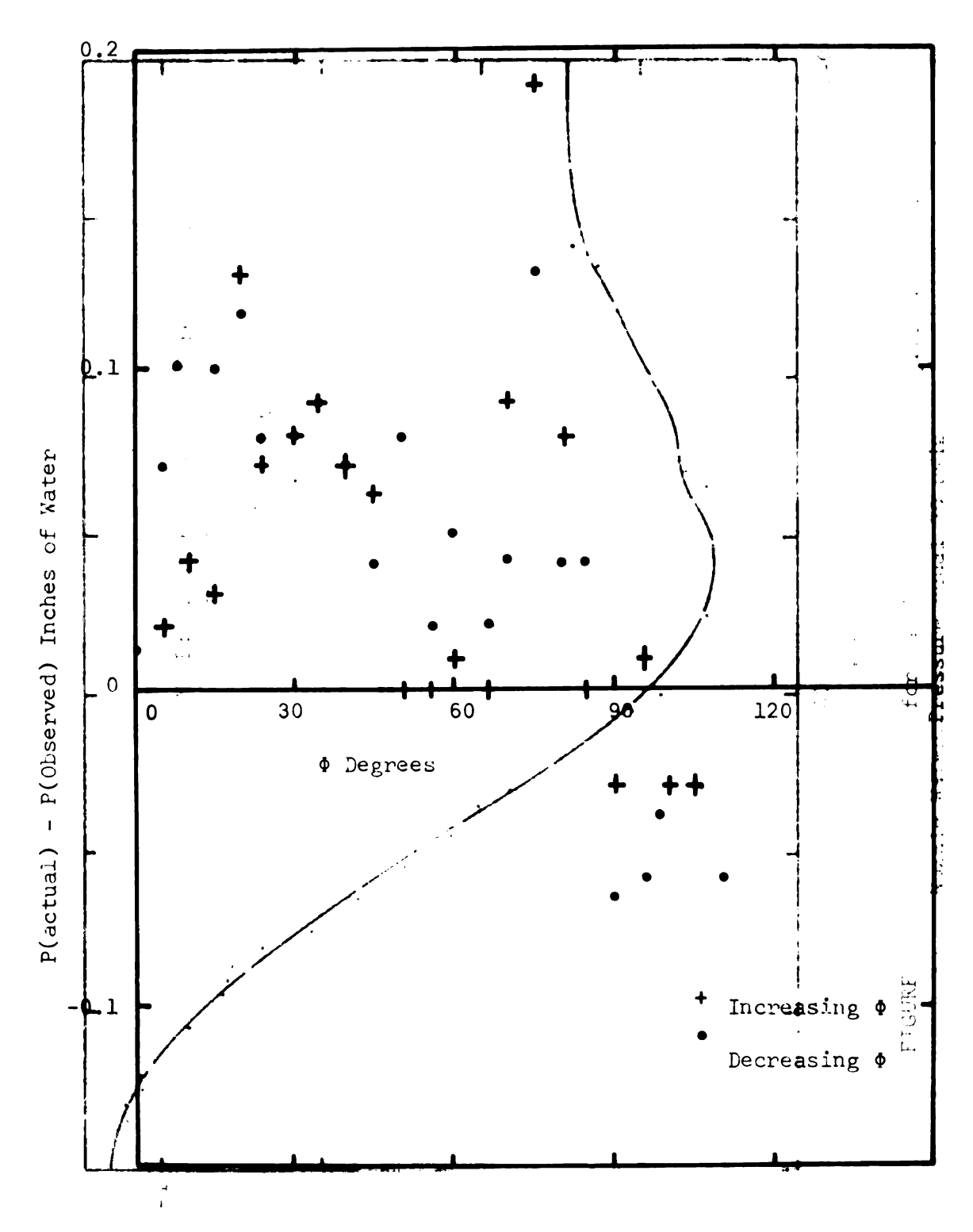


FIGURE 27 Difference Between Actual and Observed Pressure,
Observed Pressure Measured By Water Injection
Method

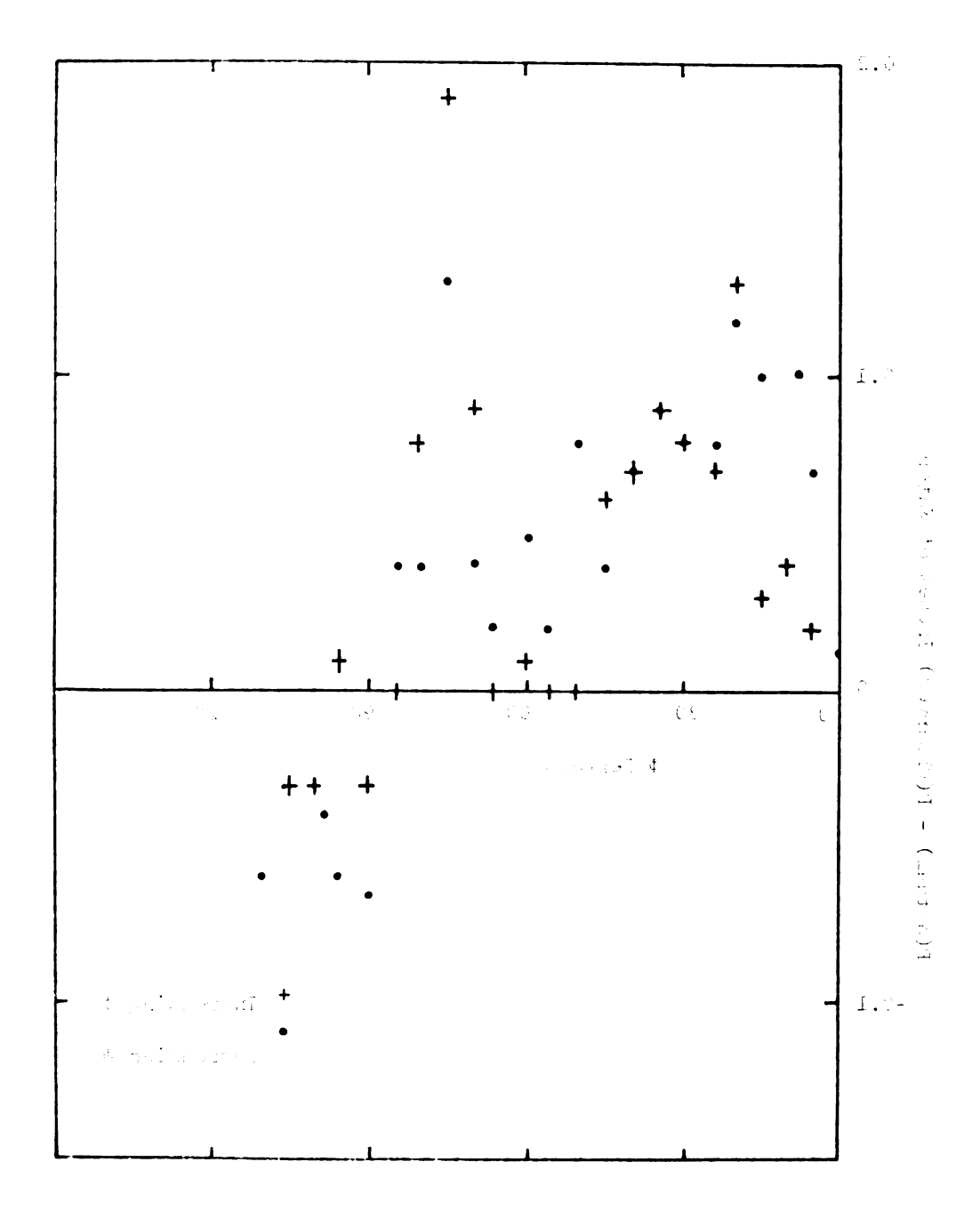
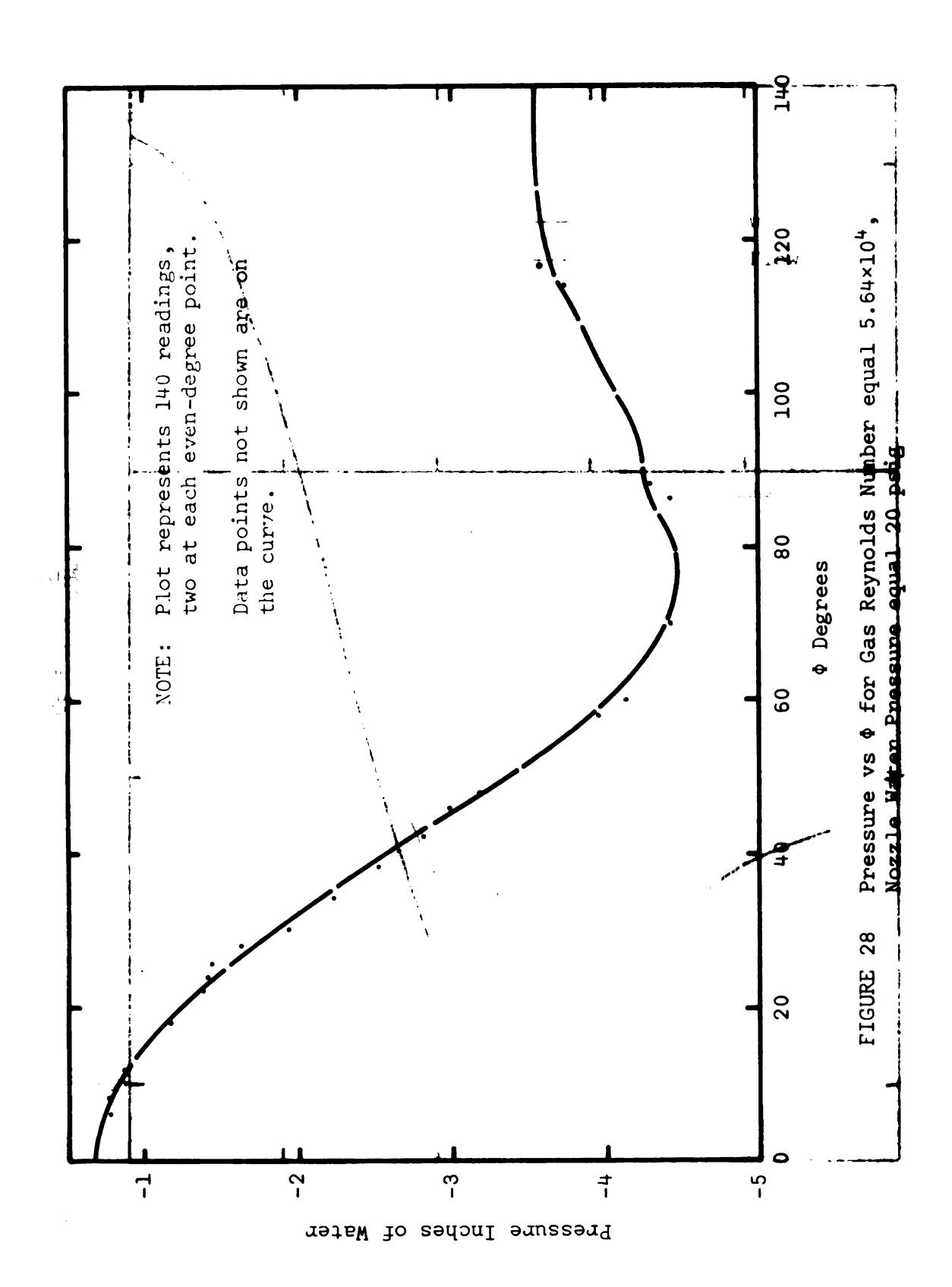
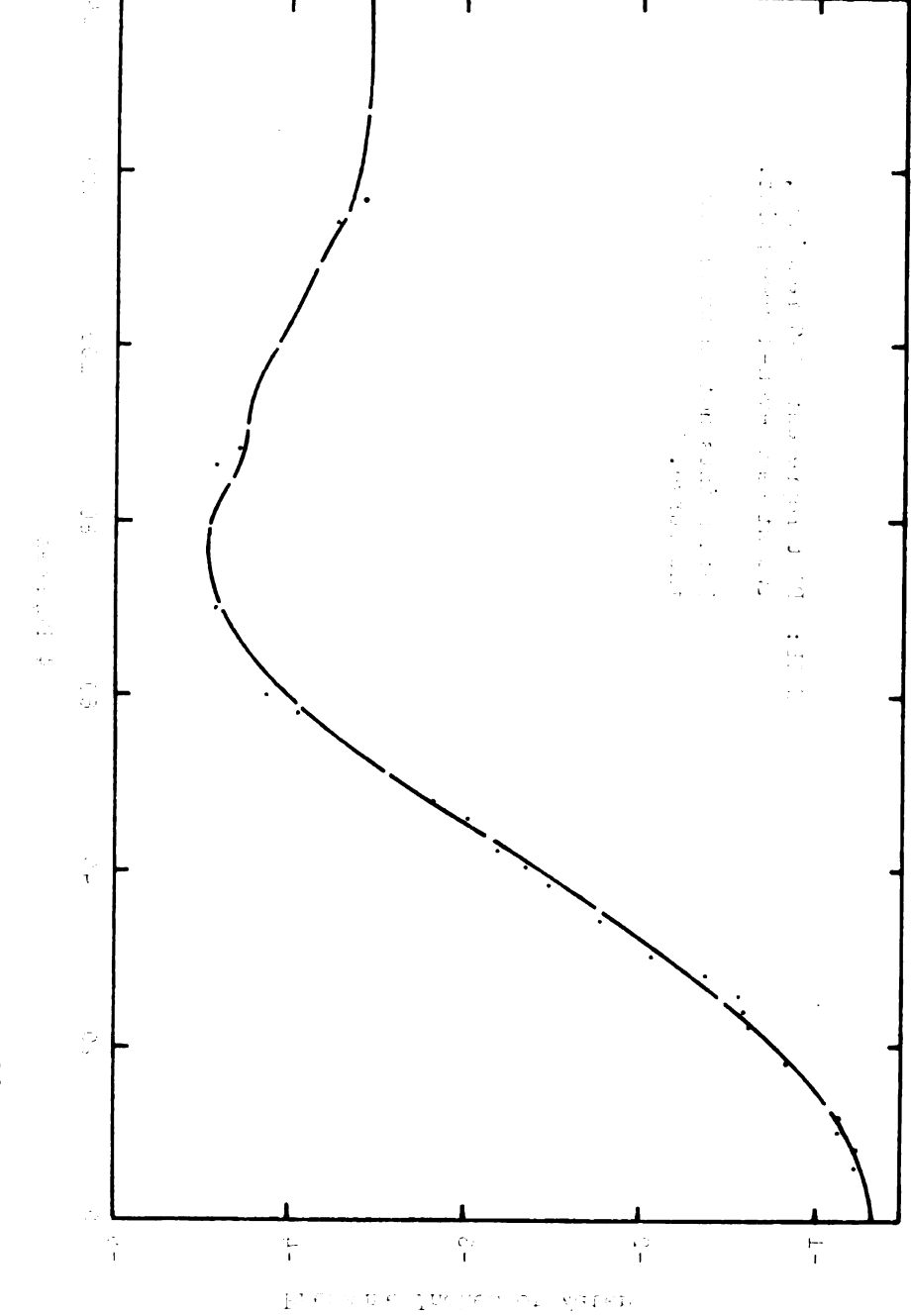


FIGURE 27 Difference Petwoon Autual and Goorvel Floridate, Oursayel Prescure Posternelly War of Educial Mothod Mothod







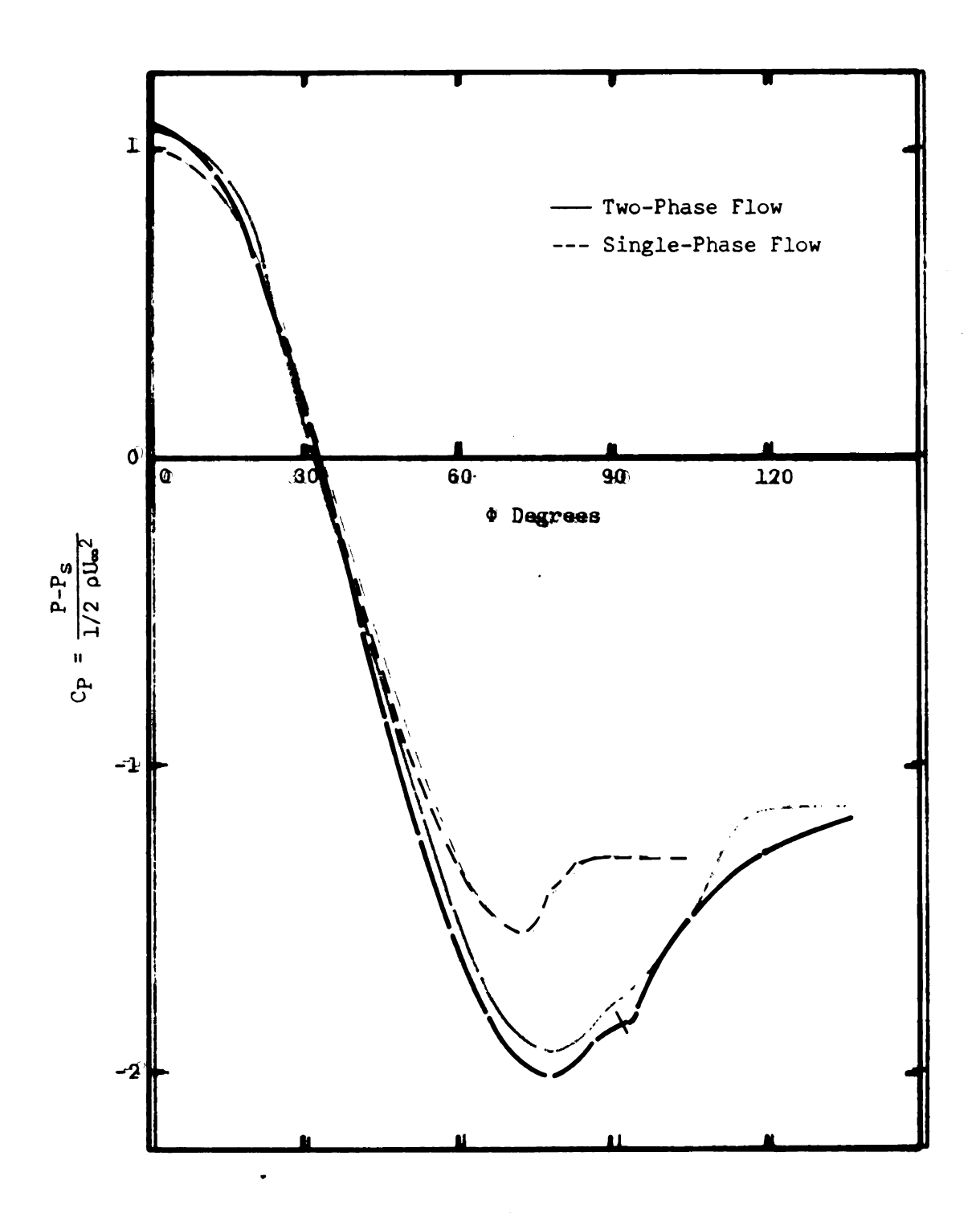


FIGURE 29 Pressure Coefficient vs Φ for Two-Phase Flow Over 1.5 Inch Diameter Cylinder, Nozzle Water Pressure equal 15 psig, Red = 522, Gas Reynolds Number equal 5.64×10⁴

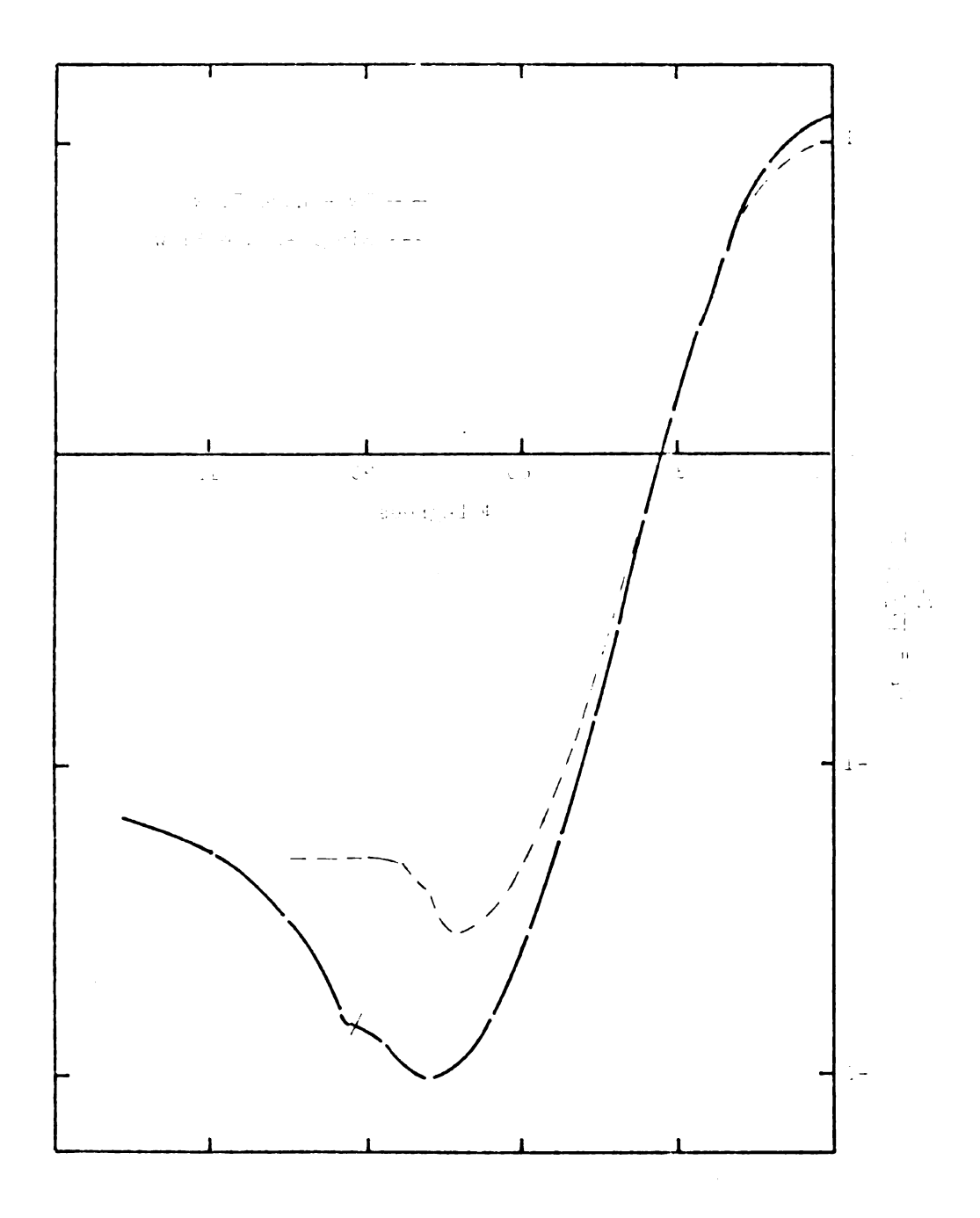


Figure 20 Figure Confficient volt to minstess Figure Cvert.

1.5 Insh Diamet a cylinera, becase have been consequently and equation of the constitution of the constit

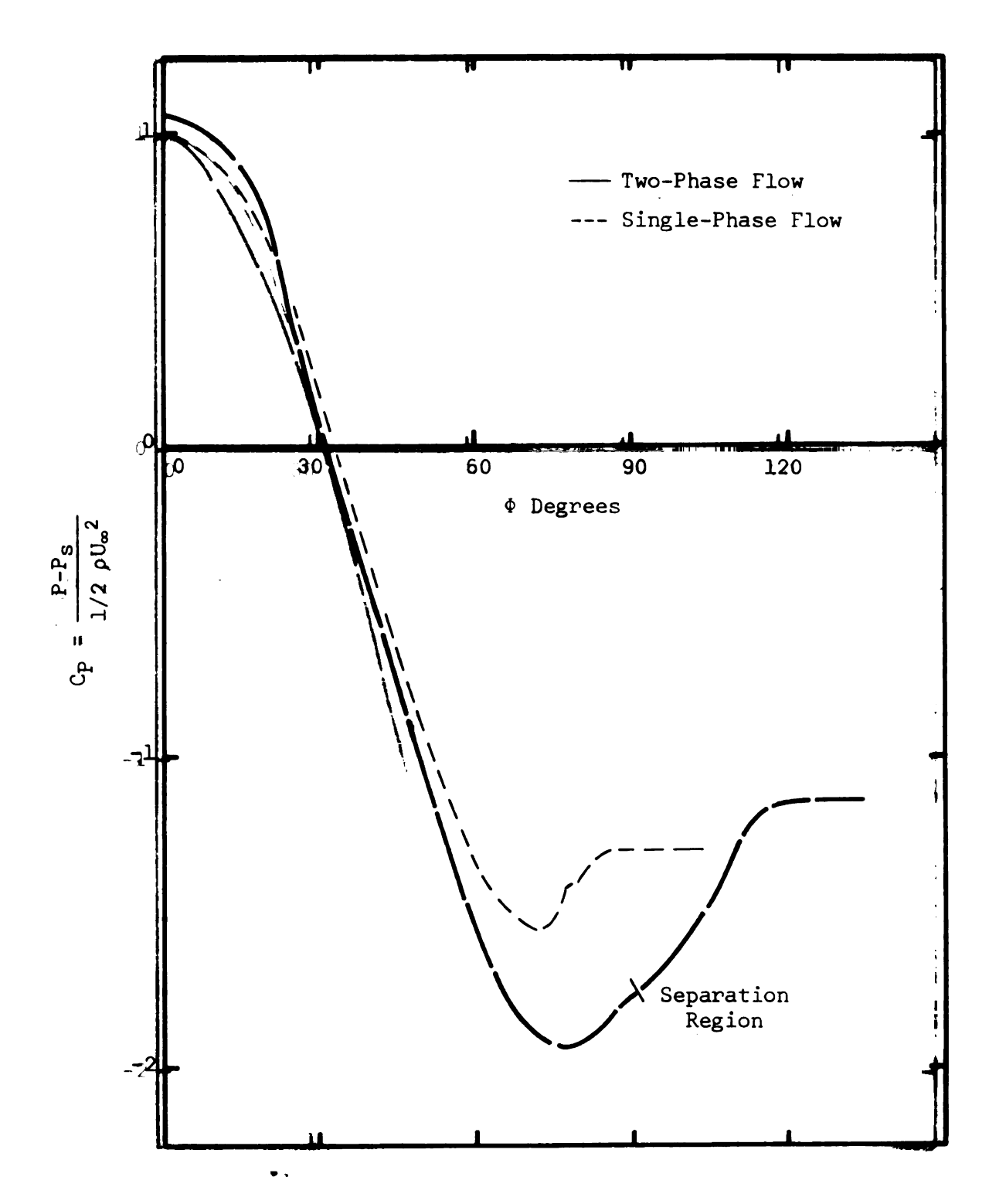
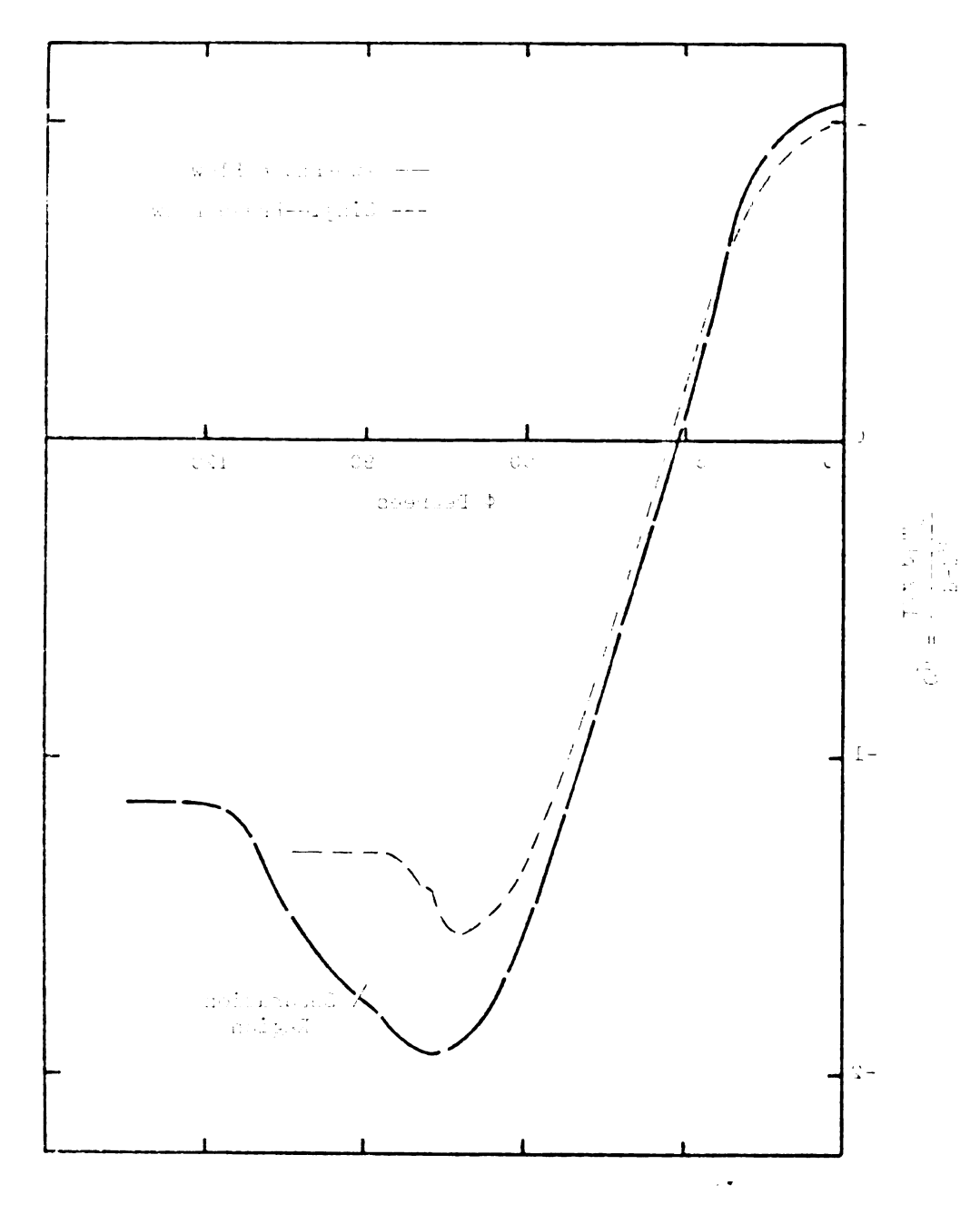


FIGURE 30 Pressure Coefficient vs Φ for Two-Phase Flow Over 1.5 Inch Diameter Cylinder, Nozzle Water Pressure equal 20 psig, Re_d = 458, Gas Reynolds Number equal 5.64×10⁴



F13002 30 Freamme Cuerficient volvium-Lucco isom over 1.5 fuch Diameter Cylinder, I ambe where Euclide equal V0 [siz, Feg = 468, Oac Repart a Euclide equal 5.69810*

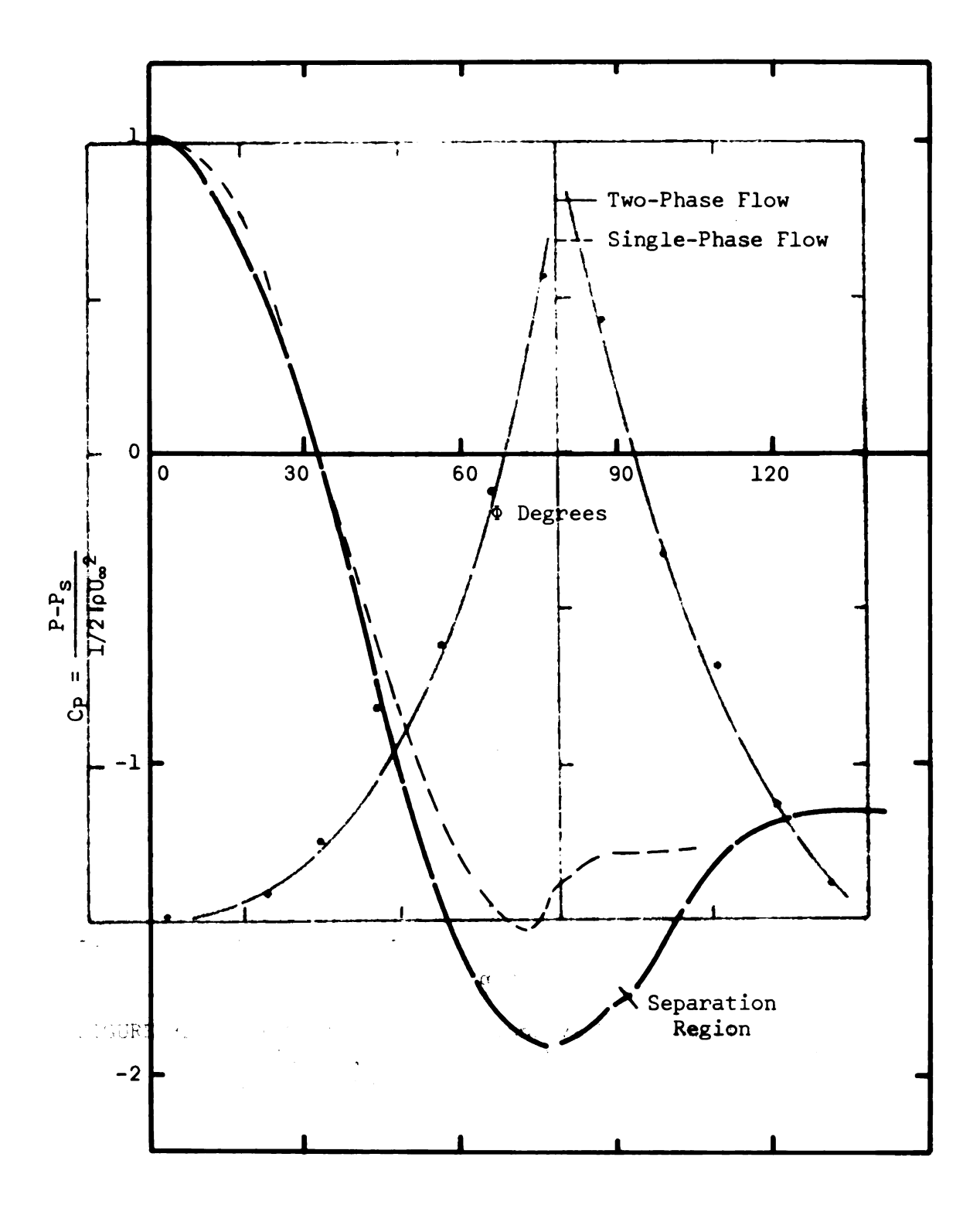


FIGURE 31 Pressure Coefficient vs Φ for Two-Phase Flow Over 1.5 Inch Diameter Cylinder, Nozzle Water Pressure equal 25 psig, Red = 380, Gas Reynolds Number equal 5.64×10⁴

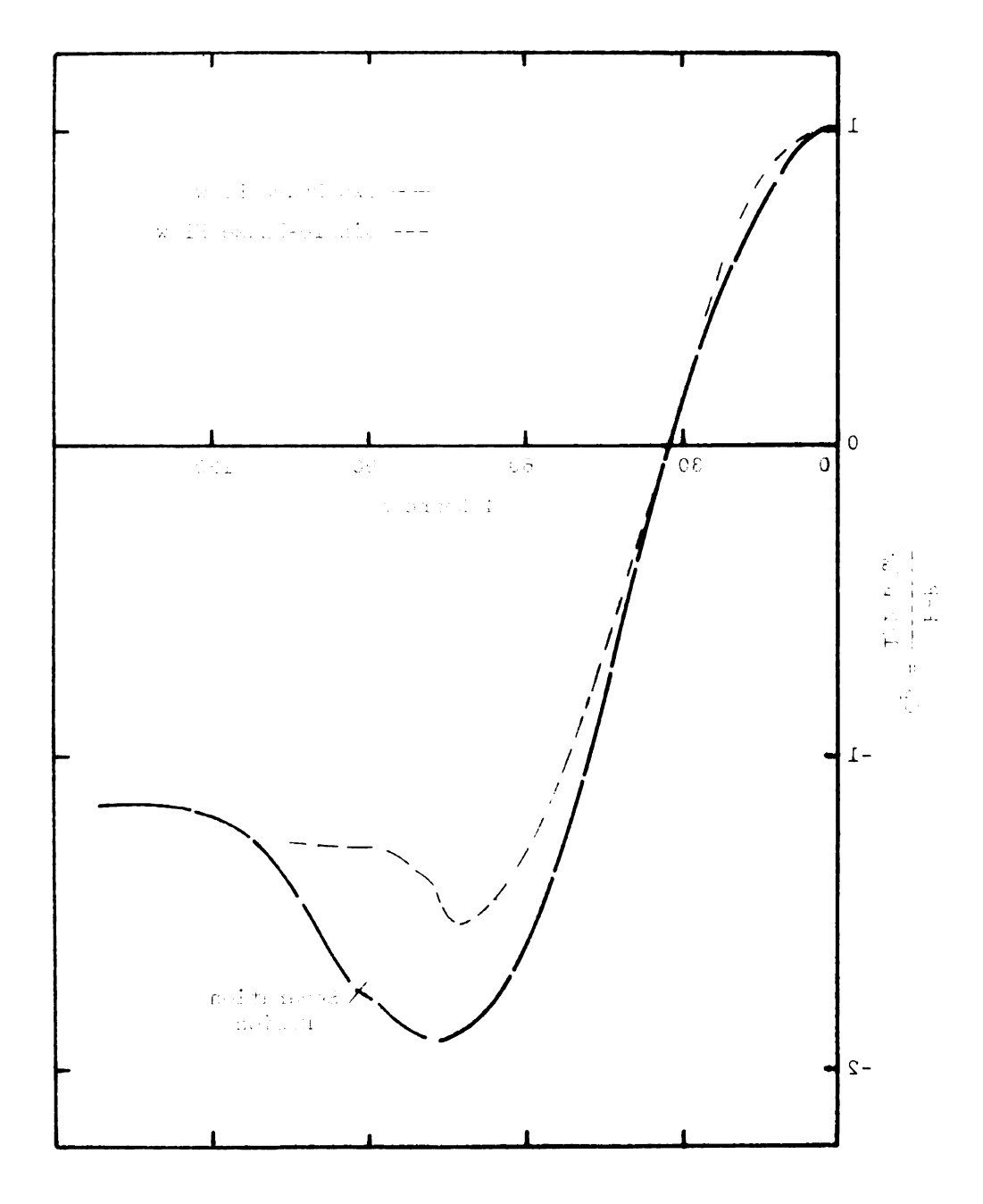


FIGURE 31 Freedome Coefulcious voltum laceThese Flow Green 1.5 Imam i buletem (piimner, Hozale Nouse Chemman equal 25 juin, Reg = 800, Chambertanius cuit megunt 5.64% of 5.64

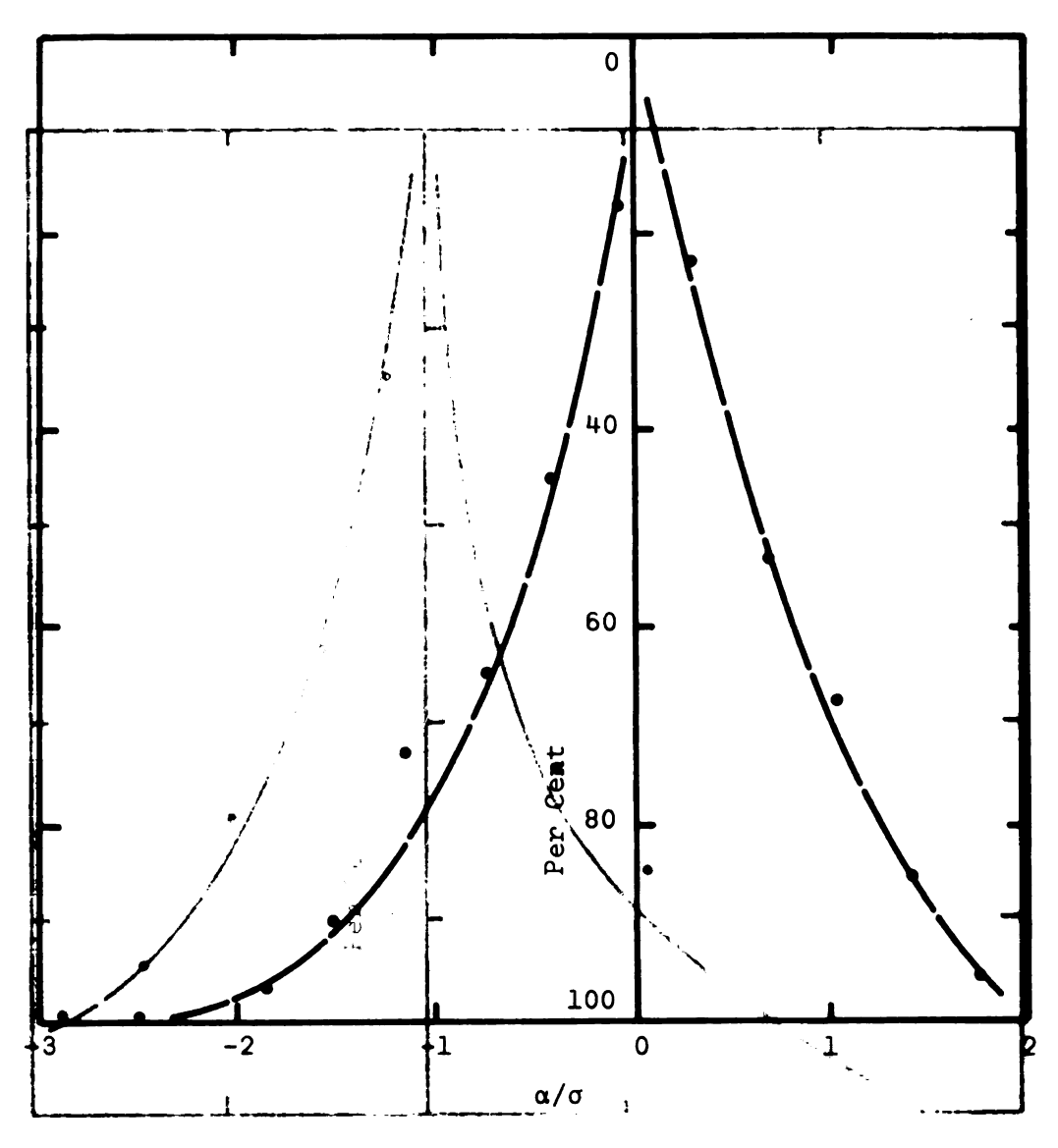
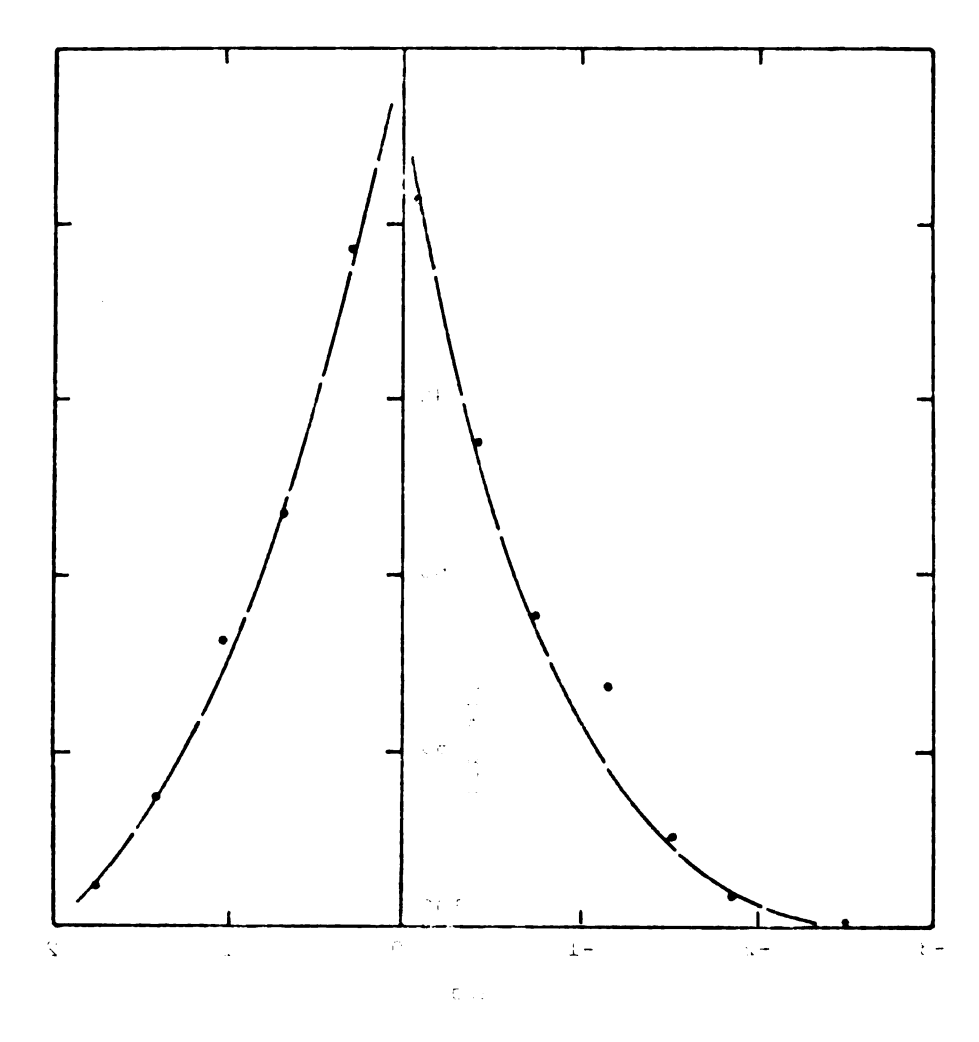


FIGURE 32 Per Cent of Observations vs Fraction of Standard Deviation, Gas Reynolds Number equal 5.64×10⁴, Nozzle Water Pressure equal 15 psig



amedicals of multiplice of a capabolic formal parel (\$6 Dari) at the capabolic formal and the ca

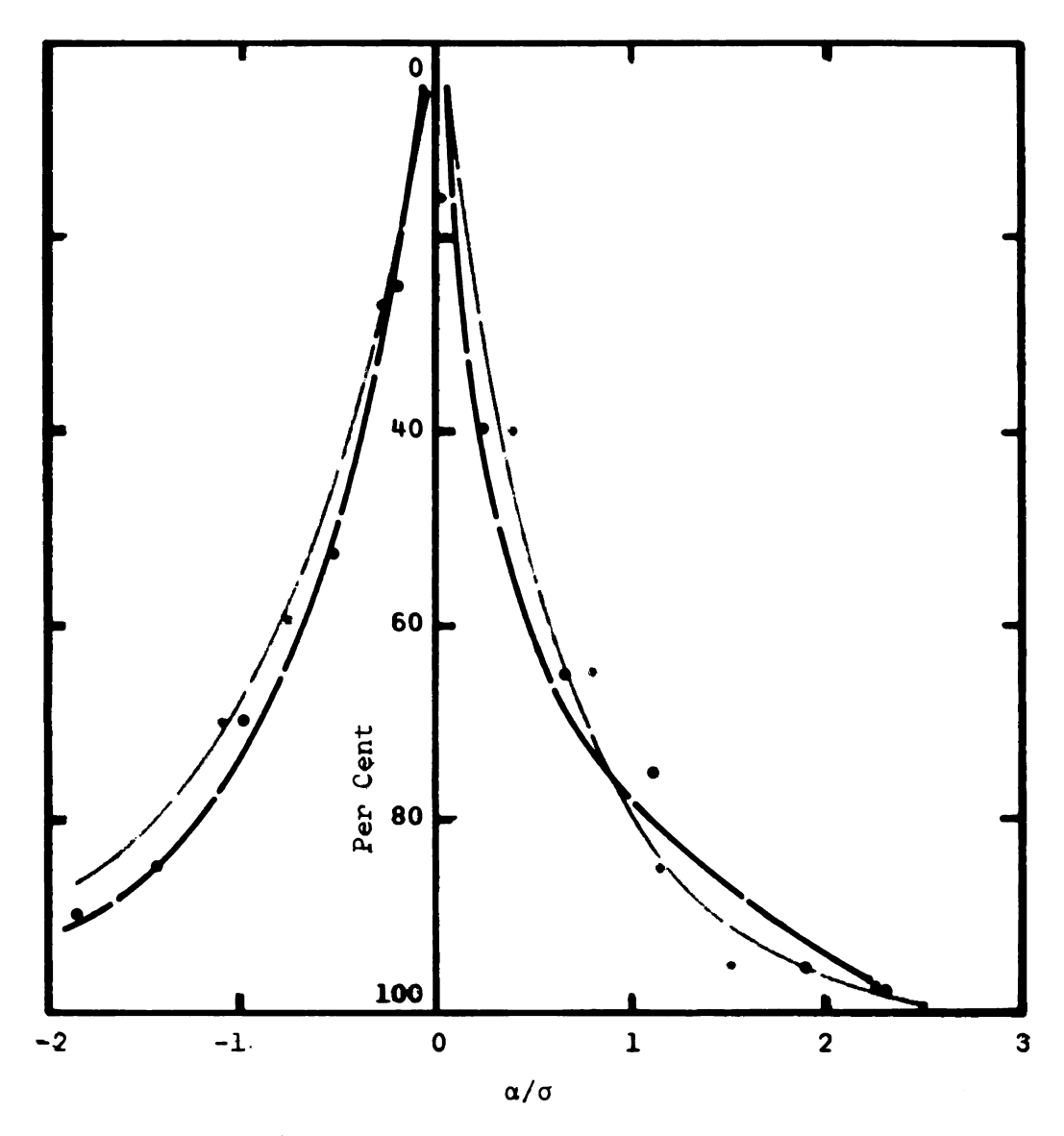
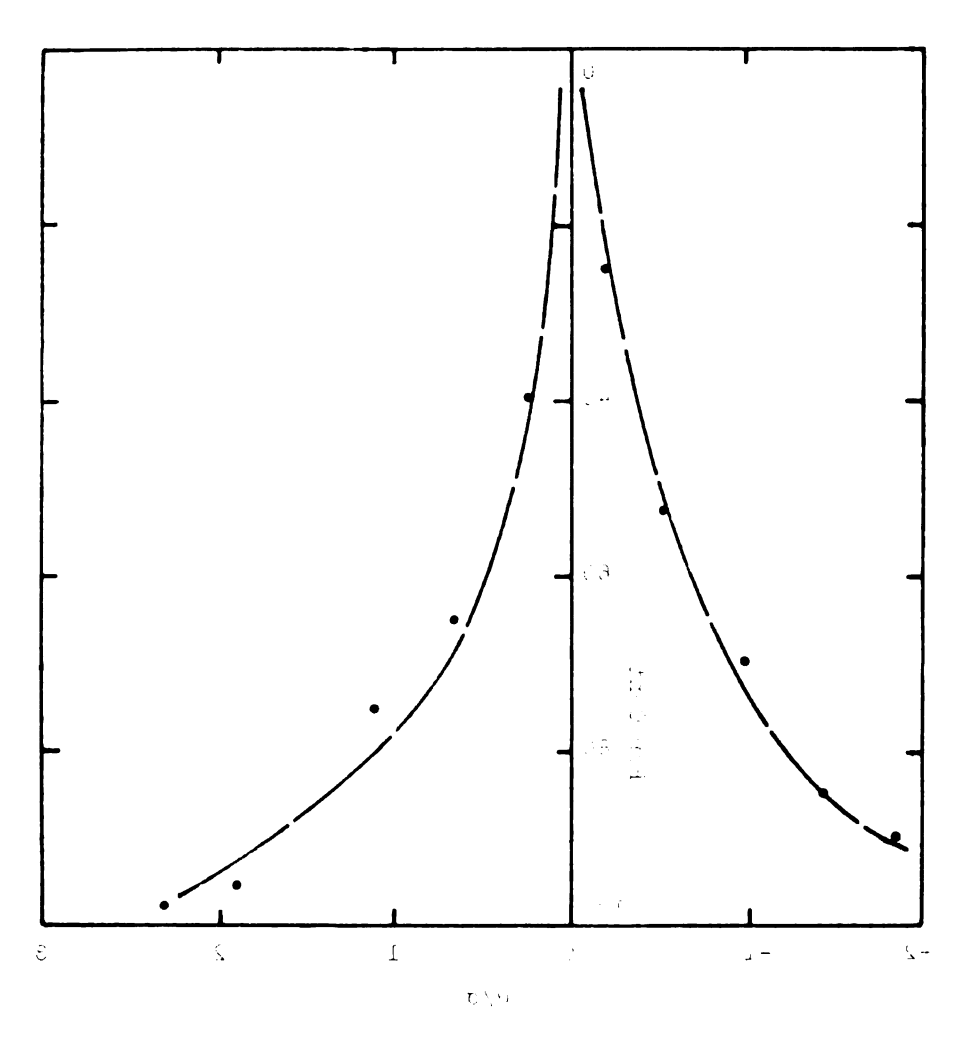


FIGURE 33 Per Cent of Observations vs Fraction of Standard Deviation, Gas Reynolds Number equal 5.64×10⁴, Nozzle Water Pressure equal 20 psig



Described to notificable variations of distributions of the LEVIT , where the property described in the Levil control of the control of the

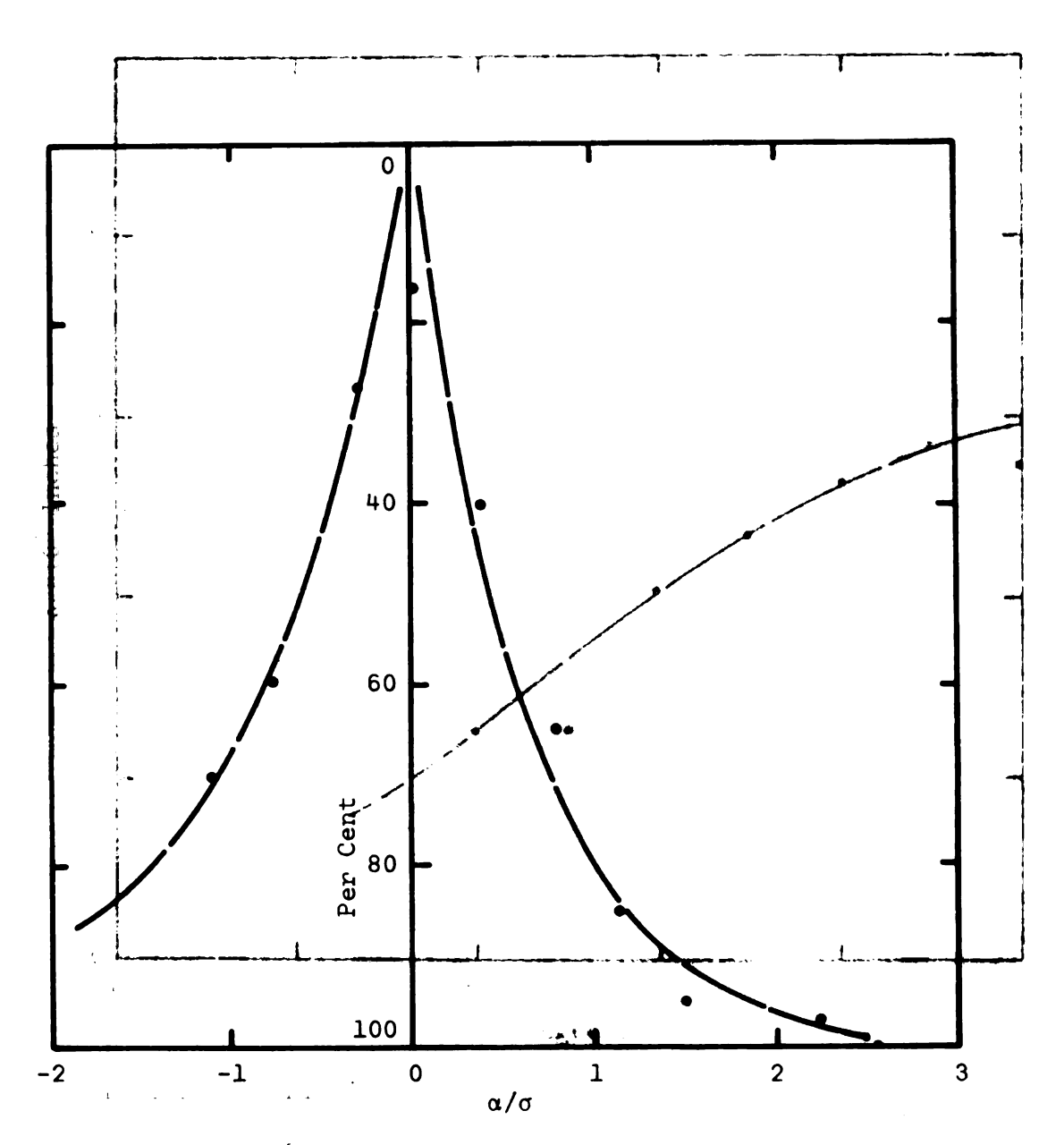
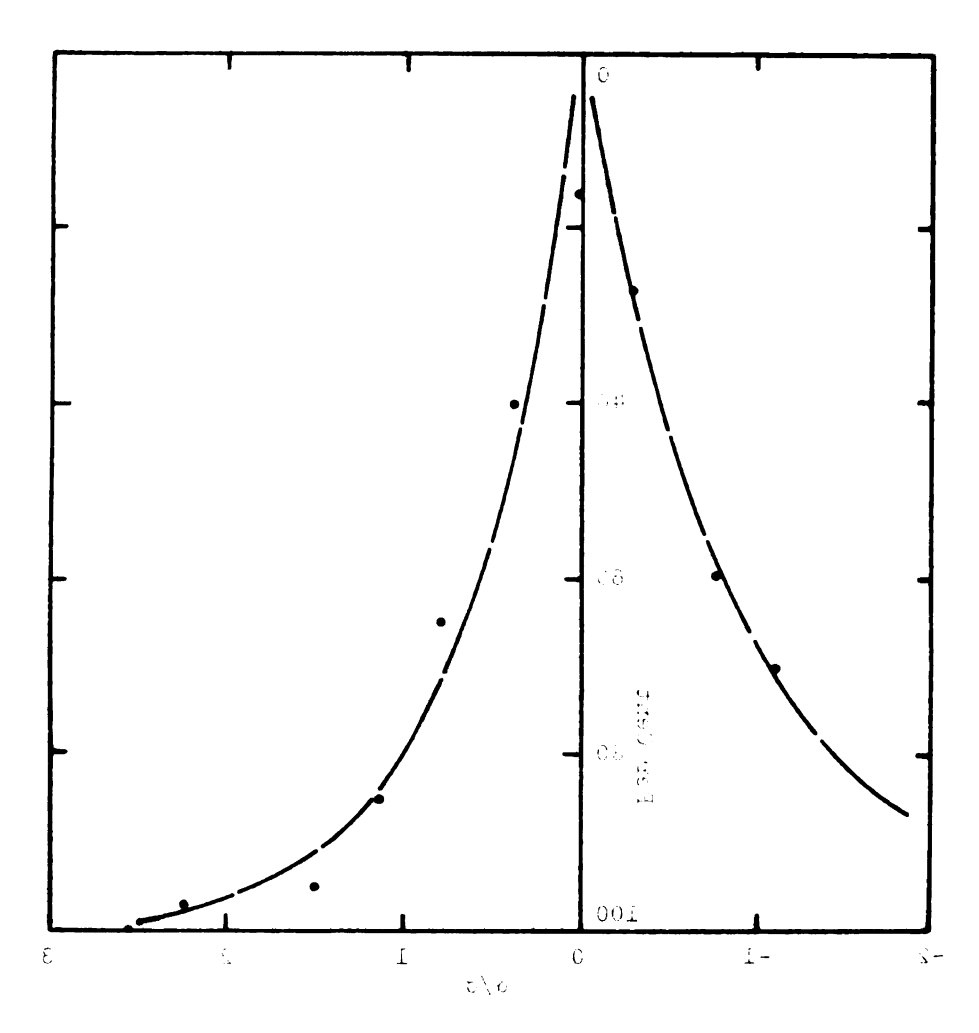


FIGURE 34 Per Cent of Observations vs Fraction of Standard Deviation, Gas Reynolds Number equal 5.64×10⁴, Nozzle Water Pressure equal 25 psig



is the Toron interpretation of the contract of the Table 1. The Table

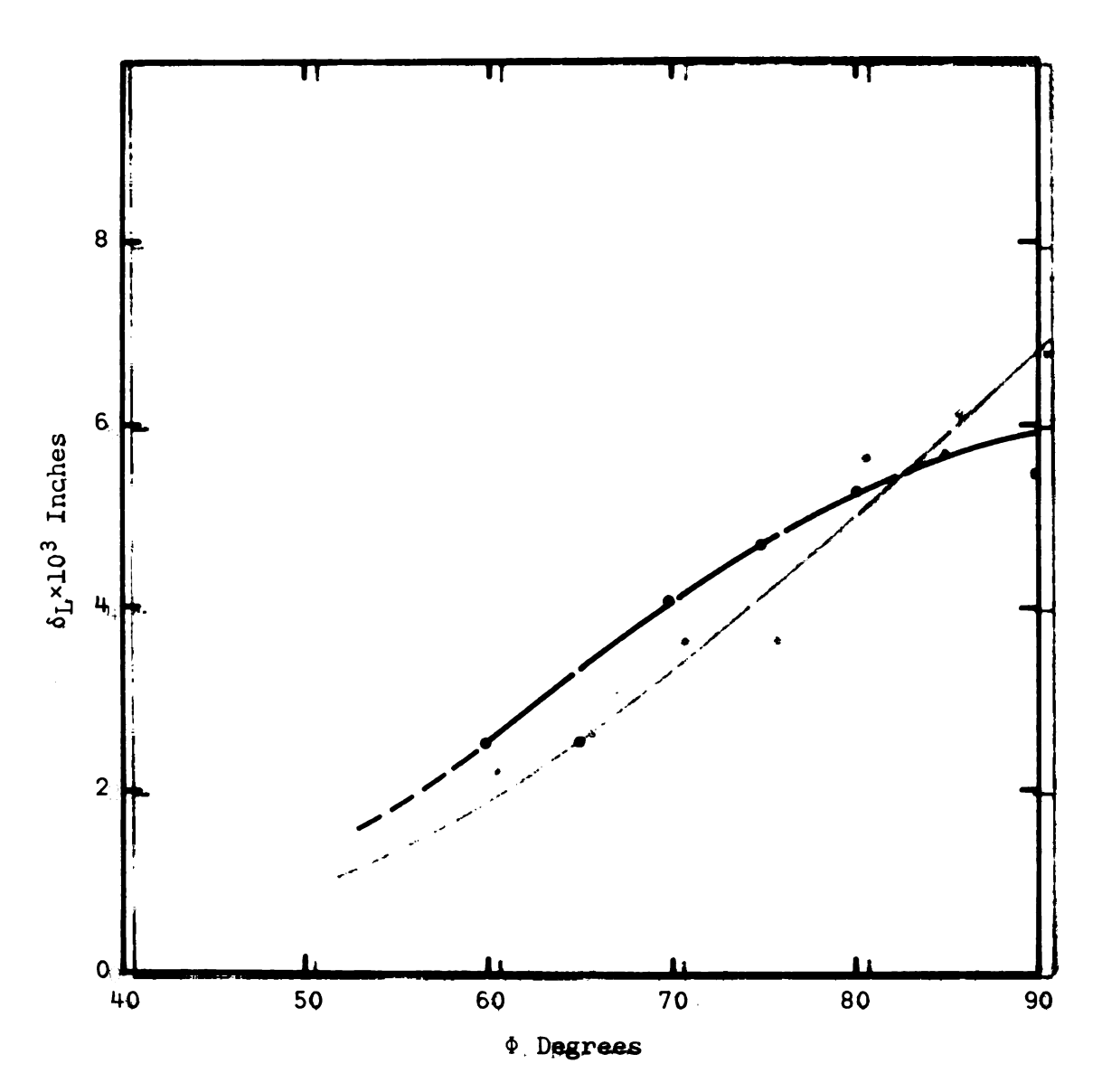
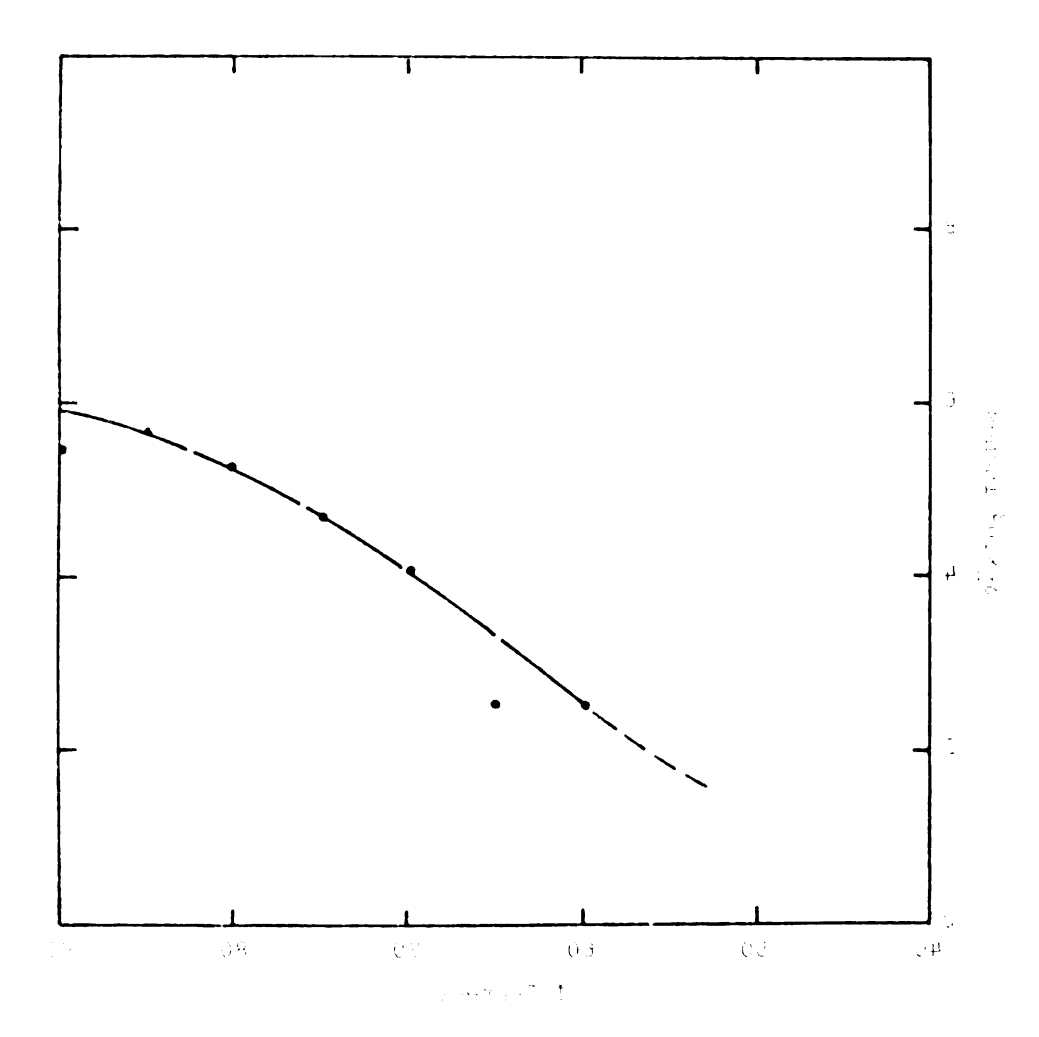


FIGURE 35 Liquid Boundary-Layer Thickness vs Φ for Gas Reynolds Number equal 5.64×10⁴, Nozzle Water Pressure equal 15 psig



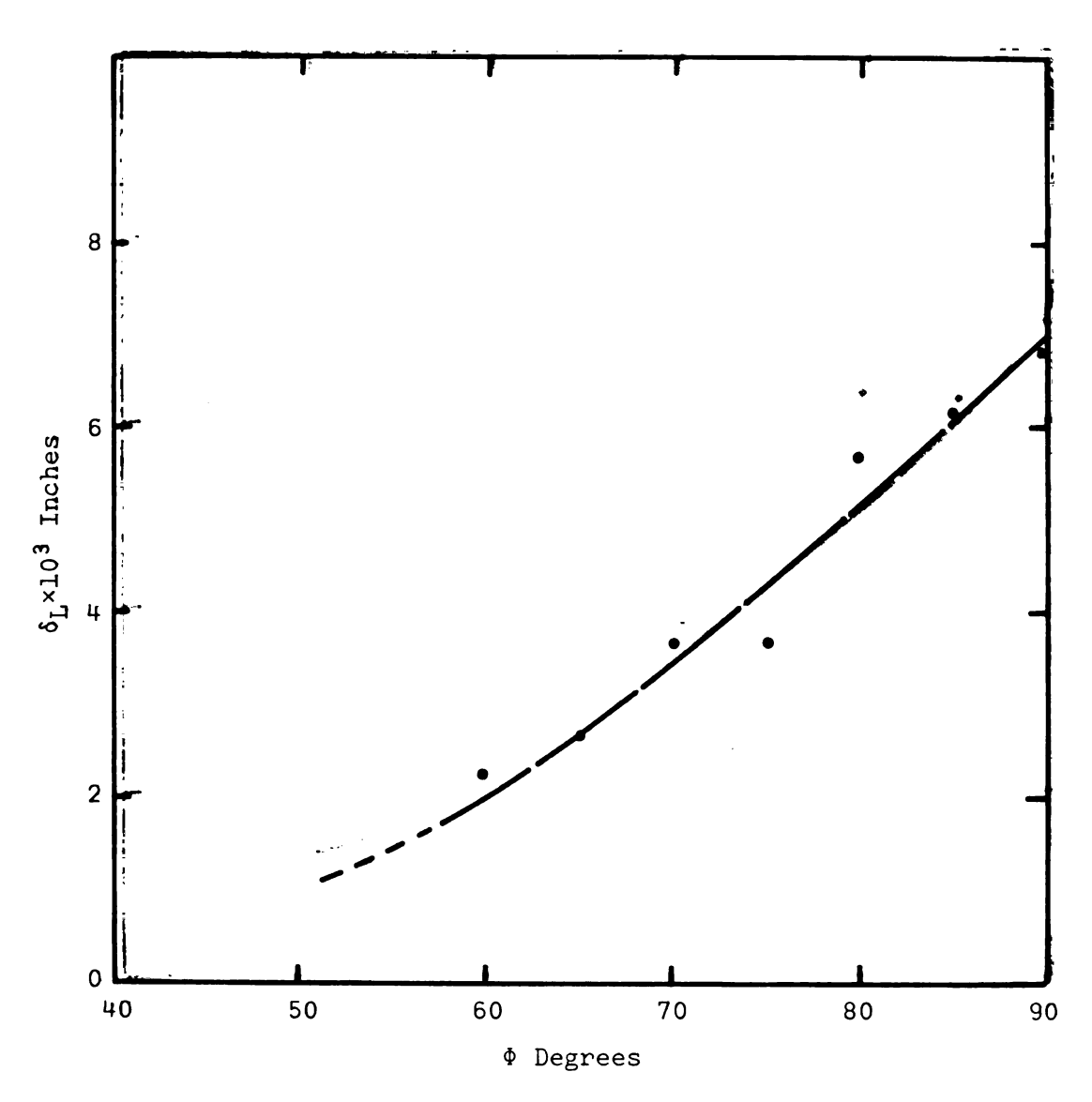
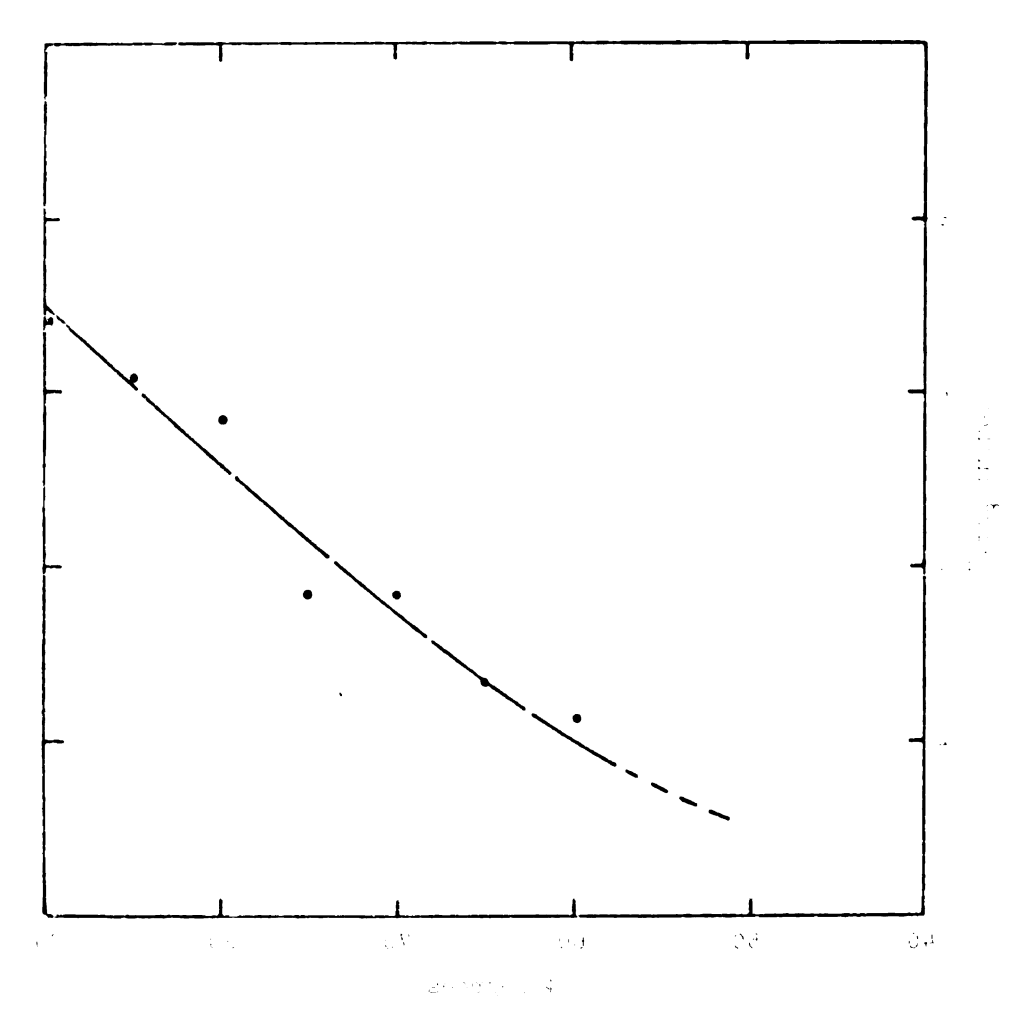
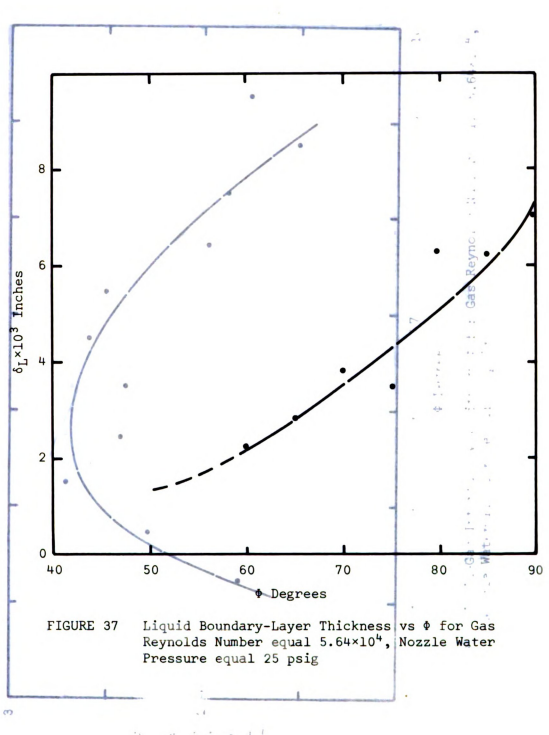


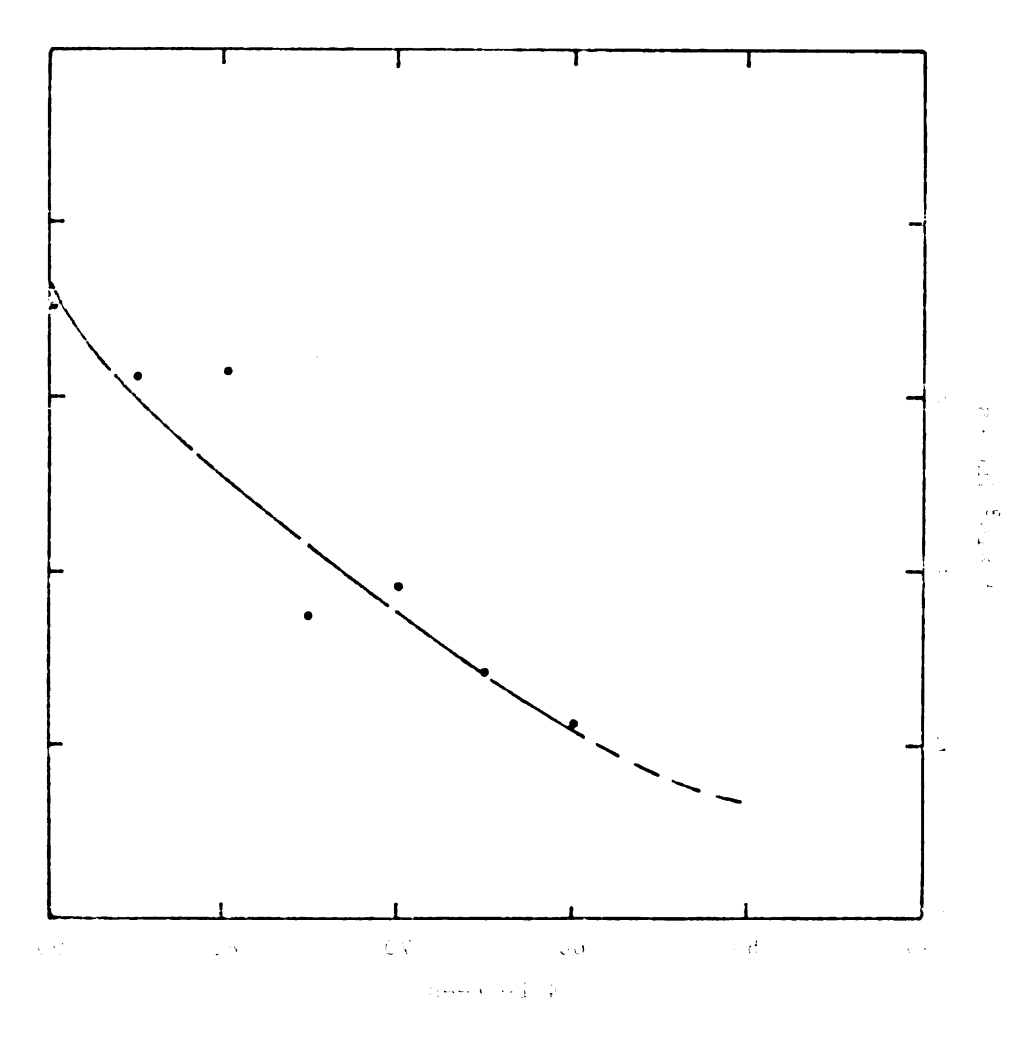
FIGURE 36 Liquid Boundary-Layer Thickness vs Φ for Gas Reynolds Number equal 5.64×10⁴, Nozzle Water Pressure equal 20 psig



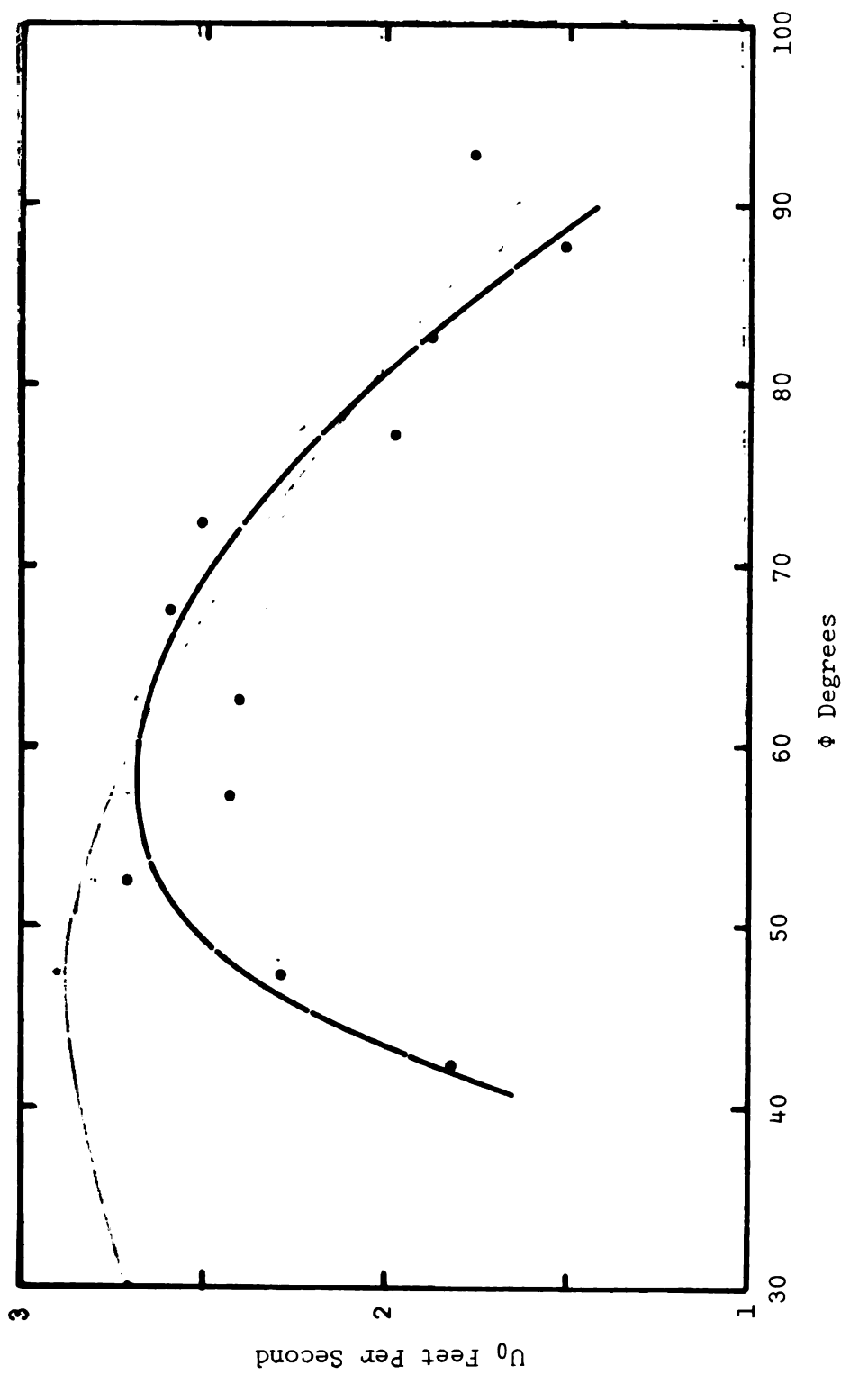
The control of the co



2 2 1 2 4- 11

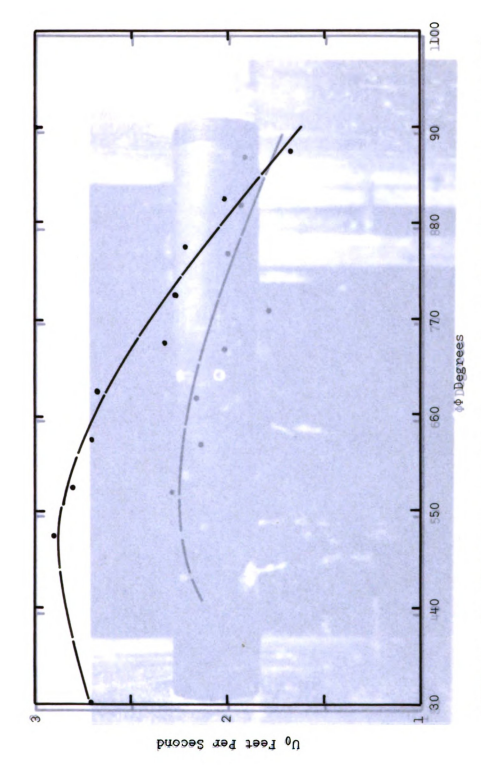


and the consense of the second with a second with the second of the second consense of the second consense of

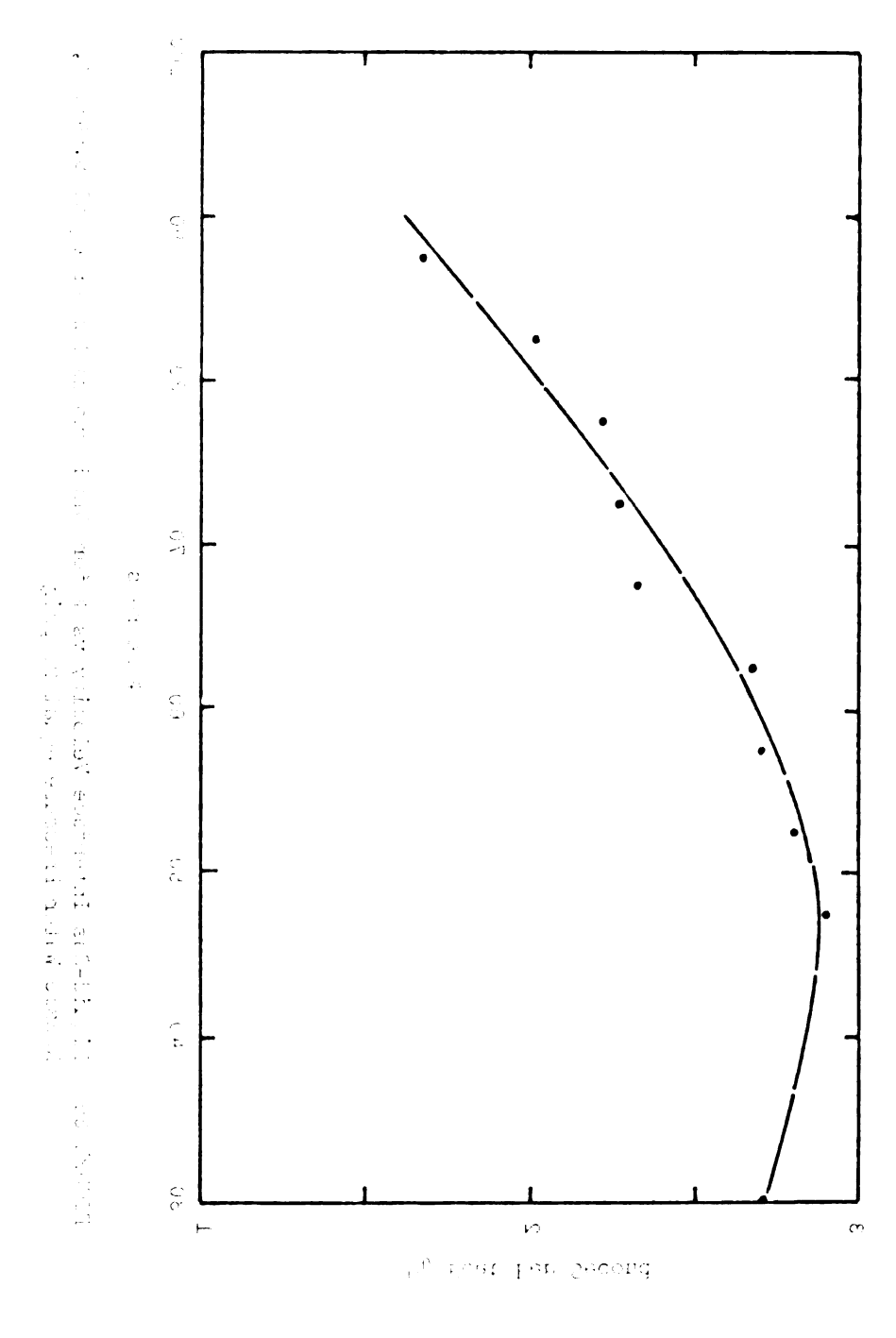


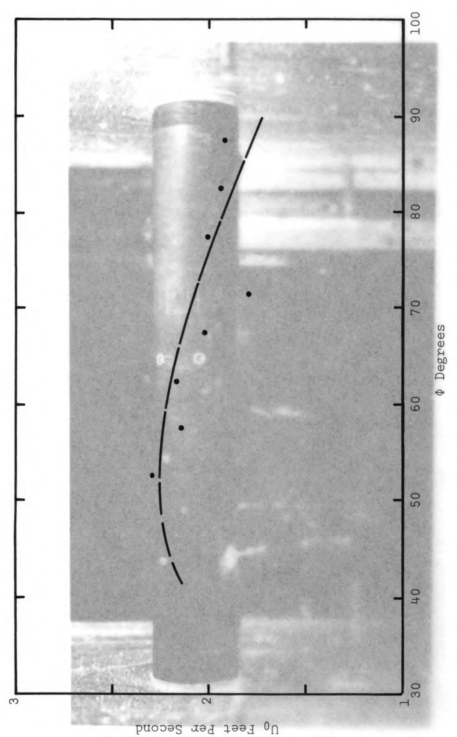
Liquid-Gas Interface Velocity vs ϕ for Gas Reynolds Number equal 5.64×10⁴, Nozzle Water Pressure equal 15 psig FIGURE 38

ig vect Per Document

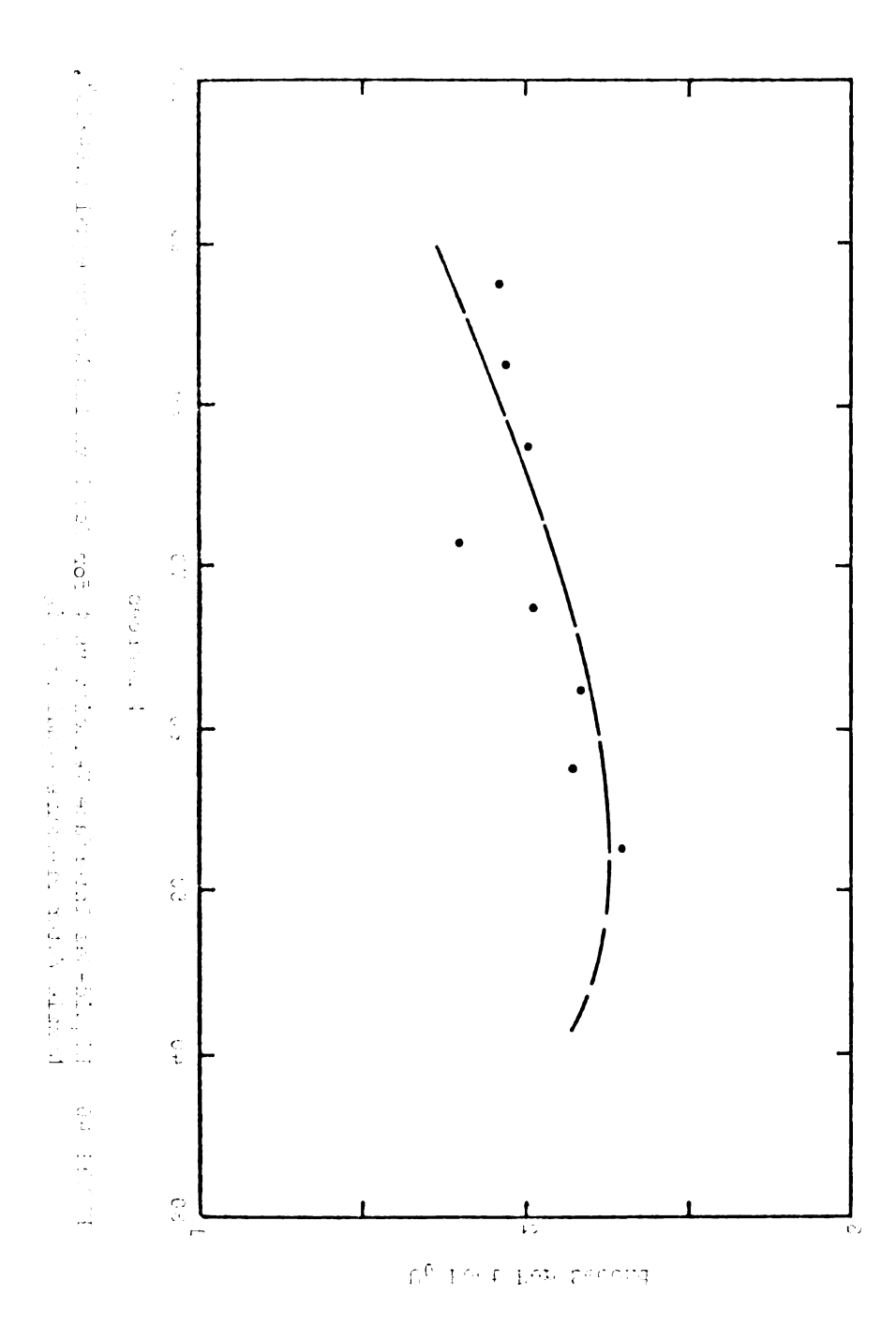


Liquid-Gas Interface Velocity vs # for Gas Reynolds Number equal 5.64×10⁴, Nozzle Water Pressure equal 20 psig FIGURE 39





Liquid-Gas Interface Velocity vs Φ for Gas Reynolds Number equal 5.64×104, Nozzle Water Pressure equal 25 psig FIGURE 40





Boundary-Layer Separation for Gas Reynolds Number equal 5.64×10 4 and Water Pressure equal 20 psig at Spray Nozzle FIGURE 41

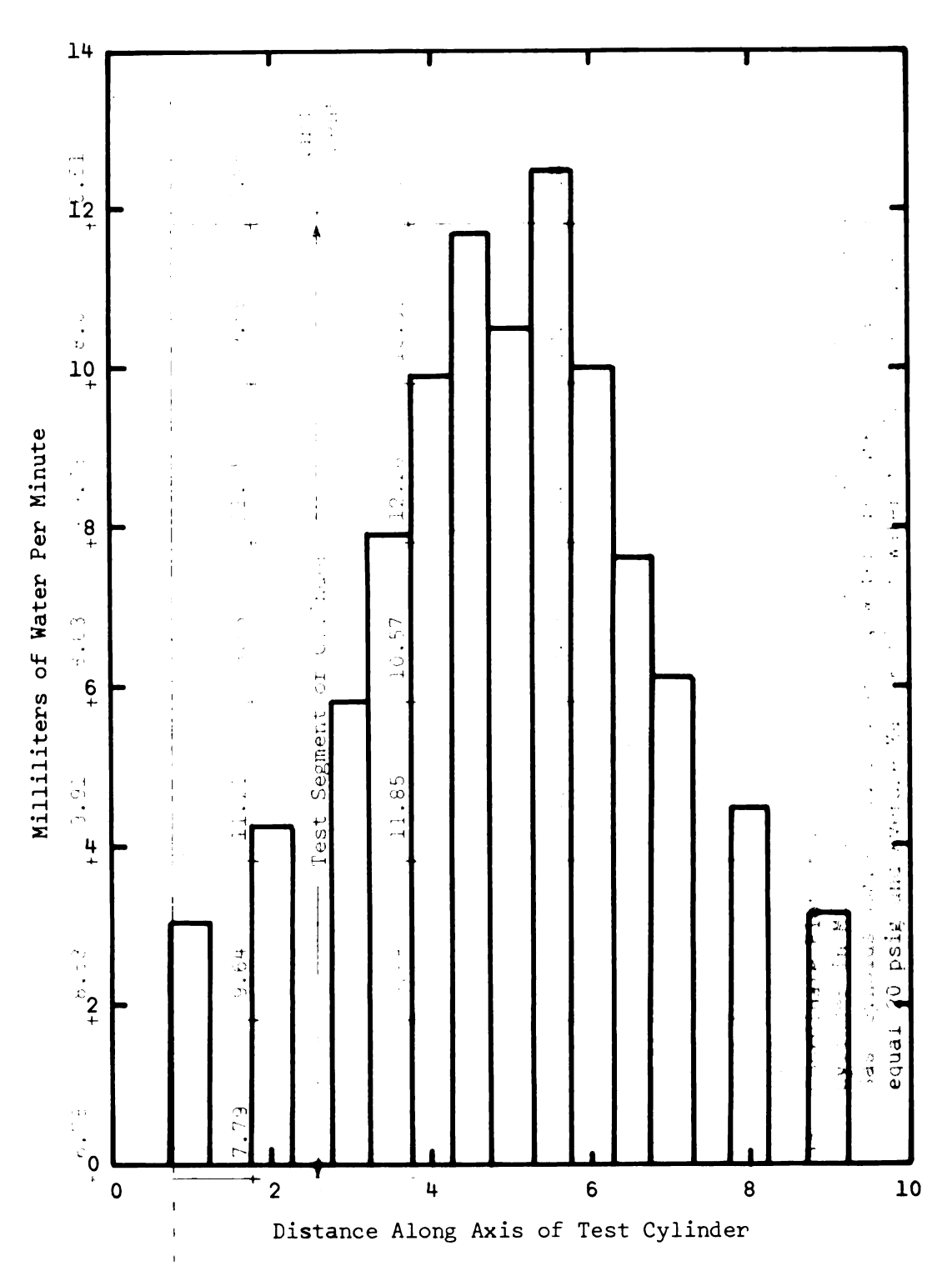
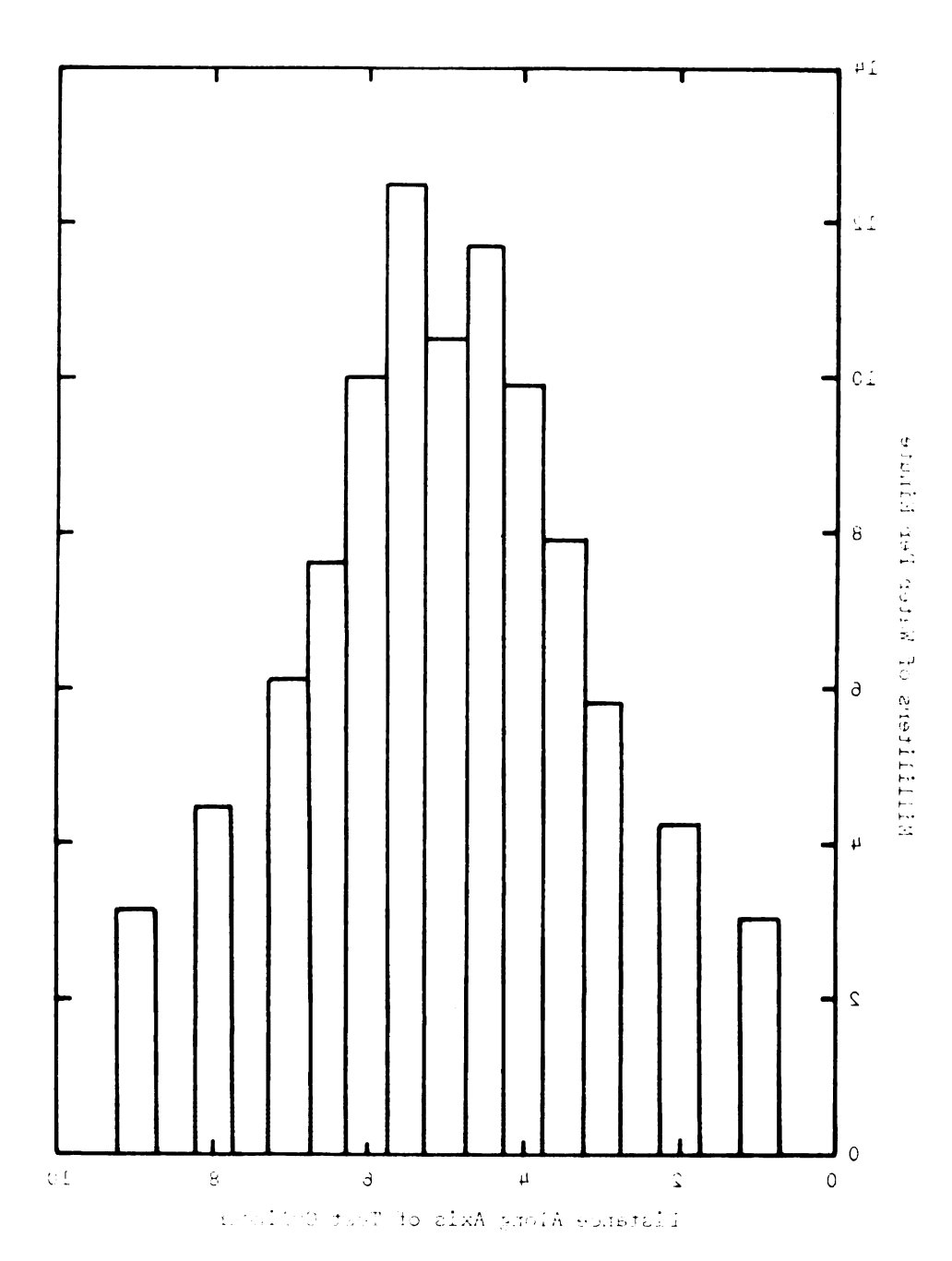
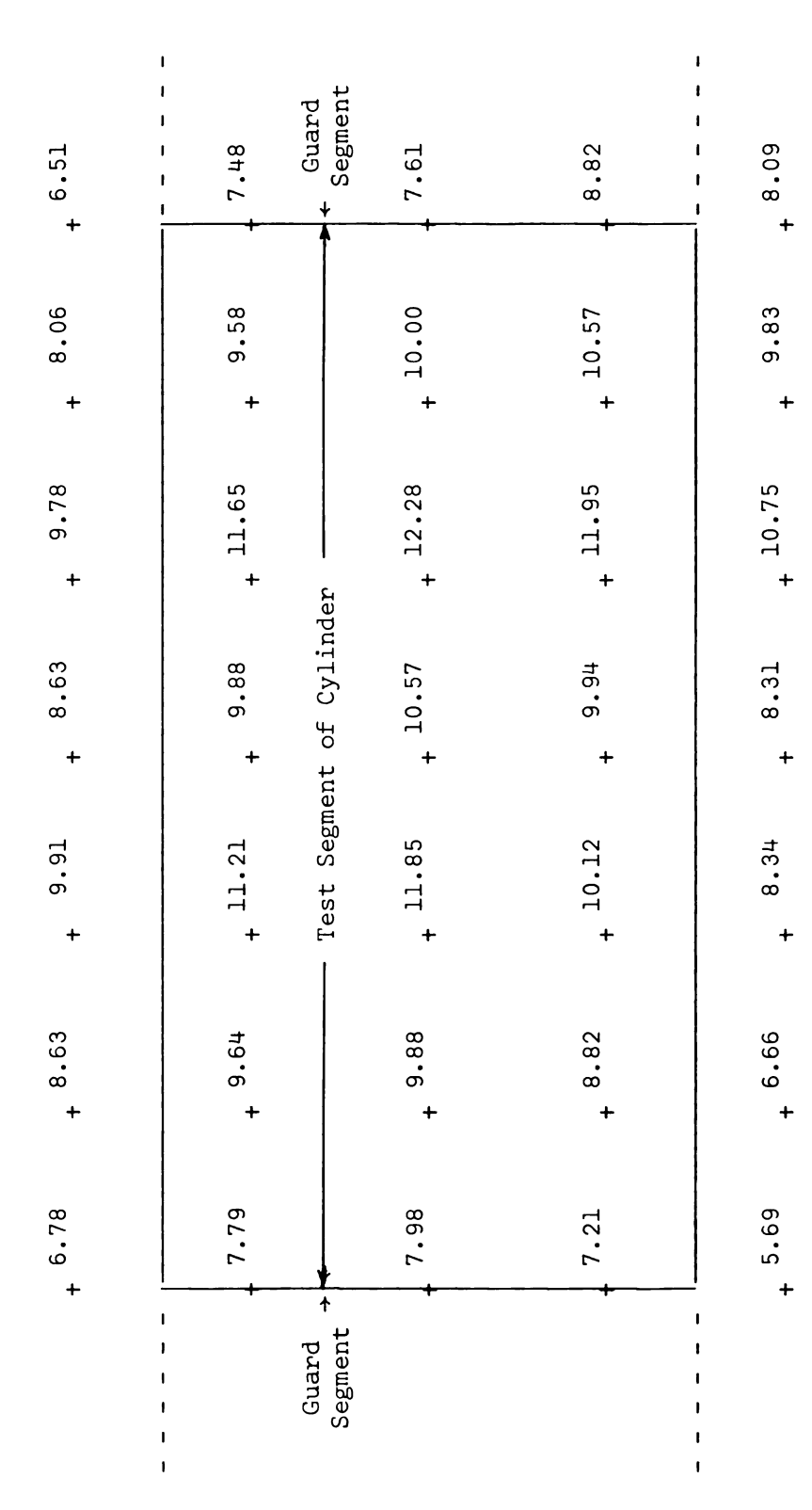


FIGURE 42 Water Spray Distribution Milliliters Per Minute Along Axis of Test Cylinder, for 1/2 Inch Collecting Tube, Nozzle Nr. 2116, Gas Reynolds Number equal 5.64×10⁴ and Water Pressure at Spray Nozzle equal 20 psig



FISURE 42 Water Spray Distribution Millilit as les M'ante Abloma Axis of Test Cylinder, for 1/2 lach Cylinder, Nozzle Mr. 2115, etc. Reventis Munice etc. 15. esc. 4 and Water Pressure at Gyray Norde etc. 20 plus and Water Pressure at Gyray Norde etc. 20 plus



Coordinate Plot of Water Spray Distribution Over Test Segment of Cylinder in Milliliters Per Minute for One-Half Inch Capture Tube, Gas Reynolds Number equal 5.64×10 4 , Water Pressure at Spray Nozzle equal 20 psig and Average Mass Ratio of Water to Air equal 0.045 FIGURE 43

124



FIGURE 44 Water Vortex Separating from Liquid Film and Indicating Direction of Vortex Rotation

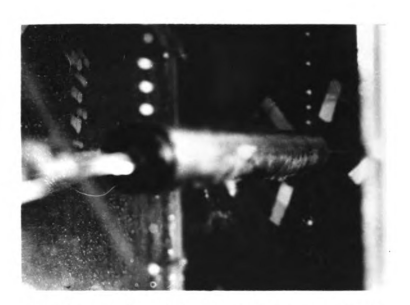


FIGURE 45 Series of Vortices Extending into Liquid Boundary Layer

125

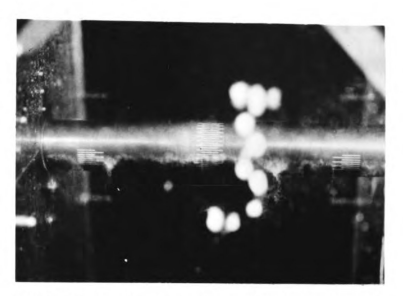


FIGURE 46 Boundary-Layer Separation for Gas Reynolds
Number equal 3.55×10⁴ and Water Pressure
equal 20 psig at Spray Nozzle

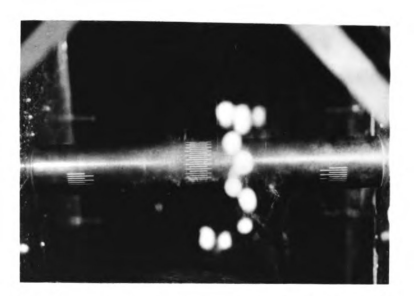
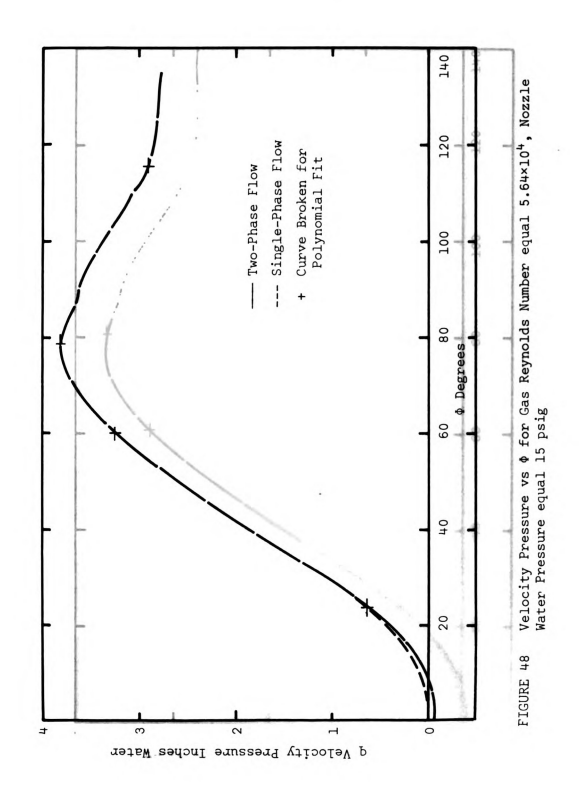
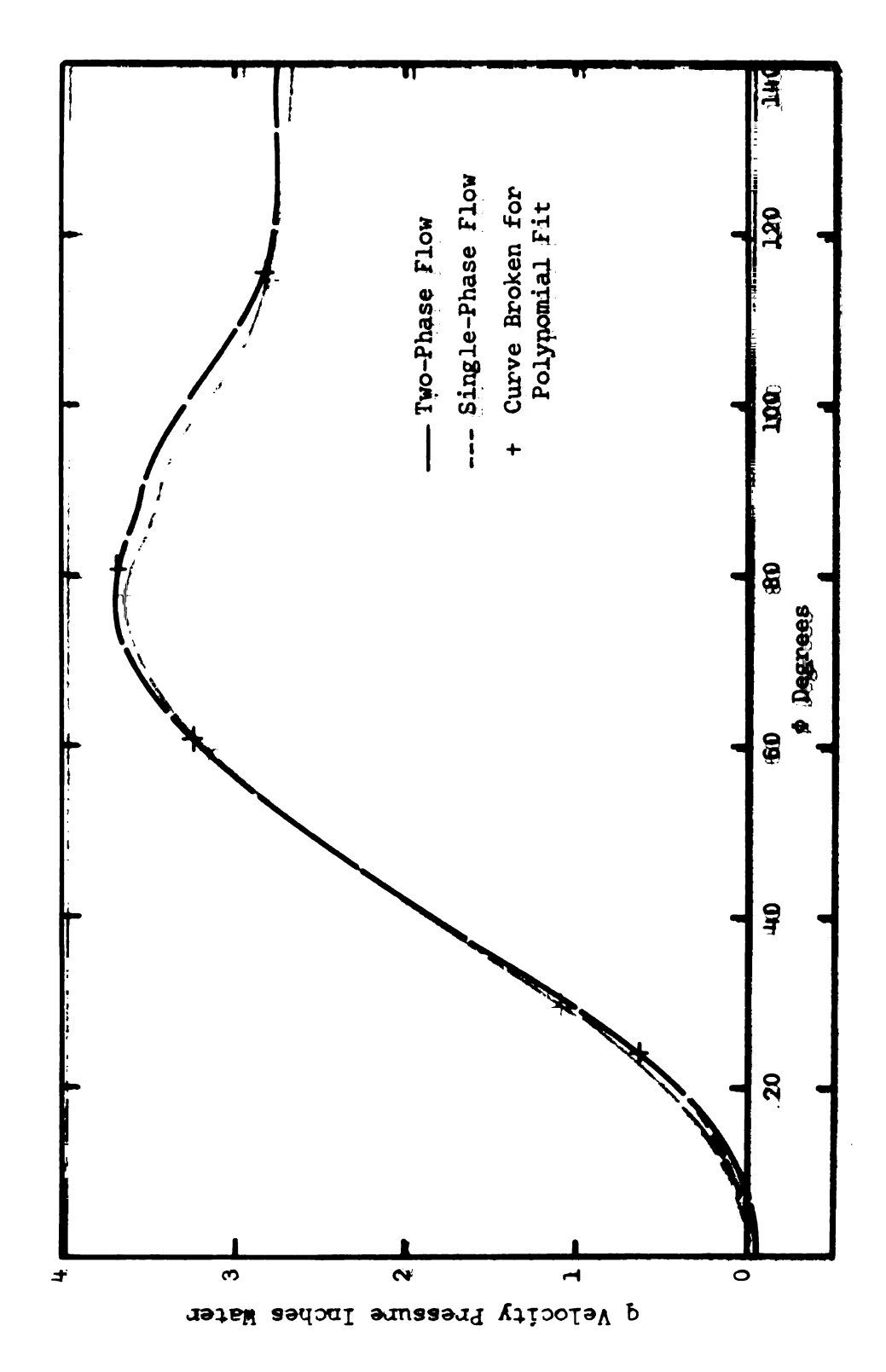


FIGURE 47 Boundary-Layer Separation for Gas Reynolds Number equal 1.04×10⁵ and Water Pressure equal 20 psig at Spray Nozzle

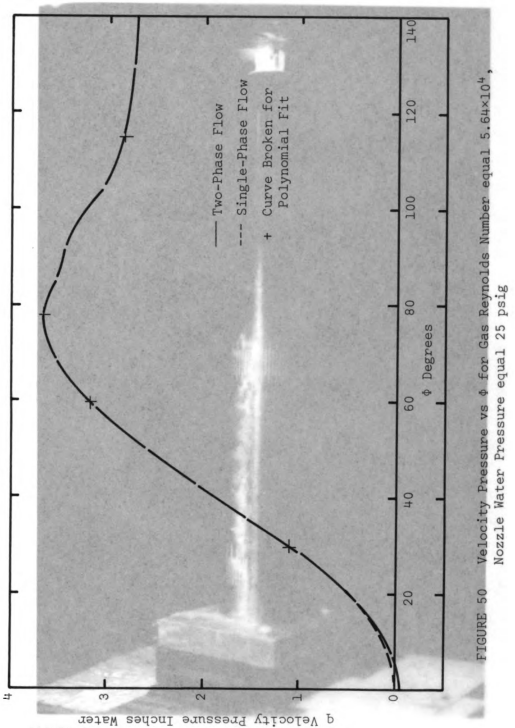


. The same substitution is a substituted for the substitute V:-:-74 11 11 11 $q \approx 100 {\rm deg}$ brosone inches where



Velocity Pressure vs & for Gas Reynolds Number equal 5.64×10⁴, Nozzle Water Pressure equal 20 psig FIGURE 49

Mandalo wates tas san e eorat (O'ate Netoniak besekts na e eorat (O'ate (C) (25.41.67 · ((C) g Velocity trespace Inches Water



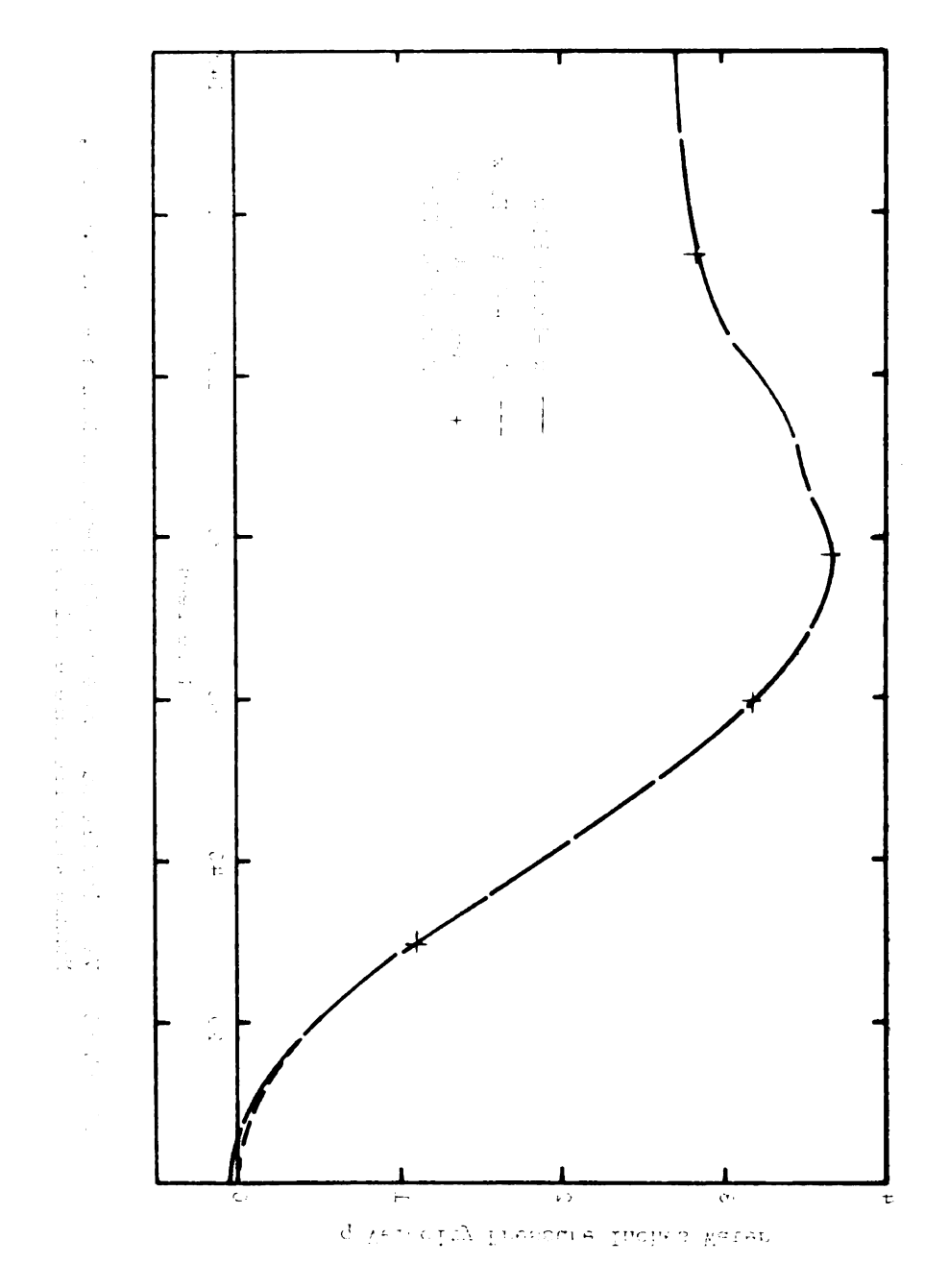




FIGURE 51 Boundary-Layer Separation on a Vertical Cylinder in Horizontal Two-Phase Flow, Gas Reynolds Number equal 5.64×10⁴

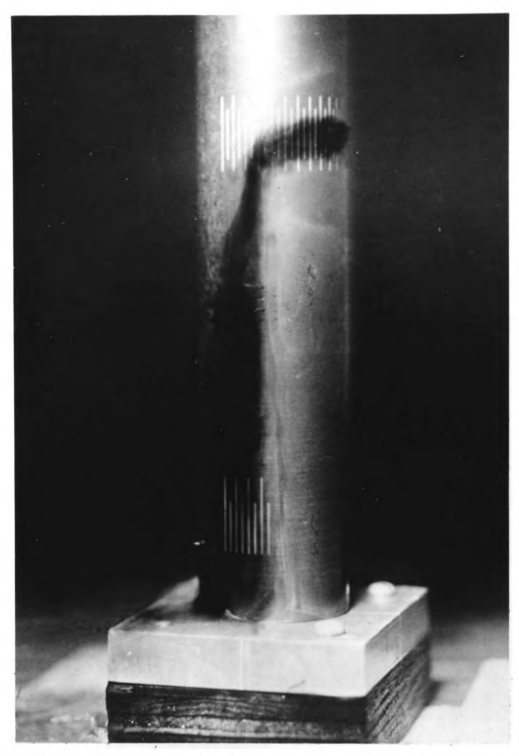


FIGURE 52 Boundary-Layer Separation on a Vertical Cylinder in Horizontal Two-Phase Flow with Dye Injected into Liquid Boundary Layer, Gas Reynolds Number equal 5.64*10*

APPENDIX C

TABLES

TABLE 1
HEAT TRANSFER DATA

Run Nr.	T _w Average Cylinder	T_{∞} Free Stream	V _∞ Free Stream	Re [†]	- Nu [†]
1	122.2	92.5	149	1.1 ×10 ⁵	224
2	115.2	79	136	9.16×10 ⁴	214
3	118.5	85.5	137	9.1 ×10 ⁴	221
4	124	86.5	107	7.13×10 ⁴	194
5	136	88	107	7.13×10 ⁴	195
6	135	90	48	3.24×10 ⁴	130
7	125	92	48	3.24×10 ⁴	133

 $[\]mbox{\dag}$ Reynolds Number Re and Average Nusselt number $\mbox{\tt Nu}$ are based on cylinder diameter D.

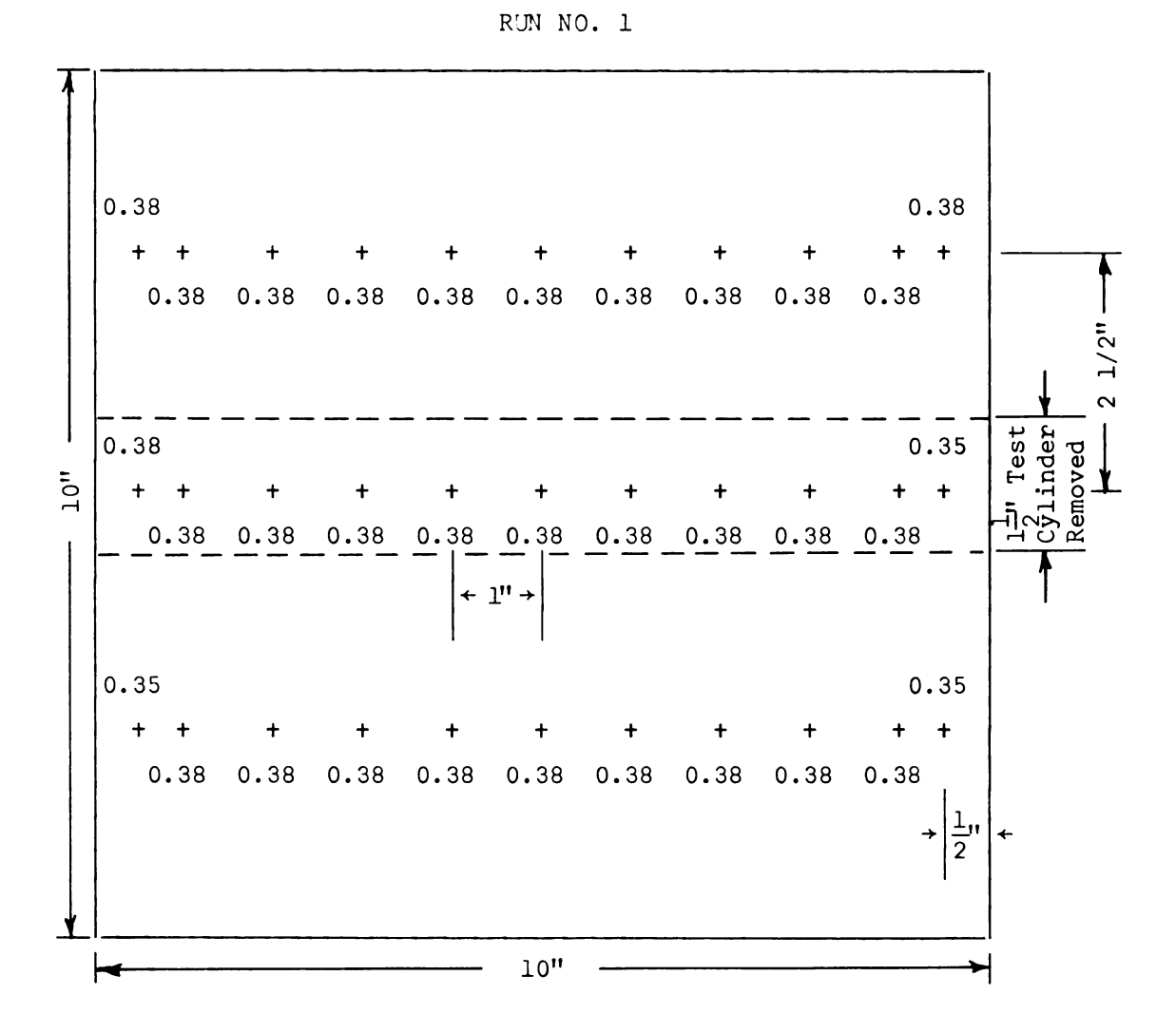
TABLE 2
VELOCITY PROFILES

Run Nr.	Free S	Stream	0.5 Inch From Wall		
	V _{max} ft/sec	V _{min} ft/sec	V _{max} ft/sec	V _{min} ft/sec	
1	42	42	42	40	
2	91	90.5	90.5	88	
3	125	123.5	124.5	121.5	
4	139	137.5	139	130	
5	176	175	176	171	

TABLE 3

VELOCITY PRESSURE IN INCHES WATER, WITH TEST CYLINDER REMOVED,

AT TEST STATION IN AFIT 10"*10" VERTICAL WIND TUNNEL

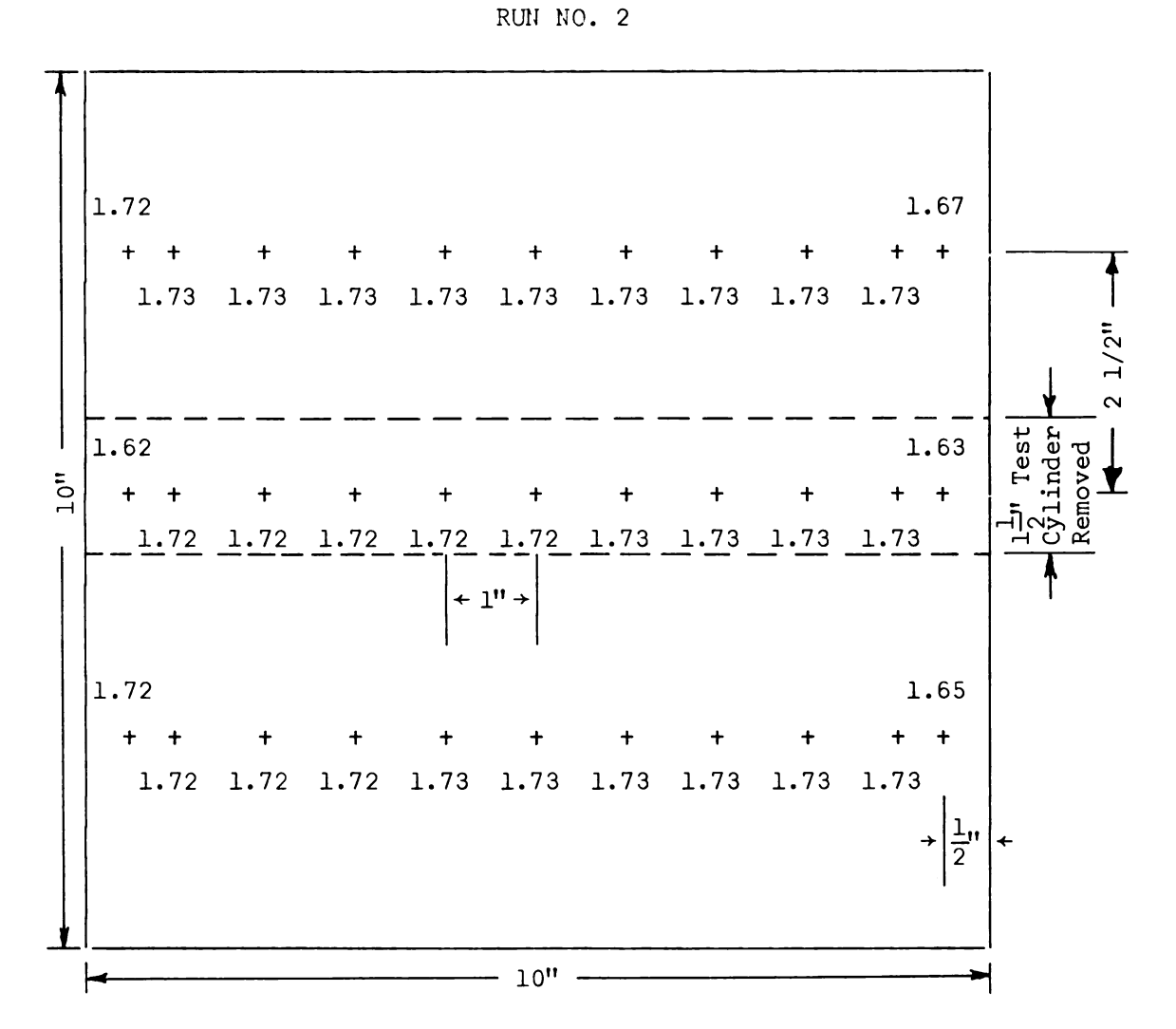


 $P_b = 29.325'' \text{ Hg}$ $T_{\infty} = 78^{\circ}\text{F}$

VELOCITY PRESSURE IN INCHES WATER, WITH TEST CYLINDER REMOVED,

AT TEST STATION IN AFIT 10"×10" VERTICAL WIND TUNNEL

TABLE 4



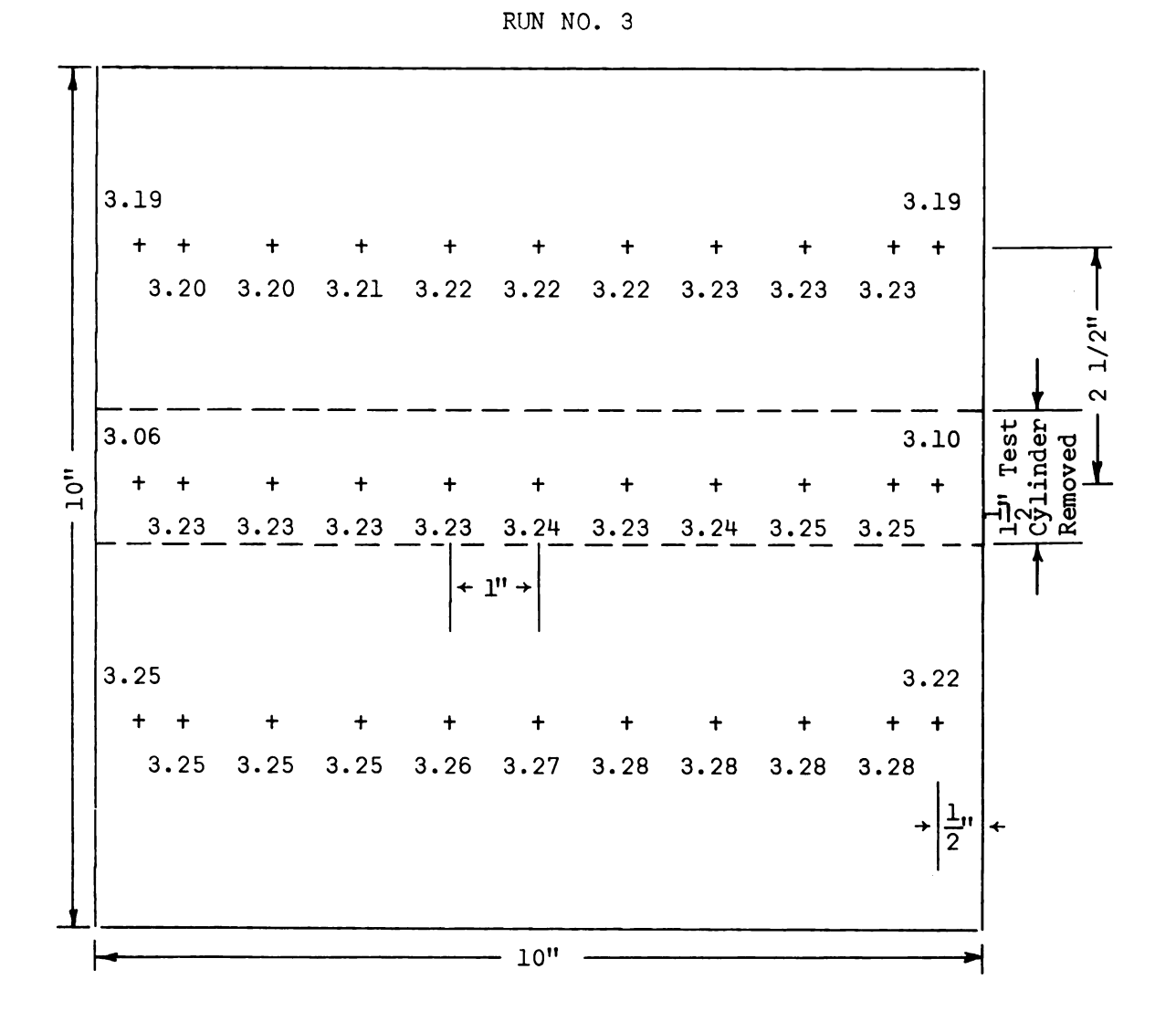
 $P_b = 29.34$ Hg

 $T_{\infty} = 90^{\circ}F$

TABLE 5

VELOCITY PRESSURE IN INCHES WATER, WITH TEST CYLINDER REMOVED,

AT TEST STATION IN AFIT 10"×10" VERTICAL WIND TUNNEL



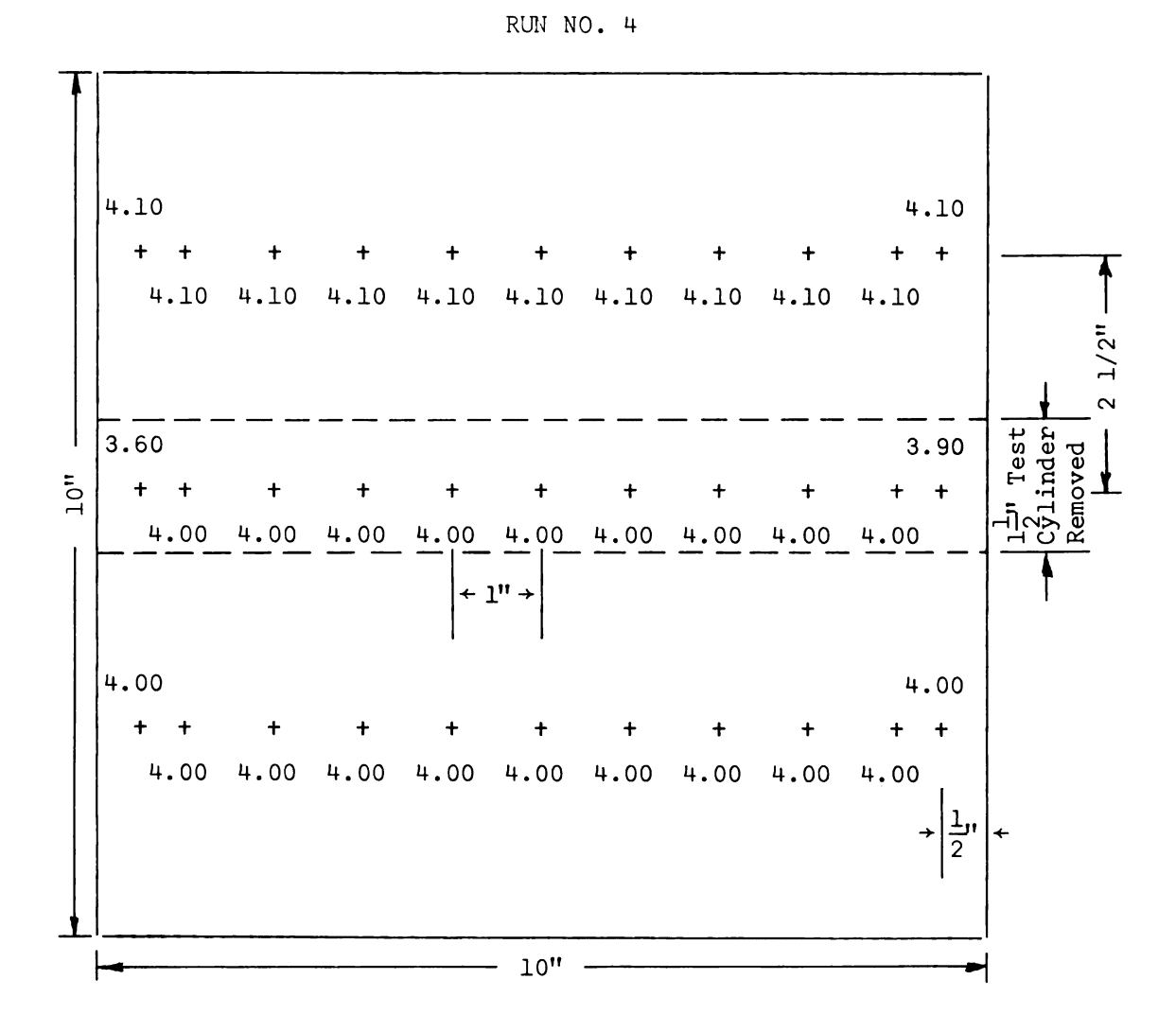
 $P_b = 29.34"$ Hg

 $T_{\infty} = 90^{\circ}F$

VELOCITY PRESSURE IN INCHES WATER, WITH TEST CYLINDER REMOVED,

AT TEST STATION IN AFIT 10"×10" VERTICAL WIND TUNNEL

TABLE 6



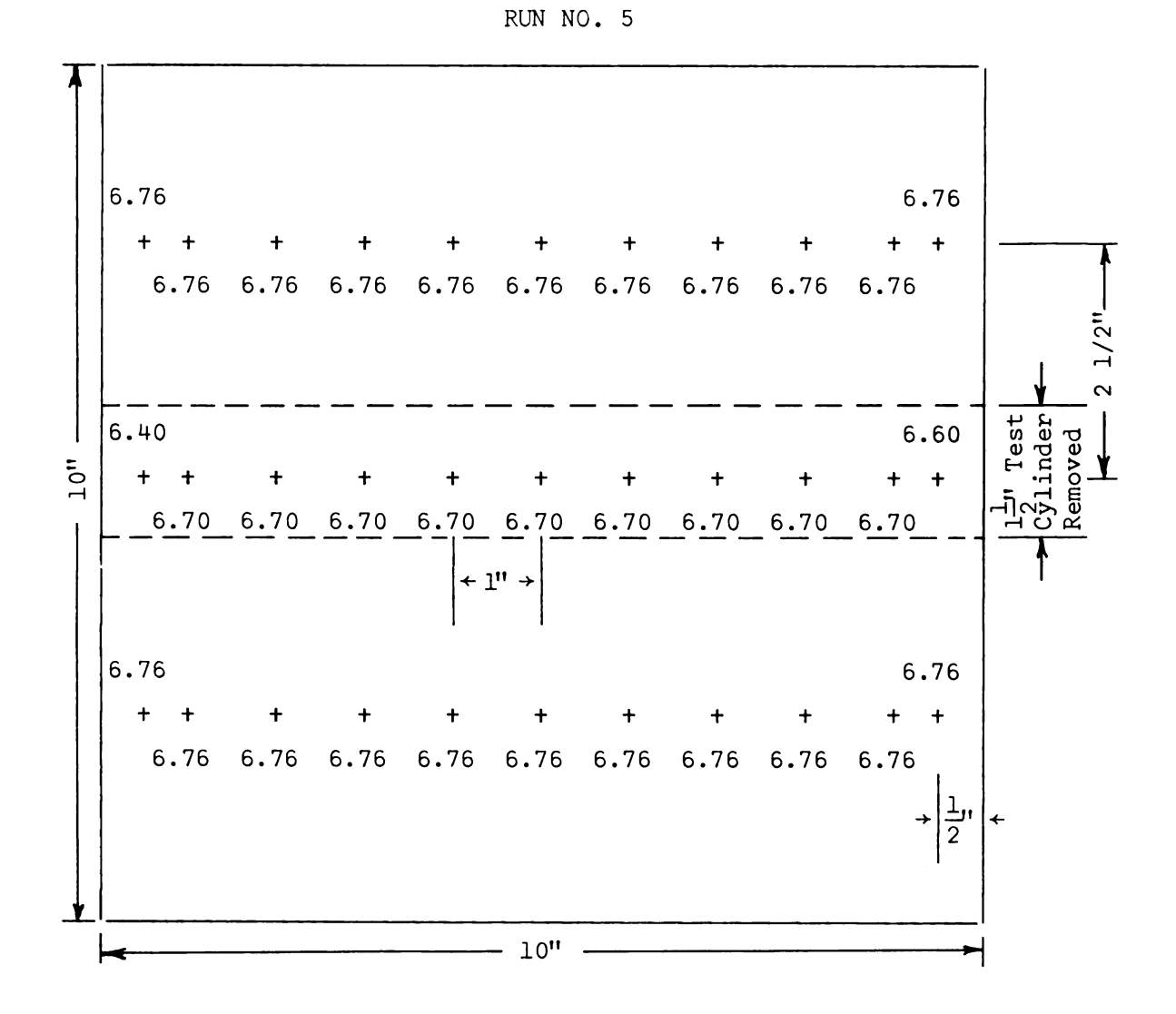
P_b = 29.32" Hg

 $T_{\infty} = 83^{\circ}F$

VELOCITY PRESSURE IN INCHES WATER, WITH TEST CYLINDER REMOVED,

AT TEST STATION IN AFIT 10"×10" VERTICAL WIND TUNNEL

TABLE 7



 $P_b = 29.325"$ Hg

 $T_{\infty} = 78^{\circ}F$

TABLE 8

DROPLET VELOCITY DATA

P _w psig	U _∞ ft/sec	U _d ft/sec	U _d ' ft/sec	U _d " ft/sec	Q ml/min	U _L ft/sec
15	76	43.0	43.4	41.1	1675	34.0
20	76	44.8	45.3	43.8	2000	40.5
25	76	50.3	51.8	48	2270	45.0

- $P_{\mathbf{W}}$ Water pressure at spray nozzle
- U_d Average droplet velocity
- U_d ' Maximum observed droplet velocity
- U_d Minimum observed droplet velocity
 - Q Water volumetric flow rate at spray nozzle (milliliters per minute)
- $\mathbf{U}_{\widetilde{\mathbf{L}}}$ Average water velocity at spray nozzle

TABLE 9

DROPLET SIZE DISTRIBUTION AND REYNOLDS NUMBER DATA

P _w n m			Maximum α/σ less than unity		Droplet size classification in per cent of total observed droplets				a'	Red
			Per Cent	α/α 11/16 1 3/64 1 1/32 1 1/64 1			_			
15	40	3036	65	0.79	5.8	9.1	29.9	56.2	0.031	520
20	40	4085	70	0.98	2.2	9.1	24.8	63.9	0.029	458
25	40	4390	65	0.76	2.5	8.8	32.5	56.2	0.030	380

- $\boldsymbol{P}_{\boldsymbol{W}}$ Water pressure at spray nozzle
 - n Number of observations
- α/σ Fraction of standard deviation
- d' Equivalent droplet diameter (the droplet diameter which would yield the same numbers of droplets and mass rate of flow)
- $\operatorname{Re}_{\operatorname{d}}$ Droplet Reynolds number based on equivalent diameter
 - m Total number of observed droplets

TABLE 10

LAMINAR BOUNDARY LAYER DATA

Φ radians	- I II / II I		λ	β	
o	0	3.526	7.052	1	
0.01	0	3.53289	7.06543	1	
0.1	0	3.53662	7.03791	1	
0.2	0	3.56821	6.99417	1	
0.3	0	3.62181	6.92010	1	
1.5	0	7.97245	1.12789	1	
1.8	0	14.73692	-6.62234	1	
1.88	0	21.00751	-12.78518	1	
0.11	0.01	3.53357	7.02444	0.95445	
1.5	0.01	7.97011	1.12756	0.9949	
1.8	0.01	14.53323	-6.60392	0.99487	
1.88	0.01	20.78130	-12.64750	0.99475	
0.11	0.02	3.52763	7.01262	0.90891	
1.5	0.02	7.96801	1.12727	0.98997	
1.8	0.02	14.49424	-6.58624	0.98973	
1.88	0.02	20.57323	-12.52088	0.98950	
0.11	0.03	3.52064	6.99873	0.86336	
1.5	0.03	7.96614	1.12700	0.98496	
1.8	0.03	14.45669	-6.56918	0.98460	
1.88	0.03	20.38086	-12.40380	0.98425	
0.11	0.04	3.51211	6.98178	0.81781	
1.5	0.04	7.96450	1.12677	0.97995	
1.8	0.04	14.42054	-6.55275	0.97946	
1.88	0.04	20.20219	-12.29506	0.97900	
0.11	0.05	3.50132	6.96032	0.77227	
1.5	0.05	7.96311	1.12657	0.97494	
1.8	0.05	14.38575	-6.53694	0.97433	
1.88	0.05	20.03561	-12.19368	0.97376	

TABLE 11
TURBULENT BOUNDARY LAYER DATA

P _w	Φ radians	θ	Н	Reθ	2q/τ ₀
15	0.20	0.001281	1.40		
15	0.24	0.00090	1.37129	9	89
15	1.32	0.00247	1.22373	118	250
15	1.36†	0.00251	1.22373	125	254
15	1.60	0.00375	1.23100	178	284
15	1.64††	0.00399	1.23255	188	288
15	1.88	0.00572	1.24465	254	315
20	0.20	0.001281	1.40		
20	0.24	0.00090	1.37129	9	89
20	1.28	0.00230	1.22449	111	244
20	1.32†	0.00241	1.22472	118	249
20	1.60	0.00381	1.23244	179	284
20	1.64 ^{††}	0.00406	1.23413	189	289
20	1.88	0.00593	1.24759	258	316
25	0.20	0.001281	1.40		
25	0.24	0.00093	1.37364	12	102
25	1.28	0.00238	1.22923	114	247
25	1.32	0.00251	1.22927	121	251
25	1.60	0.00390	1.23707	181	285
25	1.64††	0.00416	1.23883	191	290
25	1.88	0.00594	1.25131	257	316

 $Re = 5.64 \times 10^4$

 $\mathbf{P}_{\mathbf{W}} \quad \text{ Water pressure at spray nozzle}$

† Region of pressure minimum

†† Region of observed boundary-layer separation

APPENDIX D

BIBLIOGRAPHY

- 1. The Babcock and Wilcox Co. "Gas Suspension Coolant Project," AEC Contract No. AT (30-1) 2316, Final Report No. BAW-1159 (1959).
- 2. Elperin, I.T. "Heat Transfer of Two-Phase Flow with a Bundle of Tubes," <u>Inzhenerno-Fizicheski</u> <u>Zhurnal</u>, Vol. IV, No. 8, August 1961, pp. 30-35.
- 3. Martinelli, R.C., Boelter, M.K., Taylor, T.H.M., Thomsen, E.G., and Morrin, E.H. "Isothermal Pressure Drop for Two-Phase Two-Component Flow in a Horizontal Pipe," Trans. ASME, February 1944, pp. 139-151.
- 4. Lockhart, R.W. and Martinelli, R.C. "Proposed Correlation of Data for Isothermal Two-Phase, Two-Component Flow in Pipes," Chem. Eng., January 1949, pp. 39-48.
- 5. McManus, Jr. Howard Norbert. "An Experimental Investigation of Film Establishment, Film Profile Dimensions Pressure Drop and Surface Conditions in Two-Phase Annular Flow," Ph.D. dissertation, University of Minnesota, 1956.
- 6. Chiu, H.H. "Boundary Layer Flow with Suspended Particles," Report 620 Department of Aeronautical Engineering, Princeton University, August 1962.
- 7. Tribus, Myron. "Modern Icing Technology," Lecture Notes, Engineering Research Institute, University of Michigan, January 1952.
- 8. Tifford, A.N., Ohio State University. "Exploratory Investigation of Laminar Boundary Layer Heat Transfer Characteristics of Gas Liquid-Spray Systems," Aerospace Research Laboratories Report, ARL 64-136, September 1964.
- 9. Goldstein, M.E., Yang, Wen-Jei, Clark, John A. "Boundary Layer Analysis of Two-Phase (Liquid-Gas) Flow Over a Circular Cylinder and Oscillating Flat Plate," Department of Mechanical Engineering, University of Michigan, August 1965.
- 10. Kestin, J. and Maeder, P.F. "Influence of Turbulence of Transfer of Heat from Cylinder," NACA Technical Note 4018, October 1957.
- 11. Curle, N. The Laminar Boundary Layer Equations. Oxford Mathematical Monographs, Oxford Press, 1962, pp. 60-61.
- 12. Pohlhausen, K. "Zur näherungsweisen Integration der Differentialgleichung der laminaren Grenzschicht," ZAMM I (1921) pp. 252-268.
- 13. Schlichting, Hermann. Boundary Layer Theory, McGraw-Hill Book Company, Inc., New York (1960).

- 14. Doenhoff, A.E. von and Tetervin, N. "Determination of general Relations for the Behavior of Turbulent Boundary Layers."

 NACA Report No. 772 (1943) pp. 381-405.
- 15. Squire, H.B. and Young, A.D. "The Calculation of the Profile Drag of Aerofoils." R. & M. No. 1838, British A. R. C., 1938.
- 16. Gruschwitz, E. "Die turbulente Reibungsschicht in ebener Strömung bei Druckabfall und Druckanstieg." Ing.-Archiv, Bd.II, Heft 3, September 1931, pp. 321-346.
- 17. Schmidt, E. and Wenner, K. "Wärmeabgabe über den Umfang eines angeblasenen geheizten Zylinders." Forsch. Ing.-Wes. Bd.12, 65-73 (1941). Engl. transl. NACA TM 1050 (1943).
- 18. Hewitt, G.F., King, R.D. and Lovegrove, P.C. "Techniques for Liquid Film and Pressure Drop Studies in Annular Two-Phase Flow," AERE-R3921, Harwell, U.K., 1962.
- 19. Magiros, P.G. "Entrainment and Pressure Drop in Horizontal Two-Phase Gas-Liquid Flow," MS in Chem. Engrg. thesis, University of Houston, 1960.
- 20. McManus, Jr. H.N. "Experimental Methods in Two-Phase Flow," Multi-Phase Flow Symposium, American Society of Mechanical Engineers, 1963, pp. 75-78.
- 21. Hilpert, R. "Wärmeabgabe von geheizten Drähten und Rohren im Luftstrom." Forsch. Ing.-Wes. Bd4, 215 (1933).
- 22. Giedt, W.H. "Investigation of Variation of Point Unit Heat-Transfer Coefficient Around a Cylinder Normal to an Air Stream," Transactions of the ASME, May 1949, pp. 375-381.
- 23. Görtler, H. "Über eine dreidimensionale Instabilität laminarer Grenzschichten an konkaven Wänden." Nachr. Wiss. Ges. Göttingen, Math. Phys. Klasse, New Series 2, No. 1 (1940).

